Titre: Title:	Modeling in the Viscoelastic Behavior of Polyimide Matrix at Elevated Temperature
Auteur: Author:	Thibaut Crochon
Date:	2014
Type:	Mémoire ou thèse / Dissertation or Thesis
Référence: Citation:	Crochon, T. (2014). Modeling in the Viscoelastic Behavior of Polyimide Matrix at Elevated Temperature [Thèse de doctorat, École Polytechnique de Montréal]. PolyPublie. https://publications.polymtl.ca/1563/

UNIVERSITÉ DE MONTRÉAL

MODELING OF THE VISCOELASTIC BEHAVIOR OF A POLYIMIDE MATRIX AT ELEVATED TEMPERATURE

THIBAUT CROCHON
DÉPARTEMENT DE GÉNIE MÉCANIQUE
ÉCOLE POLYTECHNIQUE DE MONTRÉAL

THÈSE PRÉSENTÉE EN VUE DE L'OBTENTION
DU DIPLÔME DE PHILOSOPHIÆ DOCTOR
(GÉNIE MÉCANIQUE)
OCTOBER 2014

UNIVERSITÉ DE MONTRÉAL

ÉCOLE POLYTECHNIQUE DE MONTRÉAL

Cette thèse intitulée:

MODELING OF THE VISCOELASTIC BEHAVIOR OF A POLYIMIDE MATRIX AT ELEVATED TEMPERATURE

présentée par: CROCHON Thibaut
en vue de l'obtention du diplôme de: Philosophiæ Doctor
a été dûment acceptée par le jury d'examen constitué de:

M. DUBOIS Charles, Ph.D., président
M. LÉVESQUE Martin, Ph.D., membre et directeur de recherche
Mme LI Chun, Ph.D., membre et codirectrice de recherche
M. TSCHARNUTER Daniel, Ph.D., membre
M. FAYOLLE Bruno, Ph.D., membre

DEDICATION

To my family

À ma famille

ACKNOWLEDGEMENTS

I would like to first thank Pr. Martin Lévesque and Dr. Chun Li for their guidance and trust throughout this project. Your confidence allowed me to explore hypotheses that made my work interesting, challenging and, I hope, useful.

The time and expertise provided by the National Research Council Canada in Ottawa for the thermogravimetric analyses done during this project is also greatly appreciated. I would particularly like to thank Mahmud Kamal for his generous help and advice on the realization of my experiments.

I would like to acknowledge the contributions of my coworkers on this project, François Landry, Simon Dulong and Amine El-Mourid at École Polytechnique de Montréal, John Montesano and Marina Selezneva at Ryerson University in Toronto. The technical advice and support of Bénédict Besner, Isabelle Nowlan and Antoine Bouchard (Polytechnique) is also gratefully acknowledged.

I would like to thank the Consortium for Research and Innovation in Aerospace in Québec (CRIAQ), Rolls Royce Canada and Pratt & Whitney Canada (PWC) for financially supporting this project. I would also like to thank Stephen Caulfeild for welcoming me for a two months internship at PWC.

Finally, I would like to express my gratitude to my family and my friends for supporting me throughout the good and bad times of the past five years. I could not have done it without you.

RÉSUMÉ

L'utilisation de composites à matrice polymère (CMPs) s'est grandement répandue dans l'industrie du transport au cours des dernières décennies. Ces matériaux offrent un rapport rigidité/masse supérieur à celui des métaux et permettent d'alléger les véhicules et d'augmenter leur efficacité énergétique. Pour ces raisons, les principales compagnies aéronautiques et aérospatiales ont commencé à utiliser les CMPs dans des applications structurelles telles que les ailes, le fuselage et même les moteurs d'avion.

L'utilisation des CMPs dans des applications telles que les moteurs d'avions nécessitent des matériaux capable de résister à des conditions d'utilisation extrêmes, entre autres des températures élevées, ainsi que des chargements mécaniques importants et un environnement oxydant. Dans de telles conditions, la matrice polymère est susceptible de posséder un comportement viscoélastique dépendant de son chargement et de la température. De plus, à proximité des moteurs, la combinaison des hautes températures et de l'environnement accélère les vieillissements physiques et chimiques. Tous ces paramètres doivent être pris en considération afin de pouvoir prédire le comportement du matériau tout au long de son utilisation.

Le principal objectif de cette thèse était d'étudier le comportement viscoélastique d'une telle matrice et de développer une loi de comportement capable de tenir compte de tout type de conditions d'utilisation. Ce modèle devait ensuite être implémenté dans un logiciel commercial d'éléments finis tel que ABAQUS ou ANSYS.

Premièrement, le vieillissement chimique de la matrice à la température d'utilisation a été étudié. à cette fin, une analyse thermogravimétrique fut réalisée sur des échantillons de poudre dans une atmosphère d'air. Deux types de tests furent menés à bien : *i*) des tests cinétiques durant lesquels la poudre est chauffée à un rythme constant jusqu'à sa sublimation complète ; *ii*) des test isothermes durant lesquels les échantillons sont maintenus à une température unique pendant 24 heures. Le premier type de tests fut utilisé pour développer un modèle de dégradation reproduisant avec grande précision les résultats expérimentaux. La prédiction des résultats des essais isothermes a rencontré beaucoup moins de succès, en particulier pour les basses températures. à ces températures, une phase d'oxydation précède la phase de dégradation chimique. Or le modèle développé est incapable de représenter ce phénomène. D'autres essais de dégradation isothermes furent conduits sur des échantillons de traction plutôt que sur de la poudre. Ces tests furent menés à la température de service, pour des périodes de temps bien supérieures. Les masses, volumes et propriétés mécaniques furent mesurés après 1, 4, 9 et 17 mois. Les résultats ont montré qu'après 17 mois, la matrice avait

perdue près de 5% de sa masse et jusqu'à 19%, 30% et 10% de son module d'Young, contrainte à la rupture et déformation à la rupture, respectivement.

La seconde étape a consisté à étudier le comportement viscoélastique de la matrice dans diverses conditions d'utilisation afin de développer une loi de comportement. Cette loi fut développée à partir du travail accompli par Schapery en 1964, basé sur les principes de la Thermodynamique des Procédés Irréversibles. L'avantage principal des lois de comportement de type Schapery réside dans la prise en charge des effets des différents paramètres, tels que les contraintes, la température ou le vieillissement physique, par des fonctions nonlinéaires explicites. Des échantillons de traction du matériau furent testés à la température de service. Les déformations furent mesurées à l'aide de rosettes afin d'obtenir le comportement en 3D. Les résultats de ces essais montrèrent un coefficient de Poisson indépendant du temps, indiquant donc que son spectre des temps de retard est identique à celui de la fonction de souplesse. De plus, à cette température, le comportement viscoélastique était indépendant du niveau de chargement. Ces deux informations ont permis de conclure que le matériau était viscoélastique linéaire et que son comportement pouvait être représenté par une loi 1D. à partir de cette conclusion, et aussi du fait du manque de matériau, il fut décidé de réaliser l'étude de l'impact de la température et du vieillissement physique à l'aide de tests en flexion 3 points. Conformément à la méthodologie développée par Struik, le matériau fut chauffé à la température de vieillissement avant d'être soumis à une série de tests de fluage à intervalles croissants. Les résultats de ces essais indiquèrent que le matériau devenait plus rigide avec le vieillissement. De même, l'augmentation de la température fut accompagnée d'une augmentation de la souplesse. Un modèle fut développé dans lequel les fonctions nonlinéaires de Schapery furent obtenues à partir des données expérimentales. Le modèle fut ensuite validé à l'aide d'histoires de chargement complexes contenant plusieurs tests de fluage, ainsi que plusieurs sauts de température. Les résultats expérimentaux furent reproduits par le modèle avec une excellente précision.

Enfin, la dernière étape consistait à implémenter la loi de comportement dans un logiciel d'éléments finis. à cette fin, une nouvelle procédure fut développée au lieu des méthodes classiques qui utilisent la forme intégrale des lois de comportement de Schapery, la nouvelle procédure utilise les équations d'évolution qui sont à la base de l'intégrale. Ces équations sont résolues à l'aide des schémas de différences finies tels que Euler implicite, Crank-Nicholson ou Runge-Kutta. Les modèles numériques ainsi obtenus peuvent alors aisément être implémentés dans un logiciel éléments finis.

Au cours de cette thèse, un examen exhaustif des propriétés mécaniques d'une matrice polyimide a été réalisé. Les résultats obtenus montrent que, pour ce type de matériau, la température d'utilisation est si élevée que le vieillissement chimique prend une importance

considérable dans leur durabilité. Ce constat n'avait pas été anticipé au début de ce travail et le vieillissement chimique n'a pas été pris en considération dans la loi de comportement. De plus, il a aussi été remarqué que le comportement viscoélastique n'était pas dépendant du niveau de contrainte mais seulement de la température et du vieillissement physique.

ABSTRACT

The use of Polymer Matrix Composite Materials (PMCMs) has steadily increased in the transport industry over the past few decades. These materials offer a higher stiffness/mass ratio than their metallic counterparts and therefore allow for a reduction in the mass of the vehicle, which leads to an increased energy efficiency. Leading aerospace and aeronautics companies progressively using PMCMs for structural applications, such as wings, fuselage and more recently, aircraft engines.

Use of PMCMs in aircraft engines requires materials able to withstand extreme service conditions, such as elevated temperatures, high mechanical loadings and an oxidative environment. In such an environment, the polymer matrix is likely to exhibit a viscoelastic behavior dependent on the mechanical loading and temperature. In addition, the combined effects of elevated temperature and the environment near the engines are likely to increase physical as well as chemical aging. These various parameters need to be taken into consideration for the designer to be able to predict the material behavior over the service life of the components.

The main objective of this thesis was to study the viscoelastic behavior of a high temperature polyimide matrix and develop a constitutive theory able to predict the material behavior for every of service condition. Then, the model had to have to be implemented into commercially available finite-element software such as `ABAQUS` or `ANSYS`.

Firstly, chemical aging of the material at service temperature was studied. To that end, a thermogravimetric analysis of the matrix was conducted on powder samples in air atmosphere. Two kinds of tests were performed: *i*) kinetic tests in which powder samples were heated at a constant rate until complete sublimation; *ii*) isothermal tests in which the samples were maintained at a constant temperature for 24 hours. The first tests were used to develop a degradation model, leading to an excellent fit of the experimental data. Then, the model was used to predict the isothermal data but which much less success, particularly for the lowest temperatures. At those temperatures, the chemical degradation was preceded by an oxidation phase which the model was not designed to predict. Other isothermal degradation tests were also performed on tensile tests samples instead of powders. Those tests were conducted at service temperature for a much longer period of time. The samples masses, volume and tensile properties were recorded after 1, 4, 9 and 17 months. The results of those tests showed that after 17 months, the matrix lost about 5% of its mass and volume and as much as 19%, 30% and 10% of its Young's modulus, stress and strain at break, respectively.

The second step consisted in studying the viscoelastic behavior of the matrix under various conditions and develop a constitutive theory to model its mechanical behavior. That theory

was developed using the framework laid out by Schapery in 1964, using the Thermodynamics of Irreversible Processes. The main advantage of Schapery-type constitutive theories is that the effects of various parameters such as stresses, temperature and physical ageing can be taken into account by using user-defined explicit nonlinearizing functions. Tensile samples of the material were tested at service temperature using strain gages rosettes in order to study the matrix 3D behavior. It was found that the Poisson's ratio was time-independent, meaning that its retardation times spectrum was the same as the compliance function. Furthermore, at this temperature, it was found that the viscoelastic behavior was independent of the stress level. Those two observations led to the conclusion that the material was linearly viscoelastic and could be represented with a 1D constitutive theory. From this conclusion, and also due to the scarcity of material available, it was decided to use 3-point bending tests for studying the impact of temperature and physical ageing. Following Struik's methodology, the material was heated at ageing temperature and then series of creep tests at increasing intervals were performed. It was found that the material became stiffer as the ageing time increased, but it also became softer for increasing temperatures. A model was developed in which Schapery's nonlinearizing functions were obtained from experimental data. The model was validated with complex thermo-mechanical histories comprising several creep tests as well as temperature up- and down-jumps. The experimental data were predicted with excellent accuracy.

Finally, the last step consisted in implementing the constitutive theory into a finite-element software. To that end, a new procedure was developed. Instead of the classical methods which deal with Schapery's hereditary integral, the method went back to the evolution equations which are the basis of the integral. The evolution equations were solved with well-known finite-difference schemes such as Backward-Euler, Crank-Nicholson or Runge-Kutta. The numerical model thus obtained could then easily be implemented into finite-element software.

In this thesis, a thorough examination of the mechanical properties of a polyimide matrix was conducted. It was found that for such materials, the service temperature is so elevated that chemical ageing has a defining importance on components life.. This was not anticipated at the beginning and therefore not taken into account in the constitutive theory. Furthermore, it was found that viscoelastic behavior was only dependent on temperature and physical ageing, but not on the stress levels.

TABLE OF CONTENTS

LIST OF TABLES

LIST OF FIGURES

INTRODUCTION

The use of Polymer Matrix Composite Materials (PMCMs) has steadily increased in the transport industry over the past few decades. These materials offer a higher stiffness/mass ratio than their metallic counterparts and, therefore, allow for reducing vehicles masses, which leads to an increased energy efficiency. Leading aerospace and aeronautics companies are increasingly using PMCMs for structural applications, such as wings, fuselage and more recently, aircraft engine components.

Use of PMCMs in aircraft engines requires materials able to withstand extreme service conditions, such as elevated temperatures, high mechanical loadings and a highly oxidative environment. In such an environment, the polymer matrix is likely to exhibit a viscoelastic behavior depending on the mechanical loading and temperature. In addition, the combined effects of elevated temperature and the environment near the engines are likely to increase physical, as well as chemical, ageing. These various parameters need to be taken into consideration for the designer to predict the material behavior over the components service lives.

Pratt and Whitney Canada, Rolls Royce Canada, the Consortium for Research and Innovation in Aerospace in Quebec (CRIAQ) and the Natural Sciences and Engineering Research Council (NSERC) of Canada pooled their resources to fund a four-year project aiming at understanding the aging, static, and fatigue performance of a specific high temperature composite. The project involves 3 universities (Polytechnique - lead, Concordia University and Ryerson University) as well as the National Research Council in Ottawa.

The project was decomposed it into three sub-projects: *i*) the first sub-project, which is the subject of this thesis, dealt with the polymer matrix viscoelastic and long term behavior modeling. It involved 1 Ph.D student as well as 2 M.Sc students; *ii*) the second sub-project dealt with the development of an homogenization model for predicting the static properties of the composite. It involved 1 Ph.D student; *iii*) the last sub-project dealt with fatigue aspects inside the composite and involved 1 Ph.D student as well as 1 M.Sc student.

The current study focused particularly on the behavior of an innovative polyimide resin, manufactured by Maverick Corporation (product no. MVK-10), which provides excellent high-temperature stability and processing versatility. MVK-10 is considered as a potential replacement for the carcinogenic PMR-15 matrix used in high temperature applications for many years. This study aimed at developing tools for predicting the the polyimide resin's long-term behavior under elevated temperature applications. It addressed three objectives, namely MVK-10 thermal stability assessment under realistic service conditions, the development of a constitutive theory capable to take into consideration the effects of stress, tempera-

ture and physical ageing on the viscoelastic properties of the material and the implementation of this theory into a Finite-Element software. Two M.Sc students significantly contributed to the experimental aspects of the project. François Landry (Landry, 2010) developed the setup for testing the material at elevated temperatures and Simon Dulong realized most of the testing reported in this thesis on the actual polymer matrix.

This thesis is organized as follows. Chapter 1 presents a literature survey on polymers and the impact of temperature and environment on their mechanical behavior. Chapter 2 introduces the objectives of the project with respect to the findings of Chapter 1. Chapter 2 describes the relationship between the research objectives and the publication strategy. The three articles resulting from this work are included in Chapters 3 to 5. Chapter 3 presents the effects of chemical ageing on the material's stability. Chapter 4 studies the impact of stress, temperature and physical ageing on the viscoelastic behavior. Chapters 5 presents a novel methodology for implementing general Schapery-type constitutive theories into finite element packages such as `ABAQUS` or `ANSYS`. Chapter 6 discusses the relationships between the articles as well as complementary work performed during this project. The contributions from this thesis are finally summarized and topics for future studies are recommended.

CHAPTER 1

LITERATURE SURVEY

1.1 Polymers and polyimides

A polymer is a macromolecule whose structure is a repetition of single units called monomers and linked together by covalent bonds. The nature and composition of the monomers, as well as their arrangement inside the molecules, are responsible for overall material's properties. Polymers are generally classified as either thermoplastics or thermosets, according to bonding types. In thermoplastics, macromolecules are linked to one another by van der Waals bonds only, while in thermosets, they can also be linked by covalent bonds. Therefore, thermosets cannot be melt and recycled since the heat necessary to overcome the covalent bonds between the macromolecules would also overcome the bonds inside the macromolecule, leading to the material's decomposition. However, this also leads to better thermo-mechanical properties, when compared to thermoplastics.

Polymers are often characterized by their glass transition temperature, T_g. At this temperature, the polymer changes from a solid-like state to a liquid-like state, resulting in a severe decrease of the mechanical properties (of around 3 orders of magnitude) and thus in a material unfit for structural applications.

Developed in the 1960s, polyimides are a special class of thermosetting polymers aimed at specific high-temperature structural applications. They set themselves apart from other polymers by exhibiting high mechanical properties, as well as exceptional thermal and thermo-oxidative properties (Li *et al.*, 1999). Furthermore, while the processing of these matrices has been a major issue for a long time, recent progresses have led to the development of new chemical formulas suitable for less expensive out-of-autoclave manufacturing processes.

The designation of polyimides stands for all polymers containing an imide group (see

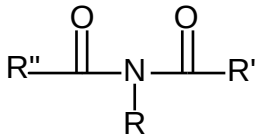

Figure 1.1: Represention of an imide group. An imide group is composed of two acyl groups (R'-C=O and R"-C-O) bound to a nitrogen N.

Table 1.1: Thermomechanical properties of various polyimides (PMR-15, DBMZ-15 and BMI) at room temperature compared to epoxy

Properties	PMR-15	DMBZ-15	BMI	General epoxy
T_g(°C)	350	290	293	~ 125
Tensile modulus (GPa)	3.5	3.2	3.8	~ 3
Failure stress (MPa)	92	130	55	~ 50
Failure strain (%)	2.6	3.2	1.6	~ 4

Fig. 1.1) in their base monomer. They are usually synthesized by polycondensation of a dianhydride (such as PMDA, ODPA, etc.) and a diamine (ODA, etc.) (Kirby, 1992; Talon, 2007), allowing for very high cross-linking density, and thus for amorphous thermosetting polymers with very high T_gs (see 1.2).

For many years, the PMR-15 polyimide matrix developed by NASA Lewis Research Center was the preferred polyimide for structural applications since it offered stable performances at high temperatures, while being easy and relatively cheap to process (Jones, 2009). While its use has decreased in recent years since one of its core components was found to be carcinogenic, PMR-15 remains the benchmark against which the performances of new polyimide systems are compared to. Table 1.1 lists the thermomechanical properties of PMR-15, DMBZ-15 (which was developed as a substitute for PMR-15) and of various other polymer systems (Chuang, 2001; Liang *et al.*, 2007). Typical polymides thermo-mechanical properties includes very high tensile modulus, tensile strength and T_g, but low elongation at break, when compared to typical epoxy resins.

High-end applications generally require to use materials at the upper limit of their possibilities. In the case of polymers, it generally translates into service temperatures slightly below their T_g. At those temperatures, most polymers exhibit progressively reduced ductility and embrittlement, chackling, cracking and general reduction in most other desirable physical properties (Beyler et Hirschler, 2001). The origins of these changes, referred to as ageing, are diverse: *i*) possible continuation of the curing process in the case of thermosetting polymers, also known as curing ageing (White, 2006); *ii*) changes in the polymer's chemical composition, i.e., chemical or thermal ageing; *iii*) volume relaxation following the rapid heating or cooling of the polymer as it evolves towards a new thermodynamic equilibrium, i.e., physical ageing (Hutchinson, 1995).

1.1.1 Thermal or chemical ageing

The American Society for Testing and Materials (ASTM) defines thermal degradation as a process occurring when a material submitted to high temperatures suffers a decrease in its

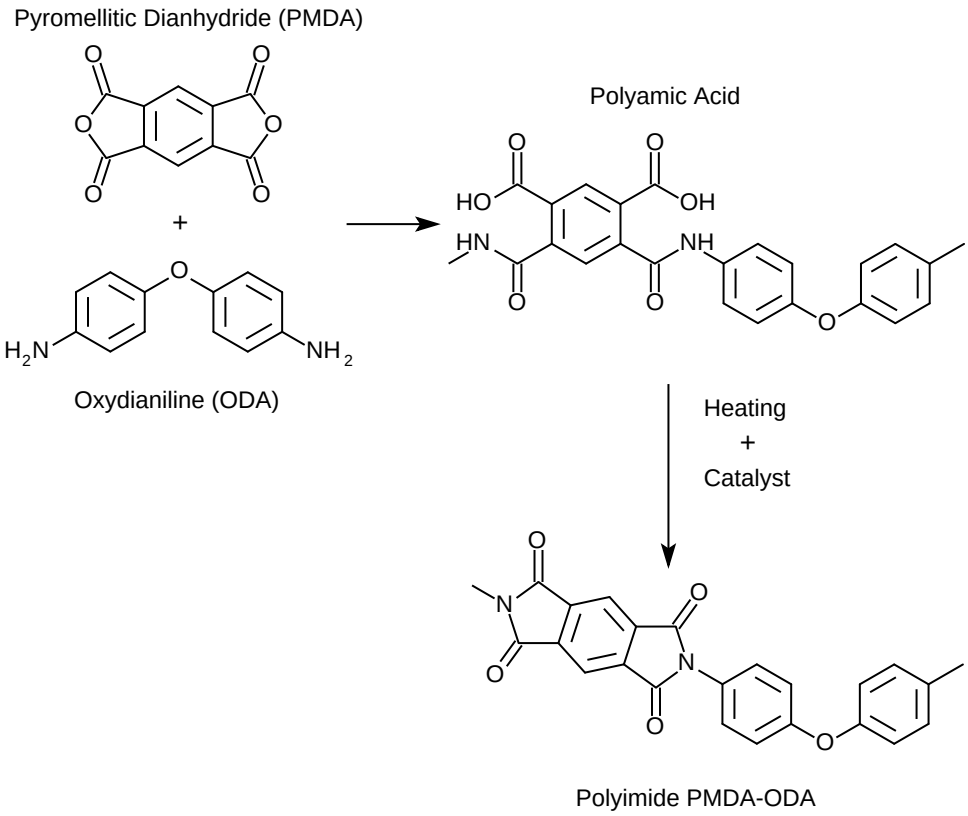

Figure 1.2: Genesis of the PMDA-ODA polyimide similar to the polyimide *Kapton* developed by DuPont (Talon, 2007). Polycondensation is a two-step polymerization process. The first step consist of obtaining a polyimic acid from the reaction between the amino group and the anhydride. This reaction occurs in the presence of polar solvent at a temperature below 50°C to prevent the cyclization and preserve solubility (Kirby, 1992). Then, heating the polyimic acid around 300°C, and the addition of a catalyst, allow for the elimination of water and the obtention of the polyimide.

mechanical, electrical or physical properties.

Polymer degradation can generally be explained by one of the following four chemical reaction mechanisms, or by any combination of them. Those mechanisms can be divided into two classes which are the main and the side chain reactions (Beyler et Hirschler, 2001). The first reaction involving the main chains is the breaking of bonds or chain-scission. This results in the production of monomers and oligomers of smaller molecular weights. An other reaction involving the main chain is the cross-linking between residual polymer chains, leading to molecules of higher weights and possibly of carbonaceous residues. Side chain reactions consists of eliminating the side groups from the main chains, generally resulting in the production of volatile products that are eliminated. Side groups can also react between themselves, forming cyclic structures with high concentration of carbon atoms, leading to the formation of chars.

The most common mechanism is the chain-scission. It is a multiple-step process following the pattern of an autoxidation process. This process involves four major steps:

1. The initiation step involves the formation of a free radical either by a random scission of the main polymer chain or by a scission at the end of the chain. A typical initiation is the loss of a hydrogen atom from the polymer chain, thus creating a free radical and an unpaired electron.
2. The propagation (or depropagation) step involves a variety of reactions: *i*) the intramolecular transfer of an hydrogen atom from the main molecular chain to a free radical situated at close proximity, leading to a random scission of the main molecular chain; *ii*) the intermolecular transfer of an hydrogen atom between a saturated chain and a free radical situated on an other main chain, also leadings to a chain scission; *iii*) a depolymerization process that generally consists of two carbon atoms separation.
3. The branching step consists of the cross-linking between chemical species formed during the propagation step. This step can also be promoted by the presence of oxygen that accelerates the production of free radicals (Jang et Wilkie, 2005). One example of such reaction is the formation of hydroperoxide from a free radical, an oxygen molecule O_2 and an hydrogen atom.
4. The termination is the concluding step of the decomposition mechanism. It consists of suppressing all remaining free radicals in order to obtain only inert chemical species.

The importance of quantifying thermal degradation under service conditions cannot be overstated. For example,Ruggles-Wrenn et Broeckert (2009) showed that, when aged at its service temperature (288°C) in an air atmosphere for 1,000 hours, a sample of plain PMR-15 matrix lost 3.5% of its initial mass. Over the same period, its elastic modulus increased

by 13% while its failure stress and strain dropped from 20MPa and 1.25% to 12MPa and 0.60%, respectively. This kind of results shows that, while the matrix could be considered as thermally stable for 1,000 hours at service temperature, its mechanical properties could significantly be deteriorated..

1.1.2 Physical ageing of polymers

Physical ageing manifests itself as the variation of viscoelastic properties as a function of time without any external stimuli (Hutchinson, 1995; White, 2006). It is found to be fully reversible for amorphous polymers and its history can be erased by heating a material above its glass transition temperature for a few minutes (Struik, 1978). Since physical ageing is not triggered by any external stimuli, the driving force is generally assumed to be the material's non-equilibrium thermodynamic state (Hutchinson, 1995; White, 2006). An example of physical ageing is depicted in Figure 1.3 that represents the volume contraction as a function of time and temperature for an amorphous polymer. Above T_g, molecular rearrangements are fast and the material always stays in its equilibrium state. However, once below T_g, the molecular rearrangements are slowed down to such an extent that the material cannot keep up with the cooling rate. The material's structure is therefore "frozen-in" as long as the cooling continues and remains in a non-equilibrium state. However, once the cooling stops, the material returns progressively to its equilibrium state, the previously frozen molecular rearrangements take place and the volume and enthalpy decrease (Hutchinson, 1995).

Physical ageing not only has an effect on the material's volume, but also on its mechanical properties. The material becomes more brittle and stiffer as physical ageing progresses.

1.2 Measuring and modeling chemical ageing

1.2.1 Measuring chemical ageing

A few methods have been proposed in the literature for measuring the chemical ageing of polymers. This thesis specifically focuses on thermogravimetric analysis, infrared spectroscopy (IR) and mass spectrometry (MS). Combining these three techniques allows for a thorough examination of the degradation kinetics and of the volatilized products. Furthermore, the NRC's laboratory in Ottawa already possessed a fully-integrated TG-IR-MS apparatus prior to this project. However, other techniques such as thermal volatization analysis (Beyler et Hirschler, 2001), differential scanning calorimetry (Coats et Redfern, 1963), solid-state NMR (Rimez *et al.*, 2008), chemiluminescence (Rychlý *et al.*, 2011) or pyrolysis gas chromatography (Beyler et Hirschler, 2001) have been used.

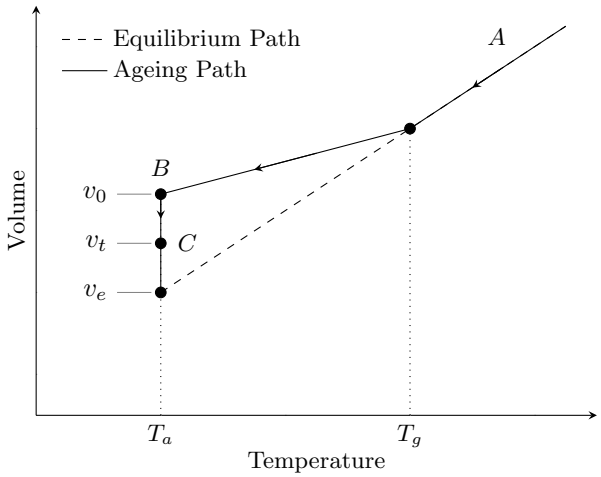

Figure 1.3: Illustration of physical ageing for a polymer quenched from a temperature above its glass transition temperature to a temperature T_a. Above T_g, the material is in thermodynamic equilibrium (A). When quenched, the volume decreases towards a volume v_0 (B) outside of equilibrium. Then, as the temperature is kept constant, molecular rearrangements can take place and the volume slowly decreases (C).

Polymers thermal degradation results in an evolution of the material weight over time (Coats et Redfern, 1963). Thermogravimetric analyses (TGA) are used to continuously measure the weight changes (losses or gains) of a sample as it is heated or cooled under a controlled atmosphere. By measuring the weight changes as a function of temperature, TGA evaluates the sample's decomposition state. It is then possible to develop models for assessing a material's thermal and oxidative stability, as well as for predicting its lifetime. Furthermore, TGA provides information on the degradation process such as the kinetics of the chemical reactions.

TGA results can be influenced by three parameters that must be taken into account when analyzing the data. The first factor is the heating rate. Increasing the heating rate leads to higher temperatures of initiation and termination of the degradation process (Coats et Redfern, 1963). The second factor is the sample itself. During decomposition, chemical reactions take place and produce or require heat, resulting in a nonlinear heating rate. Also, the diffusion of volatile products, if impaired, can lead to a lag between the specific time at which the decomposition products appear and the time at which the weight loss is measured. Finally, the temperatures at the surface and inside the sample are not identical. Therefore, to decrease the importance of those effects, it is necessary to study small samples maximizing the surface of contact with the atmosphere. The third factor is the atmosphere in which the TGA is conducted. The role of the atmosphere is to remove any volatile products from the sample's vicinity.. Two types of atmospheres can be used: inert or reactive. An inert atmosphere

(usually nitrogen, argon or helium (Gurman *et al.*, 1987)) is used to prevent interaction with the sample and secondary reactions with the volatile products. This allows for a better evaluation of the primary processes involved in the material's thermal decomposition. It should be noted that similar results can also be obtained by using a vacuum instead of an inert atmosphere. On the other hand, testing in a reactive atmosphere (usually air or oxygen) leads to important decomposition processes that are not observed in an inert atmosphere, such as oxidation or combustion (Gurman *et al.*, 1987), which result in an accelerated decomposition (Beyler et Hirschler, 2001).

One limitation of TGA is that it can only detect evolution in the material's molecular structure as long as it is accompanied by a weight change (Coats et Redfern, 1963). Furthermore, TGA only allows for a quantitative analysis of the decomposition process (Materazzi, 1997) and cannot describe the degradation mechanisms in terms of chemical reactions.

IR spectroscopy is based on the absorption of photons at specific frequencies in the infrared region (Klöpffer, 1984). Each chemical bound has its own vibration modes resulting from atom groups stretching and bending motions. Those vibration modes are excited by IR radiation at the same frequencies, resulting in a loss of some of the energy associated with those frequencies. It is therefore possible to determine the chemical composition of a sample by measuring the energy lost by the exciting light. The results of an IR spectroscopy analysis are generally represented with an absorbance graph. This graph indicates both the frequency and intensity of the light absorbed by the sample. The analysis of the absorbance graph consists of determining the frequencies of the IR spectra absorbed by the sample. Then, the components of the sample can be identified by using previous absorption results reported in the literature. It is important to note that IR spectroscopy can only determine the presence of groups in a molecule. It cannot evaluate the number of those groups, and thus cannot evaluate the full constitution of the polymer. However, when coupled to TGA, IR spectrometry can be used to analyze the composition of the volatile products created during the thermal decomposition process. This analysis is done continuously and therefore can be used to identify the chemical reactions responsible for the polymer's weight changes.

MS is a quantitative and qualitative analysis technique used to evaluate the elemental composition of a sample from its constituents atomic masses. It is based on the principles of electrodynamics for which two particles of identical mass-to-charge (m/Q) ratios follow the same path in a vacuum when submitted to the same electromagnetic field.

1.2.2 Chemical ageing modeling

Phenomenological approaches simulating the kinetics of degradation effects on properties like molecular weight, heat release, weight changes and others, can be used to model polymers

thermal degradation. These approaches assume an overall reaction type and fit a model to the kinetic data. These models have been widely used since they are easy to develop and are often sufficient to describe the kinetic degradation behavior. Various parameters identification strategies have been proposed for simple single-stage degradation mechanisms (Regnier et Guibe, 1997; Lyon, 1997; Meng *et al.*, 2007) as well as for more complex multi-stage degradation mechanisms (Budrugeac *et al.*, 2004; Li *et al.*, 2009). In their work, (Perejón *et al.*, 2011) proposed a decomposition procedure for separating the various processes in a multi-stage mechanism and identifying the model's parameters.

Lewis (Vyazovkin, 2000) introduced an adaptation of the law of mass action to the case of solid-state mechanics in which the chemical species concentrations are replaced by the degree of conversion, denoted by α. This degree of conversion can be seen as a measure of the degradation process evolution and is defined as:

$$\alpha(t,T) = \frac{m_0 - m(t,T)}{m_0 - m_f} \tag{1.1}$$

where m_0 is the sample's initial mass, m_f is its final weight and $m(t,T)$ is its mass at time t and temperature T.

The single-step reaction model assumes that the rate of conversion is a function of the temperature and the degree of conversion. Furthermore, it assumes that the degradation can be expressed as the product of two independent functions, one being dependent on temperature and the other being dependent on the degree of conversion (Šimon, 2004), leading to the following differential equation:

$$\frac{\mathrm{d}\alpha}{\mathrm{d}t}(\alpha,T) = k(T)\, f(\alpha) \tag{1.2}$$

where f is the kinetic function, representing the degradation mechanisms assumed for the chemical reaction. Typical degradation mechanisms and their associated kinetic functions can be found in various papers (Vyazovkin, 2000; Meng *et al.*, 2007; Li *et al.*, 2009; Vrandečić *et al.*, 2010; Sánchez-Jiménez *et al.*, 2010). k is the degradation rate constant that can be expressed with Arrhenius equation:

$$k(T) = A \exp\left(-\frac{E^{act}}{RT}\right) \tag{1.3}$$

where T is the absolute temperature, R is the gas constant, A is a pre-exponential factor and E^{act} is the activation energy.

One limitation of the single-step reaction model resides in the fact that the degradation mechanism is often too complicated to be reduced to a unique step (Šimon, 2004). It

is generally more accurately represented by a combination of competitive and consecutive phenomena. Each of those phenomena has different activation energies. Therefore, when using the single-step model, the activation energy evaluated from the experimental data is likely to be a combination of the activation energies of all the individual phenomena in the degradation mechanism, resulting in an apparent activation energy dependent on the degree of conversion (Vyazovkin, 2000). Assuming that the mechanism can be decomposed into a set of L independent processes, the conversion degree can then be written as the sum of the degrees of conversion of all independent processes (Perejón *et al.*, 2011):

$$\alpha\left(t\right) = \sum_{l=1}^{L} a_l \alpha_l\left(t\right) \tag{1.4}$$

where a_l represents the relative contribution of the process l to the overall degradation mechanism (and thus, $\sum_{l=1}^{L} a_l = 1$). If the kinetic triplets $\{E_l^{act}, A_l, f_l\}$ are associated to process l, then Equation (1.2) becomes:

$$\frac{\mathrm{d}\alpha}{\mathrm{d}t}\left(\alpha, T\right) = \sum_{l=1}^{L} a_n A_l \exp\left(-\frac{E_l^{act}}{RT}\right) f_l\left(\alpha_l\right) \tag{1.5}$$

The main challenge lies in the determination of the kinetic triplets $\{E_l^{act}, A_l, f_l\}$.

1.3 Viscoelasticity of polymers

1.3.1 General concepts

A material is said to have a viscoelastic behavior when it combines elastic and viscous characteristics. Elastic, because when submitted to a load, the material exhibits an instantaneous response, and viscous because the material's response depends on the loading rate. Viscoelasticity can manifest itself under two dual phenomena, namely, creep-recovery and stress-relaxation.

Creep is the tendency of a material to continue to deform through time when submitted to a constant stress. In creep-recovery tests (Figure 1.4a), the material is submitted to a constant stress σ_0 for a time t_1. The material exhibits an instantaneous response and then continues to deform with time while the stress is maintained. When the stress is removed, the elastic deformation is recovered instantaneously before the material slowly returns to its original state.

Stress-relaxation, on the other hand, is the tendency of the stress to slowly decrease in a material submitted to a constant strain. This behavior is illustrated in Figure 1.4b where the material is submitted to a constant strain ε_0. After a first instantaneous response, the

stress in the material slowly decreases with time towards a stabilized value.

Those two viscoelastic behaviors can be represented either by the creep compliance $\mathbf{S}$, in the case of creep-recovery, or by the relaxation modulus $\mathbf{C}$, in the case of stress-relaxation. Under the assumptions of linear viscoelasticity (see Section 1.3.3), strains or stresses a a given time can be obtained from:

$$\boldsymbol{\varepsilon}(t) = \int_0^t \mathbf{S}(t-\tau) : \frac{\mathrm{d}\boldsymbol{\sigma}(\tau)}{\mathrm{d}\tau}\mathrm{d}\tau \tag{1.6a}$$

$$\boldsymbol{\sigma}(t) = \int_0^t \mathbf{C}(t-\tau) : \frac{\mathrm{d}\boldsymbol{\varepsilon}(\tau)}{\mathrm{d}\tau}\mathrm{d}\tau \tag{1.6b}$$

Equation (1.6a) is called an hereditary stress-based integral since it links the instantaneous strain state to the whole stress history. Similarly, Equation (1.6b) is called an hereditary strain-based integral. Relationships taking into account ageing, temperature and stress level dependencies lead to similar relationships and are presented in the following sections.

1.3.2 Development of viscoelastic constitutive theories

The development of a constitutive theory able to describe polymers viscoelastic behavior for any kind of loading and temperature histories is a very difficult task. Difficult since polymers exhibit a wide range of mechanical behavior under various experimental conditions (Lustig *et al.*, 1996). As temperature increases, a polymer goes from exhibiting an elastic behavior at temperatures well below its T_g, to a nonlinearly viscoelastic behavior coupled with physical ageing induced by complex volume and enthalpy relaxation phenomena in the T_g region, and even non-Newtonian flow behavior or rubber elasticity above T_g.

A number of aspects need to be taken into account when developing a constitutive theory, namely

1. Its capacity to fit experimental data.
2. The fact that it relies on physically motivated arguments.
3. Its capacity to meet the principles of thermodynamics for all kinds of loading history.

Non-equilibrium thermodynamics has been widely used in the past 50 years to developed constitutive theories describing the complex behavior of polymers in their glassy state (Biot, 1954; Schapery, 1964; Cunat, 2001; Caruthers *et al.*, 2004; Drozdov, 2000). However, non-equilibrium thermodynamics still lacks an unified theory. Two main approaches have been considered in the mechanical communities, namely Rational Thermodynamics (Coleman, 1964; Lustig *et al.*, 1996; Caruthers *et al.*, 2004) and the Thermodynamic of Irreversible Processes (Biot, 1954; Schapery, 1964). Both approaches deals with the non-equilibrium

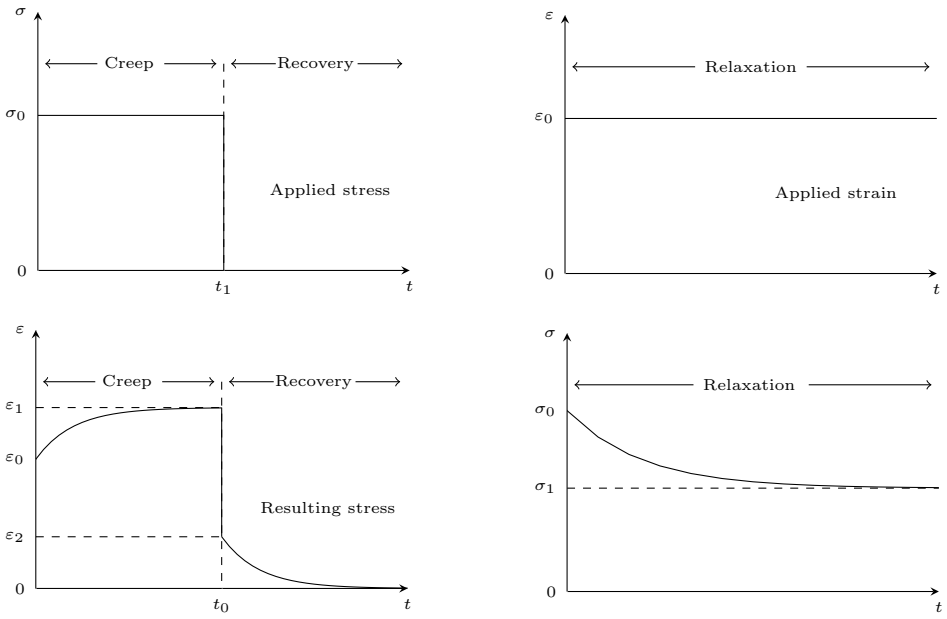

(a) Creep-recovery test (b) Stress-relaxation test

Figure 1.4: Viscoelastic behavior of a material submitted to a creep-recovery test (a) and a relaxation test (b). The polymer exhibits an instantaneous elastic response followed by a delayed viscous response.

thermodynamics state of the material by considering that, at the local scale, the material remains in equilibrium, thus allowing for the classical irreversible thermodynamic relationships to be used.

Combining the principles of continuum mechanics and thermodynamics leads to the well known Clausius-Duhem inequality:

$$\boldsymbol{\sigma} : \frac{\mathrm{d}\boldsymbol{\varepsilon}}{\mathrm{d}t} - \left(\frac{\mathrm{d}\Psi}{\mathrm{d}t} + \rho\eta \frac{\mathrm{d}T}{\mathrm{d}t} \right) - \frac{\boldsymbol{q} \cdot \boldsymbol{\nabla T}}{T} \geq 0 \tag{1.7}$$

where Ψ is Helmholtz's free energy, ρ is the mass density, η is the entropy density and $\boldsymbol{q}$ is the heat flux. The Clausius-Duhem inequality (1.7) is the basis on which most viscoelastic constitutive theories were developed (Biot, 1954; Schapery, 1964; Cunat, 2001; Caruthers *et al.*, 2004; Drozdov, 2000) and differences between Rational Thermodynamics and Thermodynamics of Irreversible Processes arise in the way this inequality is dealt with.

In Rational Thermodynamics, the time-dependent thermodynamic quantities can be derived from the time-dependent free energy Ψ (Caruthers *et al.*, 2004). By assuming that the stress tensor $\boldsymbol{\sigma}$ depends on the strain tensor $\boldsymbol{\varepsilon}$, the temperature T and the temperature

gradient ∇T, the time derivative of the free energy Ψ is given by:

$$\frac{\mathrm{d}\Psi}{\mathrm{d}t} = \frac{\partial \Psi}{\partial \boldsymbol{\varepsilon}} : \frac{\mathrm{d}\boldsymbol{\varepsilon}}{\mathrm{d}t} + \frac{\partial \Psi}{\partial T}\frac{\mathrm{d}T}{\mathrm{d}t} + \frac{\partial \Psi}{\partial \boldsymbol{\nabla T}} \cdot \frac{\mathrm{d}\boldsymbol{\nabla T}}{\mathrm{d}t} \tag{1.8}$$

Combining Equations (1.8) and (1.7) leads to:

$$-\left[\frac{\partial \Psi}{\partial \boldsymbol{\varepsilon}} - \boldsymbol{\sigma}\right] : \frac{\mathrm{d}\boldsymbol{\varepsilon}}{\mathrm{d}t} - \left[\frac{\partial \Psi}{\partial T} + \rho\eta\right]\frac{\mathrm{d}T}{\mathrm{d}t} - \frac{\partial \Psi}{\partial \boldsymbol{\nabla T}} \cdot \frac{\mathrm{d}\boldsymbol{\nabla T}}{\mathrm{d}t} - \frac{\boldsymbol{q} \cdot \nabla T}{T} \geq 0 \tag{1.9}$$

Equation (1.9) must remain true for every loading and temperature histories, meaning that the relationships

$$\frac{\partial \Psi}{\partial \boldsymbol{\varepsilon}} = \boldsymbol{\sigma} \tag{1.10a}$$

$$\frac{\partial \Psi}{\partial T} = -\rho\eta \tag{1.10b}$$

$$\frac{\partial \Psi}{\partial \boldsymbol{\nabla T}} = 0 \tag{1.10c}$$

must always be satisfied ($-\frac{\boldsymbol{q}\cdot\boldsymbol{\nabla T}}{T} \geq 0$ following Fourier's law).

The principle of material memory (Coleman, 1964) leads to a free energy defined as a functional of the strain (stress), temperature, etc... (Schapery, 2000). Therefore, Ψ can be defined as:

$$\Psi(t) = \overset{\infty}{\underset{\tau=0}{\Psi}} \left(\boldsymbol{\varepsilon}\left(t-\tau\right), T\left(t-\tau\right)\right) \tag{1.11}$$

The stress/strain relationship is ultimately established using the principles of functional differentiation and Equations (1.10) (Lustig *et al.*, 1996; Caruthers *et al.*, 2004).

In the Thermodynamics of Irreversible Processes, the free energy Ψ is assumed to be fully defined by the current values of strains and temperature as well as of so-called internal variables representing the material's current state. Those internal variables are associated with immeasurable phenomena (atomic structure, cracks,...) and are noted by $\boldsymbol{\chi}$, leading to the apparition of a new term in Equation (1.8):

$$\frac{\mathrm{d}\Psi}{\mathrm{d}t} = \frac{\partial \Psi}{\partial \boldsymbol{\varepsilon}} : \frac{\mathrm{d}\boldsymbol{\varepsilon}}{\mathrm{d}t} + \frac{\partial \Psi}{\partial T}\frac{\mathrm{d}T}{\mathrm{d}t} + \frac{\partial \Psi}{\partial \boldsymbol{\nabla T}} \cdot \frac{\mathrm{d}\boldsymbol{\nabla T}}{\mathrm{d}t} + \frac{\partial \Psi}{\partial \boldsymbol{\chi}} : \frac{\mathrm{d}\boldsymbol{\chi}}{\mathrm{d}t} \tag{1.12}$$

leading to an additional relationship, when compared compared to Equation (1.10), namely:

$$\frac{\partial \Psi}{\partial \boldsymbol{\chi}} = -\mathbf{B}^{(\chi)} : \frac{\mathrm{d}\boldsymbol{\chi}}{\mathrm{d}t} \tag{1.13}$$

where $\mathbf{B}^{(\chi)}$ is a semi-positive definite tensor. Equation (1.13) is called an evolution equation (Schapery, 2000) and is expressing the internal variables rate of change. Finally, the

stress/strain relationship is established by assuming that the free energy Ψ can be expanded using a modified second order Taylor expansion around a reference state (Lévesque *et al.*, 2008).

The main difference between Rational Thermodynamics and the Thermodynamics of Irreversible Processes lies in the way the time-dependence is introduced in the free energy function. In Rational Thermodynamics, the free energy is considered as a functional of the parameters history. In the Thermodynamics of Irreversible Processes, the time dependence of the free energy is a consequence of the evolution Equation (1.13). However, despite that difference, the two approaches lead to very similar hereditary integrals.

1.3.3 Linear viscoelasticity at constant temperature

In the case of an isothermal and adiabatic loading history, i.e. $\frac{\mathrm{d}T}{\mathrm{d}t} = 0$ and $\boldsymbol{q} = 0$, the free energy can be considered to be only dependent on the strain and internal variables tensors, i.e. $\Psi\left(\boldsymbol{\varepsilon}, \boldsymbol{\chi}\right)$. Then, the free energy can be expanded around its equilibrium state, leading to:

$$\begin{aligned}\Psi\left(\boldsymbol{\varepsilon}, \boldsymbol{\chi}\right) &= \Psi_0 + \frac{\partial \Psi}{\partial \boldsymbol{\varepsilon}} : \boldsymbol{\varepsilon} + \frac{\partial \Psi}{\partial \boldsymbol{\chi}} : \boldsymbol{\chi} + \frac{1}{2}\boldsymbol{\varepsilon} : \frac{\partial^2 \Psi}{\partial \boldsymbol{\varepsilon} \partial \boldsymbol{\varepsilon}} : \boldsymbol{\varepsilon} + \boldsymbol{\varepsilon} : \frac{\partial^2 \Psi}{\partial \boldsymbol{\varepsilon} \partial \boldsymbol{\chi}} : \boldsymbol{\chi} + \frac{1}{2}\boldsymbol{\chi} : \frac{\partial^2 \Psi}{\partial \boldsymbol{\chi} \partial \boldsymbol{\chi}} : \boldsymbol{\chi} \\ &= \Psi_0 + \frac{\partial \Psi}{\partial \boldsymbol{\varepsilon}} : \boldsymbol{\varepsilon} + \frac{\partial \Psi}{\partial \boldsymbol{\chi}} : \boldsymbol{\chi} + \frac{1}{2}\boldsymbol{\varepsilon} : \mathbf{L}^{(1)} : \boldsymbol{\varepsilon} + \boldsymbol{\varepsilon} : \mathbf{L}^{(2)} : \boldsymbol{\chi} + \frac{1}{2}\boldsymbol{\chi} : \mathbf{L}^{(3)} : \boldsymbol{\chi}\end{aligned} \tag{1.14}$$

where Ψ_0 is the free energy in the equilibrium state. In the equilibrium state, the free energy is at a local minimum, therefore the first order derivatives $\frac{\partial \Psi}{\partial \boldsymbol{\varepsilon}} = \frac{\partial \Psi}{\partial \boldsymbol{\chi}} = 0$. Furthermore, $\mathbf{L}^{(1)}$ and $\mathbf{L}^{(3)}$ must be positive definite tensors. Combining Equation (1.14) with Equations (1.10a) and (1.13) leads to:

$$\mathbf{B}^{(\chi)} : \frac{\mathrm{d}\boldsymbol{\chi}}{\mathrm{d}t} + \mathbf{L}^{(3)} : \boldsymbol{\chi} + \mathbf{L}^{(2)^{\mathrm{T}}} : \boldsymbol{\varepsilon} = 0 \tag{1.15}$$

and to the constitutive equation:

$$\boldsymbol{\sigma} = \mathbf{L}^{(1)} : \boldsymbol{\varepsilon} + \mathbf{L}^{(2)} : \boldsymbol{\chi} \tag{1.16}$$

Using the fact that $\mathbf{B}^{(\chi)}$ and $\mathbf{L}^{(3)}$ are semi-positive and positive definite tensors, respectively, it can be shown that Equations (1.15) and (1.16) leads to the constitutive equation in integral form (Lévesque *et al.*, 2008):

$$\boldsymbol{\sigma}\left(t\right) = \mathbf{C}^{(\infty)} : \boldsymbol{\varepsilon}\left(t\right) + \int_0^t \sum_{m=1}^{M} \mathbf{C}^{(m)} \mathrm{e}^{-\omega_m (t-\tau)} : \frac{\mathrm{d}\boldsymbol{\varepsilon}\left(\tau\right)}{\mathrm{d}\tau} \mathrm{d}\tau \tag{1.17}$$

where $\mathbf{C}^{(\infty)}$ is the equilibrium relaxation tensor and $\mathbf{C}^{(m)}$ are the M transient relaxation moduli associated to the M inverted relaxation times ω_m.

While Equation (1.17) is a strain-based equation, i.e. it computes stresses as a function of strains, a stress-based equation can be obtained using a very similar approach (Schapery, 1968). Instead of using the Helmholtz's free energy, the Gibbs' free energy, $G = \Psi - \boldsymbol{\sigma} : \boldsymbol{\varepsilon}$, can be considered and, after calculations, leads to:

$$\boldsymbol{\varepsilon}(t) = \mathbf{S}^{(0)} : \boldsymbol{\sigma}(t) + \int_0^t \sum_{p=1}^{P} \mathbf{S}^{(p)} \left[1 - \mathrm{e}^{-\lambda_p (t-\tau)}\right] : \frac{\mathrm{d}\boldsymbol{\sigma}(\tau)}{\mathrm{d}\tau} \mathrm{d}\tau \tag{1.18}$$

where $\mathbf{S}^{(0)}$ is the instantaneous compliance tensor and $\mathbf{S}^{(p)}$ are the P transient compliances associated to the P inverted retardation times λ_p.

For practical reasons, tridimensional viscoelastic properties are usually obtained from creep-recovery tests (Lévesque *et al.*, 2008). However, finite element packages usually require knowing $\mathbf{C}(t)$ for numerical implementation (Crochon *et al.*, 2010). Interconversion going from $\mathbf{S}(t)$ to $\mathbf{C}(t)$ can be done using interconversion algorithms such as those proposed by Luk-Cyr *et al.* (2013).

Notes

Analogue models consisting of springs and dashpots were developed for representing viscoelasticity. While those models were developed irrespectively of any thermodynamics frameworks, it should be noted that Equation (1.17) can be represented by a mechanical analogue consisting of one spring connected in parallel with M Maxwell solids (one spring and one dashpot connected in series). Similarly, the mechanical analogue of Equation (1.18) consists of one spring connected in series with P Voigt solids (one spring and one dashpot connected in parallel).

The springs and dashpots models, as well as the Thermodynamics of Irreversible Processes approaches both lead to creep compliances and relaxation moduli expressed as Prony series:

$$\mathbf{C}(t) = \mathbf{C}^{(\infty)} + \sum_{m=1}^{M} \mathbf{C}^{(m)} \mathrm{e}^{-\omega_m (t)} \tag{1.19a}$$

$$\mathbf{S}(t) = \mathbf{S}^{(0)} + \sum_{p=1}^{P} \mathbf{S}^{(p)} \left[1 - \mathrm{e}^{-\lambda_p (t)}\right] \tag{1.19b}$$

However, other functions have seldom been chosen to represent those tensors. For example, if the internal variables are considered as a continuum set (i.e. there is an infinite number of internal variables) and $\mathbf{L}^{(3)}$ is allowed to be positive semi-definite, other expressions

for constitutive theories can be obtained (Lévesque *et al.*, 2008). A very popular approach consists in using a Kohlrausch's stretched exponential function in which the spectrum of inverted relaxation and retardation times are represented by characteristic inverted relaxation and retardation times ω and λ and a stretching parameter β, leading to:

$$\mathbf{C} = \mathbf{C}^{(\infty)} + \left(\mathbf{C}^{(0)} - \mathbf{C}^{(\infty)}\right) \mathrm{e}^{-(\omega t)^{\beta}} \tag{1.20a}$$

$$\mathbf{S} = \mathbf{S}^{(0)} \mathrm{e}^{(\lambda t)^{\beta}} \tag{1.20b}$$

1.3.4 Extension to nonlinear viscoelasticity

Extension to nonlinear viscoelasticity can be obtained by modifying Equation (1.13) according to (Schapery, 1997):

$$\frac{\partial \Psi}{\partial \boldsymbol{\chi}} = -p_1 \mathbf{B}^{(\chi)} : \frac{\mathrm{d}\boldsymbol{\chi}}{\mathrm{d}t} \tag{1.21}$$

where p_1 is a positive function depending material's state. Similarly, the free energy's Taylor expansion around its equilibrium state can be modified as:

$$\Psi\left(\boldsymbol{\varepsilon}, \boldsymbol{\chi}\right) = \Psi_0 + \frac{1}{2} p_4 \boldsymbol{\varepsilon} : \mathbf{L}^{(1)} : \boldsymbol{\varepsilon} + p_3 \boldsymbol{\varepsilon} : \mathbf{L}^{(2)} : \boldsymbol{\chi} + \frac{1}{2} p_2 \boldsymbol{\chi} : \mathbf{L}^{(3)} : \boldsymbol{\chi} \tag{1.22}$$

where p_2, p_3 and p_4 are also positive functions depending on the material's state. Note that setting $p_1 = p_2 = p_3 = p_4$ leads to linear viscoelasticity. Equations (1.21) and (1.22) can be solved by introducing the notion of reduced time (Schapery, 1964):

$$\Phi(t) = \int_0^t \frac{p_2(\tau)}{p_1(\tau)} \mathrm{d}\tau \tag{1.23}$$

leading to:

$$\boldsymbol{\sigma}\left(t\right) = \frac{\partial \phi}{\partial \boldsymbol{\varepsilon}} + \left[p_3 \mathbf{I} + \frac{\partial p_3}{\partial \boldsymbol{\varepsilon}} \otimes \boldsymbol{\varepsilon}\right] : \int_0^t \sum_{m=1}^{M} \mathbf{C}^{(m)} \mathrm{e}^{-\omega_m (\Phi(t) - \Phi(\tau))} : \frac{\mathrm{d}}{\mathrm{d}\tau} \left[\frac{p_3}{p_2} \boldsymbol{\varepsilon}\left(\tau\right)\right] \mathrm{d}\tau \tag{1.24}$$

where ϕ is the strain energy function associated to nonlinearly elastic materials. If this energy is defined as $\phi = \int_0^{\boldsymbol{\varepsilon}} p_4 \boldsymbol{\varepsilon}\left(t\right) : \mathbf{C}^{(\infty)} : \mathrm{d}\boldsymbol{\varepsilon}$, then Equation (1.24) becomes:

$$\boldsymbol{\sigma}\left(t\right) = p_4 \mathbf{C}^{(\infty)} : \boldsymbol{\varepsilon}\left(t\right) + \left[p_3 \mathbf{I} + \frac{\partial p_3}{\partial \boldsymbol{\varepsilon}} \otimes \boldsymbol{\varepsilon}\right] : \int_0^t \sum_{m=1}^{M} \mathbf{C}^{(m)} \mathrm{e}^{-\omega_m (\Phi(t) - \Phi(\tau))} : \frac{\mathrm{d}}{\mathrm{d}\tau} \left[\frac{p_3}{p_2} \boldsymbol{\varepsilon}\left(\tau\right)\right] \mathrm{d}\tau \tag{1.25}$$

As for the linear case, a similar approach can be considered to obtain the stress-based

nonlinear hereditary integral:

$$\boldsymbol{\varepsilon}\left(t\right)=a_4\mathbf{S}^{(0)}:\boldsymbol{\sigma}\left(t\right)+\left[a_3\mathbf{I}+\frac{\partial a_3}{\partial\boldsymbol{\sigma}}\otimes\boldsymbol{\sigma}\right]:\int_0^t\sum_{p=1}^{P}\mathbf{S}^{(p)}\mathrm{e}^{-\lambda_p(\Omega(t)-\Omega(\tau))}:\frac{\mathrm{d}}{\mathrm{d}\tau}\left[\frac{a_3}{a_2}\boldsymbol{\sigma}\left(\tau\right)\right]\mathrm{d}\tau \quad (1.26)$$

where a_1, a_2, a_3 and a_4 are positive functions depending on the material's state and

$$\Omega(t)=\int_0^t\frac{a_2(\tau)}{a_1(\tau)}\mathrm{d}\tau \quad (1.27)$$

is the reduced time. Introducing the nonlinearizing functions g_0, $\mathbf{G}_1$, g_2 and a such as $g_0=a_4$, $\mathbf{G}_1=a_3\mathbf{I}+\frac{\partial a_3}{\partial\boldsymbol{\sigma}}\otimes\boldsymbol{\sigma}$, $g_2=\frac{a_3}{a_2}$ and $a=\frac{a_1}{a_2}$, leads to the well-known Schapery's constitutive theory:

$$\boldsymbol{\varepsilon}\left(t\right)=g_0\mathbf{S}^{(0)}:\boldsymbol{\sigma}(t)+\mathbf{G}_1:\int_0^t\sum_{p=1}^{P}\mathbf{S}^{(p)}\mathrm{e}^{-\lambda_p(\Omega(t)-\Omega(\tau))}:\frac{\mathrm{d}}{\mathrm{d}\tau}\left[g_2\boldsymbol{\sigma}(\tau)\right]\mathrm{d}\tau \quad (1.28)$$

It is important to note that the equations introduced above are not restricted to any material symmetry or nonlinearizing functions shapes. Moreover, they have been developed for 1D, 2D as well as for 3D representations. In the literature, however, some 3D equations were directly derived from the well-known stress-based 1D Schapery's constitutive theory (Schapery, 1969b)

$$\varepsilon(t)=g_0S^{(0)}\sigma(t)+g_1\int_0^t\sum_{p=1}^{P}S^{(p)}\mathrm{e}^{-\lambda_p(\Omega(t)-\Omega(\tau))}\frac{\mathrm{d}}{\mathrm{d}\tau}\left[g_2\sigma(\tau)\right]\mathrm{d}\tau \quad (1.29)$$

by introducing tensors instead of scalars for the elastic and linearly viscoelastic properties

$$\boldsymbol{\varepsilon}\left(t\right)=g_0\mathbf{S}^{(0)}:\boldsymbol{\sigma}(t)+g_1\int_0^t\sum_{p=1}^{P}\mathbf{S}^{(p)}\mathrm{e}^{-\lambda_p(\Omega(t)-\Omega(\tau))}:\frac{\mathrm{d}}{\mathrm{d}\tau}\left[g_2\boldsymbol{\sigma}(\tau)\right]\mathrm{d}\tau \quad (1.30)$$

The difference between the 3D theories (1.28) and the constitutive theory (1.30) is that the nonlinearizing function in front of the integral is a tensor in (1.28) and a scalar in (1.30) respectively. This generalization is done without any thermodynamics backing and does not guarantee that the thermodynamics principles are met for all loading histories.

It should be noted that in the nonlinear framework proposed by Schapery (1964), the reduced times are the same for all inverted relaxation times and retardation times. This assumption, called thermorheological simplicity is one of the most important in the development of such models. It assumes that the shapes of the relaxation and retardation spectra are independent of the current state of the material.

Schapery's constitutive theories introduced the nonlinearizing effects with explicit nonlinearizing functions in Equation (1.22). Those functions are purely defined by the user. Caruthers *et al.* (2004), on the other hand, introduced the nonlinear behavior by using a higher order functional expansion of the free energy around its reference state. However, it should be noted that Schapery's nonlinearizing functions could easily be chosen to be the same as those obtained by Caruthers *et al.* (2004). The two frameworks, even if they stem from different principles, lead to equivalent constitutive relationships.

1.4 The time-superposition principles

The time-superposition principle is a concept in which it is assumed that a material's properties under any service conditions, i.e. $\mathbf{C}$ or $\mathbf{S}$, can be related to its properties in a reference state, i.e. $\bar{\mathbf{C}}$ or $\bar{\mathbf{S}}$, by a so-called shift factor. One such superposition principle was first developed for describing the influence of temperature (Andrews et Tobolsky, 1951; Williams *et al.*, 1955) before being extended to other parameters such as physical ageing (Struik, 1978).

1.4.1 Time-temperature superposition principle

The time-temperature superposition principle implies that the viscoelastic functions at different temperatures can be merged into a master curve at a reference temperature $\bar{T}$ using a shift factor a_T (Andrews et Tobolsky, 1951).

Figure 1.5 illustrates the time-temperature superposition principle for the creep compliance $\mathbf{S}$. The creep compliance $\mathbf{S}$ at temperature T is obtained by shifting the creep compliance $\bar{\mathbf{S}}$ at reference temperature $\bar{T}$ along the log time axis by a shift factor a_T. Mathematically, this leads to:

$$\mathbf{S}(t) = \bar{\mathbf{S}}\left(\frac{t}{a_T}\right) \tag{1.31}$$

A few models have been proposed for determining the shift factor. Usually, when considering a material above its T_g, the shift factor is expressed using the well-known Williams-Landel-Ferry equation (Williams *et al.*, 1955):

$$\ln a_T = -\frac{C_1\left(T-\bar{T}\right)}{C_2+T-\bar{T}} \tag{1.32}$$

where C_1 and C_2 are material's parameters depending on the material and the reference temperature. Shift factors for the case where the material is below its T_g are typically

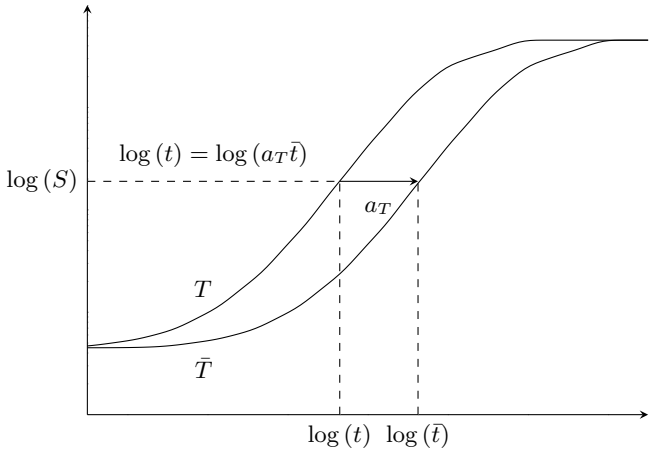

Figure 1.5: Illustration of time-temperature superposition principle for the creep compliance S.

modeled through an Arrhenius law as

$$\ln a_T = -A_T \left(\frac{1}{\bar{T}} - \frac{1}{T} \right) \tag{1.33}$$

where A_T is material's parameter.

The time-temperature superposition principle is useful for evaluating the linearly viscoelastic properties of a material in reference conditions over a wide range of decades with limited experimental data. As a matter of fact, full characterization of a material's creep compliance or relaxation modulus functions are not easily achieved for very short times, i.e. $t \leq 10^{-1}$s, or very long times, $t \geq 10^{6}$s, using typical creep or relaxation tests. However, this difficulty can be easily eluded by performing short mechanical tests at various temperatures and then shifting the results to the reference temperature (see Figure 1.6)

1.4.2 Time-ageing superposition principle

The time-ageing superposition principle is an extension of the time-temperature superposition principle to the case of physical ageing. Assuming that creep times were small enough for physical ageing to remain constant during the creep tests, Struik (1978) showed that the creep compliance function of a polymer aged for a certain amount of time t_e could be related to the reference creep compliance function for a reference time $\bar{t}_e$ with a simple shift factor a_{t_e}, leading to:

$$\mathbf{S}(t) = \bar{\mathbf{S}} \left(\frac{t}{a_{t_e}} \right) \tag{1.34}$$

Equation (1.34) can then be extended to longer tests in which physical ageing cannot be

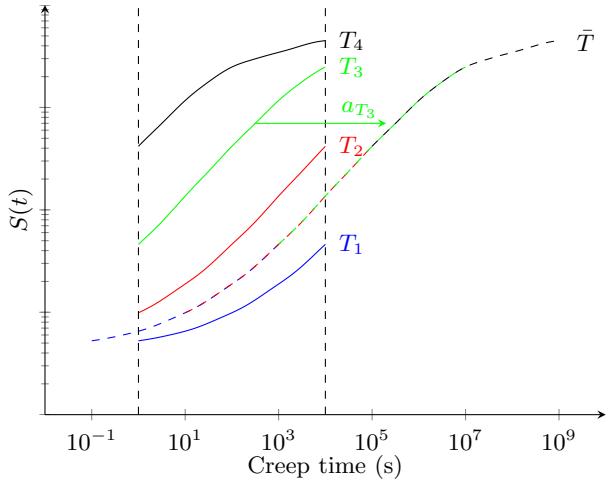

Figure 1.6: Characterization of a full creep compliance function $S(t)$ in a reference temperature $\bar{T}$ using short creep tests at various temperatures T_1, T_2, T_3 and T_4.

considered to remain constant by the following relationship (Bradshaw et Brinson, 1997b):

$$\mathbf{S}(t) = \bar{\mathbf{S}}\left(\int_0^t \frac{\mathrm{d}\tau}{a_{t_e}(\tau)}\right) \tag{1.35}$$

In the simple case where a material was quenched from a temperature above its T_g to a temperature below its T_g, and defining the ageing time t_e as the time since the ageing temperature T has been achieved, Struik (1978) proposed that the shift factor a_{t_e} be approximated by:

$$a_{t_e}\left(t_e, T\right) = \left(\frac{t_e}{\bar{t}_e}\right)^{\mu(T)} \tag{1.36}$$

where $\mu\left(T\right)$ is called the shift rate. This shift rate is dependent on the temperature at which the material was aged. In the case of isothermal ageing, it was found that $\mu\left(T\right)$ remained constant as long as the material continued to age.

In the case where more general non-isothermal ageing histories are considered, the simple relationship in Equation (1.36) is no longer valid for more general ageing histories due to memory effects (Bradshaw et Brinson, 1997b). Two approaches distinguish themselves to take into account this situation: *i*) The continuous shift factor (CSF) method proposed by Bradshaw et Brinson (1997b) based upon the notion of effective ageing time; *ii*) the KAHR-a_{t_e} method proposed by Guo *et al.* (2009) in which ageing time is defined using volume relaxation theories. Both theories lead to a more complex expression for the shift factor a_{t_e} than Equation (1.36).

1.4.3 Time-superposition principles and Schapery's nonlinear constitutive theories

It is interesting to note that the reduced time proposed by Schapery (1964) in Equation (1.27) can be assimilated to the time-superposition principles proposed above using the relationship:

$$\int_0^t \frac{a_2(\tau)}{a_1(\tau)}\mathrm{d}\tau = \int_0^t \frac{\mathrm{d}\tau}{a_T(\tau)a_{t_e}(\tau)a_1(\tau)\dots a_X(\tau)} \tag{1.37}$$

where $a_1(\tau)\dots a_X(\tau)$ stands for shift factors related to any other physical phenomenon. For example, a shift factor a_σ could be added for accounting stress induced nonlinearities.

Furthermore, it was found by some authors that vertical shift factors, b_T and b_{t_e}, are generally required when shifting experimental data for physical ageing or temperature effects (Sullivan *et al.*, 1993; Bradshaw et Brinson, 1997a). Those vertical shift factors could easily be assimilated to the others non-linearizing functions appearing in Schapery's theories. In fact, a series of correspondences between Schapery's theory recalled in Equation (1.26) and various testing conditions can be established and are presented in Table 1.2.

More generally, g_0, $\mathbf{G}_1$ and g_2 are nonlinearizing functions introduced to account for any nonlinearizing phenomena. In particular, numerous works focused on the development of stress-dependent nonlinearizing functions. For example, Schapery (1997) considered the nonlinearizing functions to be quadratic functions of stresses. Lai et Bakker (1996) proposed that function g_0 be dependent of the first stress invariant while $\mathbf{G}_1$ and g_2 would be dependent on the effective octahedral shear stress. Haj-Ali et Muliana (2004) proposed that all nonlinearizing functions be polynomial functions of the effective octahedral shear stress. Sawant et Muliana (2008) proposed temperature-dependent nonlinearizing functions by assuming that g_0 was a linear function, while $\mathbf{G}_1$ and g_2 were exponential functions of the temperature, while Muliana et Sawant (2009), in other works, assumed that all three functions were polynomial functions of temperature.

1.5 Numerical implementation of nonlinearly viscoelastic constitutive theories

Phenomenological constitutive theories, such as Schapery's, while generally developed as sets of differential equations, have mainly been used under their hereditary integral shape. Generally speaking, using an integral-type viscoelastic constitutive theory into a finite element package requires storing the loading history for all time-steps, which can be prohibitive. A number of finite element implementation strategies have been developed in order to bypass this difficulty. Introducing a recursive expression to numerically solve the integral, i.e. recursive approach (Henriksen, 1984; Beijer et Spoormaker, 2002; Haj-Ali et Muliana, 2004),

Table 1.2: Schapery's theories adapted to various experimental conditions ($g_0 = a_4$, $\mathbf{G}_1 = a_3\mathbf{I} + \frac{\partial a_3}{\partial \boldsymbol{\sigma}} \otimes \boldsymbol{\sigma}$, $g_2 = \frac{a_3}{a_2}$ and $a = \frac{a_1}{a_2}$)

	g_0	$\mathbf{G}_1$	g_2	a
Linear viscoelasticity	1	1	1	1
Ageing and temperature (no vertical shifting)	1	1	1	$a_T a_{t_e}$
Ageing and temperature (with vertical shifting)	$b_T b_{t_e}$	$b_T b_{t_e}$	1	$a_T a_{t_e}$
Schapery's nonlinear theory	$g_0(\sigma)$	$\mathbf{G}_1(\sigma)$	$g_2(\sigma)$	a_σ
Generalized Schapery's theory	$g_0(\sigma, T, t_e)$	$\mathbf{G}_1(\sigma, T, t_e)$	$g_2(\sigma, T, t_e)$	$a_T a_{t_e} a_\sigma$

or going back to a set of differential equations (Touati et Cederbaum, 1998; Poon et Ahmad, 1998, 1999) and developing a Finite-Difference (FD) model, i.e. differential approach, are all different approaches that have been studied for linearly and nonlinearly viscoelastic materials. These approaches result in the development of incremental models in which a relationship is defined between the solutions of the models at successive time-steps. Therefore, solving the hereditary integral only requires to store some quantities computed at the previous time-step instead of the whole load history, which is a major improvement.

Using an incremental model requires the time-interval $[0, t]$, in which the material behavior is studied, to be discretized into a finite number N of time-steps named t^n (which leads to $t^0 = 0$ and $t^N = t$). A time-increment $\Delta t^n = t^{n+1} - t^n$ can then be defined between two consecutive time-steps.

1.5.1 Recursive strategies

The first recursive strategy was proposed by Taylor *et al.* (1970). Their strategy was developed to compute the solution of general linearly viscoelastic constitutive theories expressed as hereditary integrals. To achieve that, Taylor *et al.* (1970) assumed that the load history varied linearly over the time-interval Δt^n and then divided the hereditary integral into recursive parts, thus establishing a recursive relationship between successive time-steps. Henriksen (1984) used a similar method for Schapery's nonlinear constitutive theories. In the case of the stress-based hereditary integral, his method leads to:

$$\boldsymbol{\varepsilon}^n = g_0^{n+1}\mathbf{S}^{(0)} : \boldsymbol{\sigma}^{n+1} + \mathbf{G}_1^{n+1} : \sum_{p=1}^{P} \mathbf{S}^{(p)} : \left(g_2^{n+1}\boldsymbol{\sigma}^{n+1} - g_2^0\boldsymbol{\sigma}^0 - \boldsymbol{q}_p^{n+1}\right) \tag{1.38}$$

where

$$\boldsymbol{q}_p^{n+1} = \int_0^{t^{n+1}} \mathrm{e}^{-\lambda_p\left(\Omega^{n+1} - \Omega\right)} \frac{\mathrm{d}}{\mathrm{d}\tau}\left[g_2\boldsymbol{\sigma}\right] \mathrm{d}\tau. \tag{1.39}$$

The hereditary integral in Equation (1.39) can be decomposed into two parts as:

$$\boldsymbol{q}_p^{n+1} = \int_0^{t^{(n)}} \mathrm{e}^{-\lambda_p\left(\Omega^{n+1}-\Omega\right)} \frac{\mathrm{d}}{\mathrm{d}\tau}\left[g_2\boldsymbol{\sigma}\right]\mathrm{d}\tau + \int_{t^n}^{t^{n+1}} \mathrm{e}^{-\lambda_p\left(\Omega^{n+1}-\Omega\right)} \frac{\mathrm{d}}{\mathrm{d}\tau}\left[g_2\boldsymbol{\sigma}\right]\mathrm{d}\tau. \tag{1.40}$$

Two simplifying hypotheses are necessary to develop a recursive relationship from Equation (1.40). The quantity $g_2\boldsymbol{\sigma}$ and the reduced-time Ω can be assumed to vary linearly with respect to τ over the time-interval Δt^n (Henriksen, 1984; Haj-Ali et Muliana, 2004):

$$\boldsymbol{q}_p^{n+1} = \boldsymbol{q}_p^n \mathrm{e}^{-\lambda_p \Delta\Omega^{n+1}} + \left(g_2^{n+1}\boldsymbol{\sigma}^{n+1} - g_2^n\boldsymbol{\sigma}^n\right) \frac{1-\exp\left[-\lambda_p\Delta\Omega^{n+1}\right]}{\lambda_p\Delta\Omega^{n+1}} \tag{1.41}$$

where

$$\Delta\Omega^{n+1} = \Omega^{n+1} - \Omega^n \tag{1.42}$$

is the reduced-time increment.

A major advantage of recursive strategies over differential strategies is that as long as their various hypotheses are respected, they compute the exact solution. Therefore, recursive strategies are often preferred over differential strategies.

1.5.2 Differential strategies

The second main strategy to the problem of Schapery-type constitutive theories implementation consists in transforming the hereditary integrals into in sets of first order differential equations before solving them with a FD scheme. The FD scheme used can range from a simple Euler Method (Zienkiewicz *et al.*, 1968; Greenbaum et Rubinstein, 1968; Poon et Ahmad, 1998, 1999) to a higher-order FD scheme such as Runge-Kutta's methods (Carpenter, 1972; Bažant, 1972).

To determine their set of differential equations, Poon et Ahmad (1998, 1999) differentiated the hereditary integral

$$\boldsymbol{y}(t) = \int_0^t \boldsymbol{f}(t,\tau)d\tau \tag{1.43}$$

Then, using δt to note an infinitesimal variation in time, Poon et Ahmad (1999) obtained the differentiation formula

$$\boldsymbol{y}(t+\delta t) - \boldsymbol{y}(t) \approx \boldsymbol{f}(t,t)\delta t + \frac{\partial}{\partial t}\boldsymbol{f}(t,t)\delta t^2 + \delta t \int_0^t \frac{\partial}{\partial t}\boldsymbol{f}(t,\tau)\mathrm{d}\tau \tag{1.44}$$

leading to

$$\begin{aligned}\frac{\mathrm{d}\boldsymbol{y}}{\mathrm{d}t} &= \lim_{\delta t\to 0}\frac{\boldsymbol{y}(t+\delta t)-\boldsymbol{y}(t)}{\delta t}\\ &= \boldsymbol{f}(t,t)+\int_0^t \frac{\partial}{\partial t}\boldsymbol{f}(t,\tau)\mathrm{d}\tau.\end{aligned} \tag{1.45}$$

Poon et Ahmad (1999) introduced the hidden state variables $\boldsymbol{y}_p$ and defined them as

$$\boldsymbol{y}_p(t) = \int_0^t \mathbf{S}^{(p)}\left[1-\mathrm{e}^{-\lambda_p\left(\Omega^{t+\Delta t}-\Omega^t\right]}\right) : \frac{\mathrm{d}}{\mathrm{d}\tau}\left[g_2\boldsymbol{\sigma}\right]\mathrm{d}\tau. \tag{1.46}$$

Therefore, Equation (1.46) leads to

$$\boldsymbol{f}(t,t) = 0 \tag{1.47a}$$

$$\frac{\partial}{\partial t}\boldsymbol{f}(t,\tau) = \frac{\lambda_p}{a}\mathbf{S}_p\mathrm{e}^{-\lambda\left(\Omega^{t+\Delta t}-\Omega^t\right)} : \frac{\mathrm{d}}{\mathrm{d}\tau}\left[g_2\boldsymbol{\sigma}\right]. \tag{1.47b}$$

and

$$\begin{aligned}\frac{\mathrm{d}}{\mathrm{d}t}\boldsymbol{y}_p(t) &= \int_0^t \frac{\lambda_p}{a}\mathbf{S}^{(p)}\mathrm{e}^{-\lambda\left(\Omega^{t+\Delta t}-\Omega^t\right)} : \frac{\mathrm{d}}{\mathrm{d}\tau}\left[g_2\boldsymbol{\sigma}\right]\mathrm{d}\tau\\ &= \frac{\lambda_p}{a}\int_0^t \mathbf{S}^{(p)}\left[1-\left(1-\mathrm{e}^{-\lambda\left(\Omega^{t+\Delta t}-\Omega^t\right)}\right)\right] : \frac{\mathrm{d}}{\mathrm{d}\tau}\left[g_2\boldsymbol{\sigma}\right]\mathrm{d}\tau\\ &= \frac{\lambda_p}{a}\left[\mathbf{S}^{(p)} : \left(g_2(t)\boldsymbol{\sigma}(t)-g_2(0)\boldsymbol{\sigma}(0)\right)-\boldsymbol{y}_p(t)\right].\end{aligned} \tag{1.48}$$

The differential Equation (1.48) can be solved for y_p using a FD scheme, leading to an expression for $\boldsymbol{y}_p^{n+1}$.

The greatest advantage of differential strategies over recursive strategies is the use of the massive amount of work that has been done on the development of FD schemes and therefore they have access to very high order incremental schemes for complex nonlinear materials and loadings.

CHAPTER 2

OBJECTIVES AND RATIONALE

The general objective of this research was to better understand the evolution of a MVK-10 polyimide matrix mechanical properties during its service life at elevated temperatures and to develop numerical tools taking into account this evolution. Another objective was to compare MVK10's performances against those of PMR15 under similar conditions. The literature review emphasized a few important aspects to investigate in that respect:

1. Chemical ageing of polymer matrices at high temperatures can lead to severe degradation. The extend of degradation must be investigated in order to be able to safely use this material in structural applications.
2. Polymers viscoelastic behavior depends on parameters such as stress, temperature and physical ageing histories. Therefore, it is necessary to fully investigate the impact of those parameters and to develop constitutive theories capable to predict those impacts. In particular, models for nonlinearizing functions dependent on stress, temperature and physical ageing have to be developed
3. Although Schapery-type constitutive theories were first developed as differential equations, actual strategies for implementing them into finite element software all use their hereditary integral forms. Recursive strategies introduced simplifying hypotheses on the non-linearizing functions in order to obtain a recursive relationships between successive time-steps while differential strategies transform back the hereditary integral in a set of differential equations which are solved with classical finite differences schemes. Implementation strategies could be developed using the original differential equations, bypassing the need to transform back the hereditary integral.

Based on the project objectives and the summary of the literature survey, 3 sub-objectives, along with their methodologies, have been defined:

1. Investigation of chemical ageing

   The first objective explored the kinetic of degradation of MVK-10 through the use of thermogravimetric analysis. Kinetic tests in air atmosphere were used to develop a three-step degradation model. The model was then used to predict degradation kinetics under isothermal conditions over 24 hours for various temperatures. Furthermore, the material's thermal stability was studied over a period of one year at service temperature. Chemical degradation progress was monitored by measuring the changes in samples

volume and mass. Finally, the mechanical properties evolution was investigated with tensile tests up to failure after 1, 4, 9 and 17 months of ageing.

An article was submitted for publication in "Polymer Degradation and Stability" on July 25$^{\text{th}}$, 2014. This journal publishes research in the field of degradation reactions and their control. The author of this thesis wrote 75% of this paper. Some of the experiments were performed by M. Kamal at NRC Laboratory in Ottawa. Professor M. Lévesque and Dr. Chun Li contributed to redaction.

2. Modeling the viscoelastic behavior of MVK-10 polyimide with respect to the stress, temperature and physical ageing history

   The second objective investigated MVK-10's mechanical behavior with respect to stress, temperature and physical ageing. The material was tested using tensile tests at service temperature to determine its linear viscoelasticity range, as well as its tri-dimensionnal (3D) behavior. Investigation of physical ageing was performed at higher temperatures using 3-point bending tests. The experimental data was used to developed a Schapery-type constitutive theory for the material. The theory was then validated using complex thermo-mechanical histories with several temperature up- and down-jumps, as well as several creep tests.

   An article was submitted to "Mechanics of Time-Dependent materials" on July 25$^{\text{th}}$, 2014. This journal publishes research on the time-dependent mechanical behavior of materials. The author of this thesis wrote 75% of this paper. $\sim$ 50% of the experiments were performed by S.Dulong. Professor M. Lévesque and Dr. Chun Li contributed to the redaction.

3. Development of a new strategies for implementing Schapery-type constitutive theories into FE software

   The third objective consisted in developing a finite-element strategy for using the model proposed in the second objective. Two new strategies for implementing Schapery-type constitutive theories into FE software. The first strategy relied on the original differential equations that lead to the integral formulation of Schapery-type constitutive theories and Finite Difference (FD) schemes. This strategy is quite different from all the other strategies found in the literature. The second strategy is an improvement of recursive strategies, used by many authors, based on the integral formulation of the constitutive theory.

   An article was published in "Mechanics of Time-Dependent materials", Volume 14, pp. 359 - 387, in 2010. This journal publishes research on the time-dependent mechanical behavior of materials. The author of this thesis wrote 75% of this paper. T. Schönherr

performed some preliminary investigation on the subject. Professor M. Lévesque and Dr. Chun Li contributed to redaction.

CHAPTER 3

ARTICLE 1: Thermal stability and evolution of the mechanical properties of an aerospace polyimide at high temperature

T. Crochon, M.Kamal, C. Li, M. Lévesque (2014). Submitted to *Polymer Degradation and Stability* on July 25$^{\text{th}}$ 2014.

3.1 Abstract

This work explores the kinetic of degradation of a high-temperature aeropsace polyimide through the use of thermogravimetric analysis. Kinetic tests in air atmosphere were used to develop a three-step degradation model. The model was then used to predict the kinetic of degradation in isothermal conditions over 24 hours. At high temperatures, the model was found to produce quite good predictions while at low temperatures, the model led to poor predictions since it cannot predict the formation of an initial oxidation layer. Furthermore, the thermal stability of the polyimide was studied over a period of one year at service temperature. The material was found to loose about 5% of its mass and volume. At the same time, its mechanical properties decreased by 19%, 30% and 10% for the Young's modulus, failure stress and failure strain, respectively.

3.2 Introduction

Heating a polymer at temperatures close to its glass transition temperature, i.e., T_g, typically leads to reduced ductility and embrittlement, chackling, cracking and general reduction in most of its other desirable physical properties (Beyler et Hirschler, 2001). The origins of these changes, referred to as ageing, are diverse: *i*) possible continuation of the curing process in the case of thermosetting polymer, also known as curing ageing (White, 2006); *ii*) change in the chemical composition of the polymer, i.e., chemical or thermal ageing; *iii*) volume relaxation following the rapid heating or cooling of the polymer as it evolves towards a new thermodynamic equilibrium, i.e., physical ageing (Hutchinson, 1995).

Thermal ageing results from a variety of phenomena such as the polymer's main chain breakdown (Beyler et Hirschler, 2001) or the formation of an oxidation layer on its surface (Bowles *et al.*, 1995). Both these mechanisms lead to the formation of new chemical species and their effects can be assessed by continuously monitoring a specimen's mass (Coats et Redfern, 1963) using ThermoGravimetric Analysis (TGA). TGA provides information on the

overall progress of thermal ageing and allows for the determination of thermal and thermo-oxidative stability of the material. It can also be used for the estimation of product lifetimes, degradation kinetics and effects of reactive atmospheres. TGA provides valuable information that can be used to select materials for certain end-use applications, predict product performance and improve product quality (Kingston *et al.*, 2010). One limitation of TGA is that it can only detect evolutions in the molecular structure as long as it is accompanied by a mass change (Coats et Redfern, 1963). Furthermore, it only allows for a quantitative analysis of the degradation mechanism (Materazzi, 1997).

Studying the thermo-oxidative stability at any temperature alone does not provide a complete assessment of a polymer durability (Bowles *et al.*, 1995). It has been shown that even at temperatures at which a material would be considered thermally stable, i.e., the overall mass change does not exceed a predetermined threshold, mechanical properties could still be significantly impacted. The problem lies with the fact that, while TGA data is monolithic, the actual degradation mechanism is a competition between the polymer breakdown which occurs throughout the material, resulting in a mass loss, and the oxidative degradation which occurs only where the oxygen diffuses, resulting in a mass gain (Tsuji *et al.*, 2000). The competitive nature of those two phenomena can result in a seemingly constant mass for the material, when, simultaneously, the mechanical properties are significantly affected.

Polymer matrix composite materials are increasingly used in aerospace applications like aircraft engines. Gas turbine blades made from composites are currently being used in General Electric GENx and CFMi LEAP-X engines. Such applications require polymer matrices able to withstand temperatures as high as 300°C, under severe mechanical loading conditions. Polyimide matrices set themselves apart from other polymers by exhibiting higher mechanical properties, as well as better thermal and thermo-oxidative properties (Li *et al.*, 1999). Recent progress in the development of new polyimides formulas, suitable for less expensive out-of-autoclave manufacturing processes, has made light-weight and high temperature polymer matrix composite materials viable options for high-temperature applications.

PMR-15 has been extensively used in the aerospace industry and has been the subject of a series of studies on the impact of temperature on its mechanical properties, both as a plain matrix or inside a composite. Particularly, Ruggles-Wrenn and Broeckert (Ruggles-Wrenn et Broeckert, 2009) showed that a bulk PMR-15 sample lost 3.5% of its initial mass after being exposed at 288°C for 1000 hours. Over the same period, its elastic modulus increased by 13% while its failure stress and strain dropped from 20MPa and 1.25% to 12MPa and 0.60%, respectively. This kind of results shows that even modest mass reductions, leading to deceptive conclusion that the material is thermally stable, can lead to significant mechanical properties loss.

The purpose of this paper was to study the impact of exposure to elevated temperature on a high-temperature aerospace polyimide suitable for Resin Transfer Molding (RTM). Material thermal properties, degradation kinetics, thermo-oxidative stability and mechanical properties were specifically studied.

This paper is organized as follows: Section 3.3 recalls general modeling aspects for thermal degradation and its impact on mechanical properties; Section 3.4 presents the procedure used to test the material. Finally, Section 3.5 deals with the analysis of the experimental data and the determination of the models' parameters.

3.3 Theoretical considerations

3.3.1 Thermal degradation model

Lewis (Vyazovkin, 2000) introduced an adaptation of the law of mass action to the case of solid-state mechanics in which the concentrations of the chemical species are replaced by the degree of conversion, denoted by α. This degree of conversion can be seen as a measure of the degradation progress and is defined as:

$$\alpha(t,T) = \frac{m_0 - m(t,T)}{m_0 - m_f} \tag{3.1}$$

where m_0 is the sample's initial mass, m_f is its final mass and $m(t,T)$ is its mass at time t and temperature T.

The single-step reaction model assumes that the rate of conversion is a function of temperature and the degree of conversion, leading to the following differential equation (Sánchez-Jiménez *et al.*, 2011):

$$\frac{\mathrm{d}\alpha}{\mathrm{d}t}(\alpha,T) = k(T)\,\alpha^m\,(1-\alpha)^n \tag{3.2}$$

where $\alpha^m\,(1-\alpha)^n$ is the Sestak-Berggren equation, which the most popular form for representing auto-catalyzed reactions. m and n are the reaction orders and k is the degradation rate constant that can be expressed with the Arrhenius equation:

$$k(T) = A\exp\left(-\frac{E^{act}}{RT}\right) \tag{3.3}$$

where T is the absolute temperature, R is the gas constant, A is a pre-exponential factor and E^{act} is the activation energy.

One limitation of the single-step reaction model resides in the fact that the degradation mechanism is often too complicated to be reduced to a unique step (Šimon, 2004). It is generally more accurately represented by a combination of competitive and consecutive

phenomena. Each of those phenomena has different activation energies. Therefore, when using the single-step model, the activation energy evaluated from the experimental data is likely to be a combination of the activation energies of all the individual phenomena in the degradation mechanism, resulting in an apparent activation energy dependent on the degree of conversion (Vyazovkin, 2000).

Isoconversional methods can be used to dissociate single and multiple steps degradation mechanisms since they provide an efficient evaluation of the activation energy without a-priori knowledge of the degradation kinetics. The Flynn-Wall-Ozawa (FWO) method (Ozawa, 1965; Flynn et Wall, 1966), the Kissinger-Akahira-Sunose (KAS) method (Vrandečić *et al.*, 2010), Friedman's method, Vyazovkin's method and Li and Tang methods (Budrugeac et Segal, 2001) are examples of such procedures. Those methods were developed for determining the kinetic triplet from a series of TGA tests performed at constant heating rates β.

Friedman's method evaluates Equation (3.2) at fixed values of α (see (Budrugeac et Segal, 2001) for further details), leading to:

$$\ln\left(\frac{\mathrm{d}\alpha}{\mathrm{d}t}\right)_{\alpha} = \ln\left[A_{\alpha}\alpha^{m}\left(1-\alpha\right)^{n}\right] - \frac{E_{\alpha}^{act}}{RT_{\alpha}}. \tag{3.4}$$

where $\left(\frac{\mathrm{d}\alpha}{\mathrm{d}t}\right)_{\alpha}$, E_{α}^{act}, A_{α} and T_{α} are, respectively, the conversion rate, activation energy, the pre-exponential factor and temperature associated to a fixed value of the degree of conversion α. Therefore, the quantity $\ln\left[A_{\alpha}\alpha^{m}\left(1-\alpha\right)^{n}\right]$ being constant, it is possible to obtain the activation energy E_{α}^{act} by plotting $\ln\left(\frac{\mathrm{d}\alpha}{\mathrm{d}t}\right)_{\alpha}$ as a function of $1/T_{\alpha}$ for the various heating rates. If the activation energy is independent of α, then the degradation mechanism is single-stage. Otherwise, a more complex multi-step reaction model must be used.

Assuming that the degradation mechanism can be decomposed in a set of Q independent processes, the conversion degree can be written as the sum of the degree of conversion of all independent processes (Perejón *et al.*, 2011; Nam et Seferis, 1991):

$$\alpha\left(t\right) = \sum_{q=1}^{Q} a_{q}\alpha_{q}\left(t\right) \tag{3.5}$$

where a_q represents the relative contribution of process q to the overall degradation mechanism (and thus, $\sum_{q=1}^{Q} a_q = 1$). Combination of Equations (3.2) and (3.3) leads to the following differential equation for each q mechanism:

$$\frac{\mathrm{d}\alpha_{q}}{\mathrm{d}t}\left(\alpha,T\right) = A_{q}\exp\left(-\frac{E_{q}^{act}}{RT}\right)\alpha_{q}^{m_{q}}\left(1-\alpha_{q}\right)^{n_{q}} \tag{3.6}$$

3.3.2 Mechanical properties degradation model

Few studies have been proposed to model the mechanical properties degradation due to thermal aging (Kim *et al.*, 2002; Fan et Li, 2013). A mathematical expression similar to Equation (3.2) can be used if it is considered that the same mechanisms leading to mass loss are responsible for the degradation of the material properties. By defining the ratio $\rho = P/P_0$, where P_0 is the initial value of material property P, the rate of degradation of P can be modeled by the Sestak-Berggren equation (Kim *et al.*, 2002) as:

$$\frac{\mathrm{d}\rho}{\mathrm{d}t}(\rho, T) = k_\rho(T)\,\rho^{n_\rho}\,(1-\rho)^{m_\rho} \tag{3.7}$$

where k_ρ, m_ρ and n_ρ are the degradation rate and reaction orders associated to mechanical property P. Property evolution for a material aged at a constant temperature has been expressed by Fan and Li (Fan et Li, 2013) [1]:

$$P(t) = P_0 \exp\left(K_P t^{\gamma_P}\right) \tag{3.8}$$

where K_P and γ_P are model parameters.

3.4 Experimental methods

3.4.1 Material

The material studied in this paper was the MVK-10 polyimide matrix from Maverick Corporation. This matrix is formulated for high temperature applications. Matrix panels, provided by the manufacturer, were prepared using RTM. The panels were cured at at a temperature slightly above its T_g for approximately 4 hours before being subsequently post-cured at the same temperature for another 17 hours.

3.4.2 Determination of T_g

The dry- and wet-glass transition temperatures, dry-T_g and wet-T_g, were investigated with a Dynamic Mechanical Analyzer (DMA) TA Q800 from TA Instruments and according to ASTM D-7028 standard. Rectangular samples for DMA testing were cut from the main panels using a high precision low speed saw equipped with a diamond wafering blade. The dimensions of the samples were $60 \times 12.70 \times 3.20\mathrm{mm}^3$. Prior to testing, dry-$T_g$ samples were left to dry for 48 hours in an oven at a temperature of 150°C before being cooled down and

1. Equation (3.8) is the solution to the Avrami equation in the isothermal case. Sestak *et al.* (1973) showed that the Avrami equation is equivalent to the Sestak-Berggren equation to a first order approximation.

stored in a desiccator. Wet-T_g samples were fully saturated with water in an environmental chamber and their masses were recorded regularly until stabilization (see Figure 3.1).

The samples were loaded at a frequency of 1Hz under strain control while the material was heated at a constant rate of $5°C \cdot min^{-1}$ and each test was repeated 3 times. As customary in aerospace applications, T_g was defined as the intersection of the two slopes associated to the onset of storage modulus.

3.4.3 Thermal degradation and stability

The thermal degradation and stability of the material were studied with TGA. Two kinds of tests were performed: *i*) kinetic tests during which samples of material are heated at a constant heating rates until no more degradation was observed. Those tests were used to determined the mechanism of thermal degradation; *ii*) isothermal tests during which the material was submitted to a constant temperature for a fixed amount of time. Those tests were used to analyzed the thermal stability of the material at various temperatures.

Thermogravimetric analysis was performed on a TGA A588 TGA-IR from PerkinElmer. The balance inside the instrument had a resolution of 1μg for a maximum weight of 1g. Samples of approximately 5mg were obtained by grinding into fine powder parts of the matrix panels with a FRITSCH Pulverisette 2 mortar grinder. The samples were conditioned at 150°C for 12 hours so as to remove any remaining humidity in order to obtain accurate initial mass measurements. The samples were placed into a crucible made of ceramic whose mass change with temperature was evaluated before each test and accounted for in the data reduction.

Kinetic tests were performed at heating rates of $5°C \cdot min^{-1}$, $10°C \cdot min^{-1}$, $15°C \cdot min^{-1}$ and $20°C \cdot min^{-1}$ in an oxidizing air atmosphere. A controlled flow of $50cc.min^{-1}$ was used for each tests to ensure a constant atmosphere. Purging of all gases was performed with a flow of $25cc.min^{-1}$ of argon. Each test was repeated three times for each heating rate.

TGA was performed on powder samples during 24 hours isothermal experiments conducted at wet-$T_g - 28°C$, wet-$T_g - 3°C$, wet-$T_g + 12°C$, wet-$T_g + 37°C$ and wet-$T_g + 87°C$. It must be pointed out here that results of isothermal tests performed on powder samples can be misleading since they maximize the surface area between the material and the environment and minimize the temperature gradient. Much larger thicknesses are used in structural applications. Therefore, isothermal tests were also performed on typical tensile test samples obtained by water jet cutting, whose dimensions are shown in Figure 3.2. To that end, samples were exposed to wet-$T_g - 28°C$ over a period of 17 months and their volumes and masses were recorded. The samples were stored in a Thermo Scientific Precision 625 High Performance environmental chamber in compliance with industry standards such as ASTM

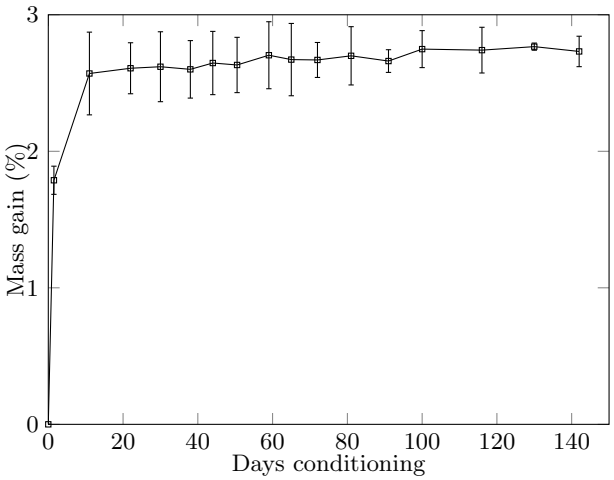

Figure 3.1: Conditioning of the samples before the wet-T_g tests. Advancement of the conditioning is measured by percentage of mass gain. The data represented is the mean values and a 95% confidence interval for the three samples tested.

E145 type IIA and UL746B, as well as with ASTM E3035 standard for heat ageing of plastics. The chamber was equipped with four thermocouples to monitor air temperature. The resulting mass losses were measured with a Sartorius CPA124S scale within ± 0.1mg. The volume contractions were estimated by measuring the width and thickness of the sample with a Mutitoyo caliper.

3.4.4 Mechanical properties

Tensile tests up to failure were performed with a MTS Insight 50kN electromechanical load frame equipped with a Lab-Temp LBO-series box environmental chamber from Thermcraft Incorporated. Temperature control was achieved by setting the temperature in the air surrounding the sample with the thermal controller while monitoring the specimen temperature with a thermocouple set in its gage section.

Tensile tests were performed at room temperature as well as at service temperature, defined as wet-$T_g - 28°$C. Tests were also performed on samples exposed to service temperature for 1, 4, 9 and 17 months. The tensile tests were performed according to ASTM D638 standard for tensile testing of plastics. A controlled displacement rate of 5mm.min^{-1} was used. Axial strains were measured with an Epsilon 3555 high-temperature un-cooled extensometer.

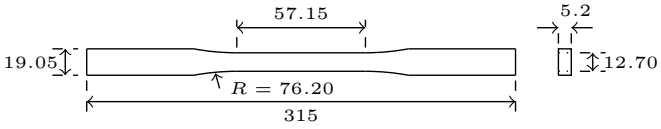

Figure 3.2: Dimensions in mm of the ASTM Type I specimen used for tensile testing (all dimensions are in mm).

3.5 Results and analysis

3.5.1 Glass Transition Temperature

The mean value for the dry-T_g was found to be close to that provided by the manufacturer. The wet-T_g was found to be 58°C inferior to the dry-T_g. The service temperature used as a reference subsequently was determined as per FAA regulations and set to wet-$T_g - 28$°C.

3.5.2 Thermal degradation

Kinetic tests

Results of the kinetic tests can be found in Figure 3.3 and are summarized in Table 3.1. For each heating rate, excellent reproducibility was observed for all three repetitions. Consequently, only the mean values are presented for each test. Figure 3.3 shows that, for a heating rate of 5°C·min^{-1}, the onset of thermal degradation is at wet-T_g+109°C (temperature corresponding to a conversion degree of 1%) which is slightly above Dry-T_g. Figure 3.3 also shows that the rate of degradation increases slowly as the material is heated up to wet-$T_g + 227$°C. Then, the bulk of the degradation occurred with a maximum conversion rate at wet-$T_g + 292$°C. Finally, the degradation was complete around wet-$T_g + 369$°C (temperature corresponding to a conversion degree of 99%) with almost no material remaining (the residual mass was less than 1%). Similar observations were made as the heating rate increased. However, the curves are slightly shifted towards higher temperatures, as well as flattened, which progressively leads to the apparition of a second maximum on the conversion rate curve.

Analysis of the dependence of the activation energy on the degree of conversion α was performed using Friedman's analysis (see Figure 3.4). The activation energy was found to be around 150kJ.mol^{-1} for $0.05 < \alpha < 0.35$ before drastically decreasing towards a minimum of 70kJ.mol^{-1} for $\alpha = 0.7$. Then, the activation energy increased anew at the end of

the degradation process. Those observations are consistent with a three-steps degradation process.

A kinetic model was developed based on these observations, as per Equation (3.5). The kinetic parameters were obtained with an optimization algorithm to solve the following problem:

$$\min_{x} \sum_{j=1}^{J} \sum_{i=1}^{I_j} \left[\left(\frac{\mathrm{d}\alpha}{\mathrm{d}t} \right)_{ij} - \left(\frac{\mathrm{d}\bar{\alpha}}{\mathrm{d}t} \right)_{ij} \right]^2 \tag{3.9}$$

where $\left(\frac{\mathrm{d}\alpha}{\mathrm{d}t}\right)_{ij}$ and $\left(\frac{\mathrm{d}\bar{\alpha}}{\mathrm{d}t}\right)_{ij}$ are, respectively, the i^{th} experimental data point and model value associated to the j^{th} heating rate. J is the number of heating rates tested and I_j is the number of experimental data points obtained for the j^{th} heating rate. x is the set of material parameters to optimize (see below).

Problem (3.9) was solved with `fmincon` from MATLAB's optimization toolbox and `sqp` algorithm. The thermal degradation was assumed to follow a three-step mechanism, leading to a set of 15 material parameters (each step is associated to a quintuplet $\left\{a_q, A_q, E_q^{act}, m_q, n_q\right\}$). The outcome of this optimization can be found in Figure 3.3 and Table 3.2. As can be seen, this model led to an excellent fit of the experimental data.

TGA isothermal tests

The first isothermal tests were performed on powder samples. The data for those tests can be found in Figure 3.5. Different behaviors are observed for the different tests temperatures.

An initial increase in the residual mass was observed for temperatures lower than wet-T_g+12°C. Furthermore, as the testing temperature decreased, the length and size of the initial mass gain increased. Those initial mass gains are typically explained by the creation of an oxidation layer around the samples. However, as the experiment progressed, the degradation inside the material became more important and the residual mass slowly decreased.

On the other hand, at temperatures higher than wet-$T_g + 12$°C, severe mass loss resulting from material break-down was observed from the beginning of the test, overshadowing any

Table 3.1: Summary of TGA data. $T_{1\%}$ and $T_{99\%}$ are the temperatures at which 1% and 99% of conversion are achieved, respectively. T_{max} is the temperature corresponding at maximum conversion rate.

β	$\mathbf{T_{1\%}}$	$\mathbf{T_{max}}$	$\mathbf{T_{99\%}}$	**Residual weight**
$5°\mathrm{C} \cdot \mathrm{min}^{-1}$	wet-$T_g + 109$°C	wet-$T_g + 292$°C	wet-$T_g + 369$°C	0%
$10°\mathrm{C} \cdot \mathrm{min}^{-1}$	wet-$T_g + 125$°C	wet-$T_g + 314$°C	wet-$T_g + 406$°C	1%
$15°\mathrm{C} \cdot \mathrm{min}^{-1}$	wet-$T_g + 127$°C	wet-$T_g + 331$°C	wet-$T_g + 427$°C	1%
$20°\mathrm{C} \cdot \mathrm{min}^{-1}$	wet-$T_g + 128$°C	wet-$T_g + 338$°C	wet-$T_g + 454$°C	0%

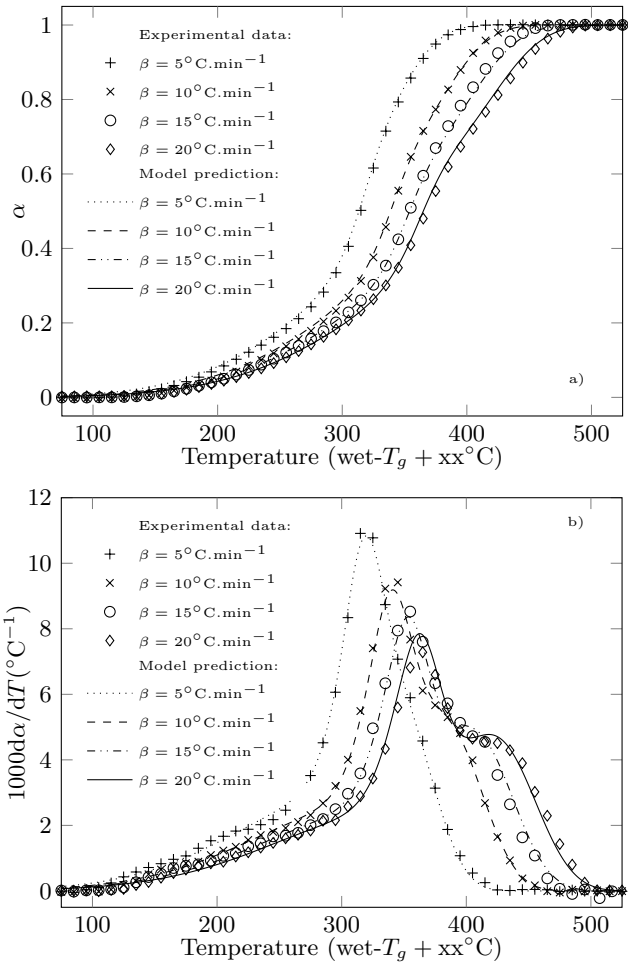

Figure 3.3: Experimental data and model predictions for a) the conversion degree and b) the conversion rate of the thermal degradation for various heating rates in oxidizing atmosphere.

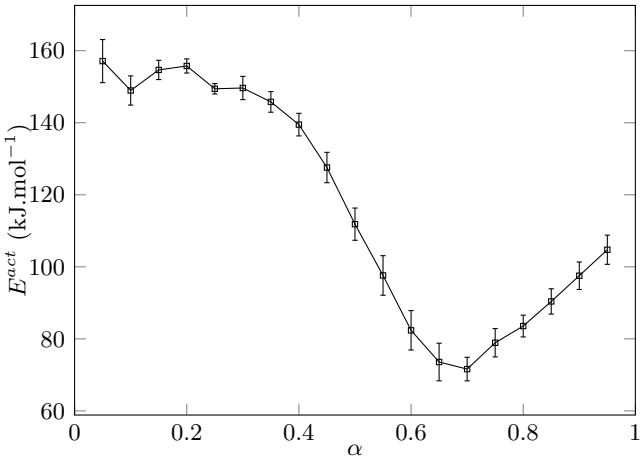

Figure 3.4: Activation Energy E^{act} as function of α data in oxidizing atmosphere.

Table 3.2: Optimized material parameters for the thermal degradation model obtained from the kinetic data

$\mathbf{q}$	$\mathbf{a_q}$	$\mathbf{lnA_q}$ $(\mathbf{s^{-1}})$	$\mathbf{E_q^{act}}$ $(\mathbf{J.mol^{-1}.^\circ C^{-1}})$	$\mathbf{m_q}$	$\mathbf{n_q}$
1	0.23	17.06	1.47×10^5	-1.00	0.73
2	0.32	20.07	1.71×10^5	0.53	1.09
3	0.45	8.87	1.03×10^5	0.48	0.95

formation of an oxidation layer.

Predictions of the isothermal tests was preformed with the kinetic model developed in Section 3.5.2 and the results can be found in Figure 3.5. It can be seen that the model predictions are overall in poor agreement with the experimental data. At lower temperatures, the model cannot predict the initial mass gains due to the formation of the oxidation layer, since the model only includes degradation. For temperatures of wet-T_g + 37°C and wet-$T_g + 87$°C, the model is capable of capturing the general trend.

Figure 3.6 shows the isothermal tests results for tensile samples. No mass or volume gains due to the formation of an oxidation layer were observed. However, close observation (see Figure 3.7) revealed that samples surface became rougher and cracks slowly started to appear and multiply as ageing progressed. This could be explained by the progressive formation of an oxidation layer, leading to an embrittlement of the surface of the material and generating tensile stresses triggering spontaneous cracking (Pochiraju et Tandon, 2006). Since the surface to volume ratio is much smaller for the tensile samples than for the powder samples, the thermal degradation in the bulk of the samples (mass loss) should be much more important than the thermal oxidation on the surfaces (mass gain). This could explain that, while, thermal oxidation can be observed, it was not measured.

3.5.3 Mechanical properties

Mechanical properties evolution with respect to ageing at service temperature can be found in Figure 3.8. The Young's modulus E^{RT}, the failure stress σ_f^{RT} and the failure strain, ε_f^{RT} were evaluated at room temperature and are used as references below.

In every test, the material exhibited a very brittle failure mode with low σ_f and ε_f, even when compared to other polyimides (Chuang, 2005; Liang *et al.*, 2007). When heated at service temperature, the mechanical properties of the material decreased significantly, with reductions of 28% for E, 52% for σ_f and 36% for ε_f. Furthermore, the mechanical properties continued to decrease as the material was further aged at service temperature. After 17 months of ageing, additional decreases of 19%, 30% and 10% were observed for E, σ_f and ε_f, respectively.

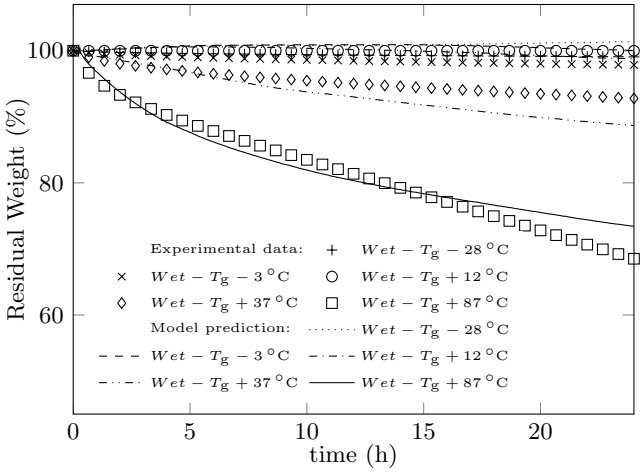

Figure 3.5: TGA data and model prediction for the isothermal degradation at various temperatures in an oxidizing atmosphere.

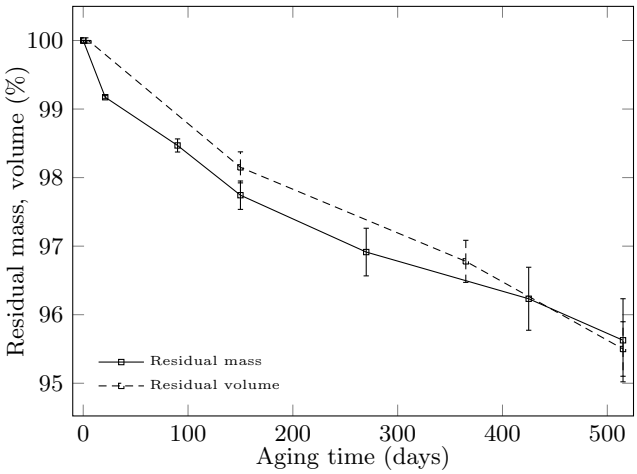

Figure 3.6: Residual mass and volume data for the isothermal degradation at service temperature of tensile samples in an oxidizing atmosphere.

Figure 3.7: Pictures of gage sections of the tensile samples after a) 4 months, b) 9 months and c) 17 months at service temperature in an oxidizing atmosphere.

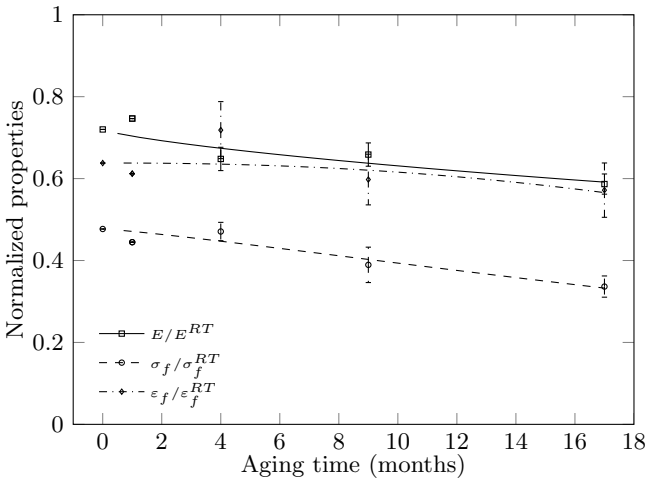

Figure 3.8: Evolution of the normalized tensile properties E, σ_f and ε_f with respect to ageing times at service temperature. Marks represent experimental data while lines represent the model predictions.

Simple models, as proposed in Equation (3.8), were developed for predicting the evolution of the mechanical properties of the material with respect to exposure time at service temperature. The models' parameters were obtained using the curve fitting algorithm `fit` from MATLAB, leading to:

$$E(t) = 0.72 \exp\left(-0.02322 t^{0.7547}\right) \tag{3.10a}$$

$$\sigma_f(t) = 0.477 \exp\left(-0.01252 t^{1.186}\right) \tag{3.10b}$$

$$\varepsilon_f(t) = 0.00637 \exp\left(-0.0001779 t^{2.3}\right) \tag{3.10c}$$

The results can be found in Figure 3.8 and the experimental data are fitted quite well. All three models predict a decrease of the material properties. In the case of σ_f and ε_f, the models predict that these decreases will accelerate with time. This is particularly true in the case of ε_f, for which the decrease is very small in the first 9 months. This is in concordance with the observation made on the surface of the samples in Figure 3.7. Up to 9 months, the formation of the oxidation layer is barely visible. After 17 months, it appears clearly.

3.6 Concluding remarks

The thermal properties, kinetic of degradation and mechanical properties of a high-temperature aerospace polyimide have been studied. Several interesting results have been obtained:

- The dry-T_g of the material was found to be slightly below the onset of thermal degradation in the kinetic tests. However, it is above the temperature at which almost immediate and severe degradation is observed during the isothermal tests (wet-$T_g + 37°C$).
- Kinetic tests in oxidizing atmosphere leads to a three-step degradation mechanism. Identification of the model's parameters led to an excellent fit of the kinetic data. However, the model was not capable of predicting the isothermal data with accuracy, demonstrating the limits of determining degradation models from purely kinetics data: *i*) accurate measurements of small mass changes, obtained for lower temperatures can be challenging; *ii*) experimental data from kinetic tests reflects mainly changes at higher temperatures and do not capture mass changes at lower temperatures; *iii*) determination of the exact number of processes is challenging.
- Isothermal degradation of powder samples at service temperature showed the formation of an oxidation layer on the surface of the samples. This oxidation could not be measured with mass reduction on the tensile samples. Visual inspection, however, revealed it presence.
- Isothermal degradation of the tensile samples showed some mass loss ($< 5\%$) after 17 months of ageing at service temperature. This could lead us to conclude that this polyimide is stable at such temperature. However analysis of the mechanical properties led to very different conclusions. Decreases of 19%, 30% and 10% from the non-aged properties were observed for E, σ_f and ε_f, respectively. Those are important changes of the material properties.
- Simple mechanical properties degradation models were developed and agreed well with obtained experimental data.

All those results show that thermal ageing of a polymer matrix is a complex matter and that a material should be thoroughly studied before being used in critical applications such as aircraft engine. Furthermore, it indicates that FAA rules for determining the service temperature of a polymer matrix may be inadequate for those high performance materials since their T_g is already near their temperature of degradation.

Acknowledgments

Financial support from Pratt and Whitney Canada, Rolls Royce Canada and the Consortium for Research and Innovation in Aerospace in Quebec (CRIAQ) is gratefully acknowledged.

CHAPTER 4

ARTICLE 2: On time-temperature dependent viscoelastic behavior of an amorphous polyimide

T. Crochon, C. Li, M. Lévesque (2014). Submitted to *Mechanics of Time-Dependent materials* on July 25$^{\text{th}}$ 2014.

4.1 Abstract

Development of new polyimide formulas has led to an increase of the use of polymer matrix composites by the aerospace industry in critical applications such as aircraft engines. In such an extreme environment, the polymer matrix is likely to exhibit a viscoelastic behavior due to the elevated temperatures. Furthermore, physical ageing is likely to appear during the service life of the material. In order for engineers to desing with such materials, constitutive theories able to take into account those effects, must be developed. This paper deals with the mechanical behavior of a new polyimide matrix tested under complex thermo-mechanical histories while accounting for physical ageing. The experimental data obtained was modeled with a newly developed constitutive theory stemming from Schapery's thermodynamical framework. The models parameters were obtained from creep-recovery data under various temperatures, ageing times and loads. The model was subsequently validated against independent complex thermo-mechanical histories. An excellent agreement between the experiments and the predictions has been obtained.

4.2 Introduction

Firstly used in non-structural applications, Polymer Matrix Composites (PMCs) are now widely used in more critical aerospace applications, such as wings, fuselage and aircraft engines. Aircraft engine applications require materials able to withstand extreme service conditions, such as elevated temperatures, high mechanical loadings and a highly oxidative environment. With rated service temperatures exceeding 300 °C, overall excellent mechanical properties and the possibility to be manufactured through easier and cheaper out-of-autoclave processes such as Resin Transfer Molding (RTM), polyimide-based PMCs set themselves as potential candidates for such applications (Li *et al.*, 1999).

Polymer matrices exposed to high temperatures and loads are likely to exhibit a viscoelastic behavior, potentially nonlinear with respect to load and temperature. In addition, the

combined effects of elevated temperature and the environment near the engines are likely to increase physical as well as chemical ageing (Xiao *et al.*, 1994). For example, Marais et Villoutreix (1998) realized a series of creep and recovery tests on PMR-15 polyimide matrix and found that the material's compliance significantly increased with increasing stress and temperature levels. Furthermore, at temperatures far below the glass transition temperature (T_g) the material seemed to exhibit a linearly viscoelastic behavior. However, as the test temperatures increased, the same stress levels led to a nonlinearly viscoelastic behavior. Therefore, adequate constitutive theories must take in account these nonlinear effects and representative experimental data have to be used to obtain meaningful material properties.

For many years, PMR-15 was the preferred polyimide for structural applications since it offered stable performances at high temperatures, while being easy and relatively cheap to process (Jones, 2009). However, its use has decreased in recent years since one of its core components was found to be carcinogenic. Alternatives to PMR-15 were subsequently developed, like the MVK-10 polyimided developed my Maverick Corporation.

The purpose of this work was to study the mechanical behavior of the MVK-10 polyimide submitted to a wide range of elevated temperatures. The dependence of the material's viscoelasticity on temperature and physical ageing was examined and a model based on Schapery's framework (Schapery, 1964) was developed and validated against independent complex thermo-mechanical hisotries.

This paper is organized as follows: Section 4.3 recalls the notions of physical ageing and shift factors. Section 4.4 presents the procedure used to test the material. Finally, Section 4.5 deals with the development of the model, as well as the determination of its parameters from the experiments.

Stresses/strains and stiffnesses/compliances are respectively represented as vectors and matrices, according to the modified Voigt notation recalled in Lévesque *et al.* (2008). A vector is denoted by a boldfaced lower case letter, i.e., $\boldsymbol{a}$ and $\boldsymbol{\alpha}$ and a matrix is denoted by a boldfaced capital Roman letter, i.e., $\mathbf{A}$.

4.3 Background

4.3.1 Physical ageing

Firstly developed for the case of polymers submitted to elevated temperatures (Williams *et al.*, 1955), the Time-Superposition Principle (TSP) has been extended to physical ageing by Struik (1978). Based on the free volume theory, the TSP relies on the effective time concept (Bradshaw et Brinson, 1997b) to compare creep responses obtained at different temperatures and ageing times. The concept implies that retardation times under any service conditions can

be related to those at reference conditions by a simple multiplicative horizontal shift factor. The the concept is mainly used for predicting polymers' long-term creep (Ohashi *et al.*, 2002; Olasz et Gudmundson, 2005; Zhao, 2008; Luo, 2007) or physical ageing responses at a given temperature by testing the material at higher temperatures over shorter time-scales.

According to the TSP, the creep compliance $S(t)$ of a material aged for a time t_e at a constant temperature T and submitted to a stress σ can be related to its creep compliance $\bar{S}(t)$ when aged for a reference time $\bar{t}_e$ at a reference temperature $\bar{T}$ and submitted to a reference stress $\bar{\sigma}$, according to:

$$S(t) = b(t_e, T, \sigma)\, \bar{S}\left(\frac{t}{a(t_e, T, \sigma)}\right) \tag{4.1}$$

where $a(t_e, T, \sigma)$ and $b(t_e, T, \sigma)$ are horizontal and vertical shift factors dependent on temperature, stress and physical ageing, respectively. Graphically, those shift factors represent the distance by which $S(t)$ must be respectively shifted horizontally and vertically in order to match the reference master curve, $\bar{S}(t)$ (Bradshaw et Brinson, 1997b). The shift factor $a(t_e, T, \sigma)$ can be decomposed into the product of three shift factors, namely the temperature shift factor a_T, the stress shift factor a_σ and the physical ageing shift factor a_{t_e} (Lai et Bakker, 1996), leading to:

$$a(t_e, T, \sigma) = a_T a_\sigma a_{t_e}. \tag{4.2}$$

The evaluation of the horizontal shift factor a_{t_e} is usually performed following the methodology proposed by Struik (1978) who considered the case where a material was quenched from a temperature above its glass transition temperature to a temperature T below its glass transition temperature. In this simple case, the ageing time t_e is defined as the time elapsed since the quench. Struik (1978) found that the shift factor a_{t_e} extracted from a creep test could be approximated by:

$$a_{t_e} = \left(\frac{t_e}{\bar{t}_e}\right)^{\mu(T)} \tag{4.3}$$

where $\mu(T)$ is the shift rate. In the case of isothermal ageing, the shift rate is assumed to remain constant as long as the material continues to age.

The simple relationship of Equation (4.3) is not valid for general non-isothermal ageing histories due to memory effects (Bradshaw et Brinson, 1997b). Two approaches dealing with general ageing histories distinguish themselves in the literature, namely: *i*) The continuous shift factor (CSF) method proposed by Bradshaw et Brinson (1997b) based upon the notion of effective ageing time; *ii*) the KAHR-a_{t_e} method proposed by Guo *et al.* (2009) in which the ageing time is defined using volume relaxation theories. The CSF method is an adaptation of Equation (4.3) to the case of non-isothermal ageing where t_e is replaced by the so-called

effective ageing time t_e^{eff} defined as the time the material would have to age under isothermal conditions to achieve the same amount of physical ageing under non-isothermal conditions. The KAHR-a_{t_e} method relies on the KAHR theory for materials volume relaxation outside thermodynamic equilibrium (Kovacs, 1963; Kovacs *et al.*, 1979). In this theory the amount of physical ageing is linked to the notion of relative depart from volumetric equilibrium δ (defined as the difference between the material's actual and equilibrium volumes) by assuming that physical ageing can be related to δ by a simple linear relationship (Struik, 1988; Guo *et al.*, 2009).

Finally, while the introduction of a complementary vertical shifting $b\,(t_e)$ is often required when dealing with physical ageing, it is generally found to have a much smaller effect than the horizontal shift factor (Sullivan *et al.*, 1993) and to exhibit an irregular behavior (Bradshaw et Brinson, 1999). Consequently, vertical shift in the case of physical ageing is considered to be negligible and is not included into the final model. Nevertheless, some authors found that, in some cases, a general trend could be observed in which the vertical shift factor decreases with increasing ageing times (Sullivan *et al.*, 1993; Bradshaw et Brinson, 1997a). This decrease of the vertical shift factor with increasing ageing times is consistent with the general increase in stiffness observed in physically aged polymers. Bradshaw et Brinson (1997a) even proposed that a linear relationship could be observed when representing the vertical shift factor as a function of the logarithm of ageing time. However, in the general case of TSP, the vertical shift factor is assumed to be only temperature-dependent.

4.3.2 Schapery's constitutive theories

The TSP is useful for evaluating the linearly viscoelastic properties of a material in reference conditions over a wide range of decades with limited experimental data. However, dealing with nonlinear behavior under challenging environmental conditions requires more general models. Many nonlinear models have been developed by enforcing that the mathematical operator relating strains and stresses meets the principles of thermodynamics, irrespectively of the loading histories (Lévesque *et al.*, 2008). Such a strategy was developed by Biot (1954) in the case of linearly viscoelastic materials within the framework of the thermodynamics of irreversible processes. It was then extended to nonlinearly viscoelastic materials by Schapery (1964) by the introduction of nonlinearizing functions. Such phenomenological theories can be seen as extensions of the TSP to complex loading and temperature histories. The horizontal shift factor is replaced by the so-called material clock which has been developed for a variety parameters including free volume (Knauss et Emri, 1981, 1987), strains (Schapery, 1966b), stresses (Schapery, 1966a), physical ageing (Schapery, 1997) or any combination of the formers (Lai et Bakker, 1996). More complex material clocks were also developed to

take into account the general state of the material by using quantities such as the entropy (Drozdov, 1997) or the internal energy (Caruthers *et al.*, 2004).

Schapery's (Schapery, 1964) framework has been extended and interpreted in a number of papers over the last forty years and led to a three-dimensional stress-based hereditary integral:

$$\boldsymbol{\varepsilon}(t) = g_0(t)\,\mathbf{S}^{(0)} : \boldsymbol{\sigma}(t) + \mathbf{G}_1(t) : \int_0^t \Delta\mathbf{S}(\Omega - \Omega') : \frac{\mathrm{d}}{\mathrm{d}\tau}\left[g_2(\tau)\,\boldsymbol{\sigma}(\tau)\right]\mathrm{d}\tau \tag{4.4}$$

where $\boldsymbol{\varepsilon}$ is the mechanical strain tensor, $\mathbf{S}^{(0)}$ and $\Delta\mathbf{S}$ are the instantaneous and transient compliances tensors, respectively. $\Delta\mathbf{S}$ can be expressed as a Kohlrausch's stretched exponential function (Guo et Bradshaw, 2007; Guo *et al.*, 2009; Guo et Bradshaw, 2009), a Prony series (Lai et Bakker, 1996; Haj-Ali et Muliana, 2004) or a power law function (Ruggles-Wrenn et Broeckert, 2009). Using Prony series leads to:

$$\Delta\mathbf{S}(t) = \sum_{n=1}^{N} \mathbf{S}^{(n)}\left(1 - \exp\left[-\lambda_n t\right]\right) \tag{4.5}$$

where $\mathbf{S}^{(n)}$ are the transient compliance coefficients associated to the inverted retardation times λ_n. Schapery (1964) introduced the notion of reduced time Ω, which is a generalization of the horizontal shift factors introduced in Equation (4.2), as:

$$\Omega(t_e, T, \sigma) = \int_0^t \frac{\mathrm{d}\xi}{a_T(\xi)\,a_\sigma(\xi)\,a_{t_e}(\xi)} \tag{4.6}$$

Finally, g_0, $\mathbf{G}_1$ and g_2 are the nonlinearizing functions introduced to represent the nonlinearly viscoelastic behavior. Those functions could be considered as generalization of the vertical shift factors $b(t_e, T, \sigma)$.

It should be noted noted that development of the three-dimensional theory in Equation (4.4) leads to

$$\mathbf{G}_1(t) = \gamma(t)\mathbf{I} + \frac{\mathrm{d}\gamma(t)}{\mathrm{d}\boldsymbol{\sigma}} \otimes \boldsymbol{\sigma} \tag{4.7}$$

where $\mathbf{I}$ is the fourth order identity tensor and γ is a function of the stress tensor. Therefore, $\mathbf{G}_1$ is a fourth order tensor in the general case. It can be reduced to a scalar and the identity tensor for a very limited number of situations (see Lévesque *et al.* (2008) for more details).

Development of models for the nonlinearizing functions have mainly focused on stresses or strains nonlinearizing effects (Lai et Bakker, 1996; Haj-Ali et Muliana, 2004; Lévesque *et al.*, 2008). For example, Schapery (1997) considered the nonlinearizing functions to be quadratic functions of stresses. Lai et Bakker (1996) proposed that function g_0 be dependent of the first

stress invariant while $\mathbf{G}_1$ and g_2 would be dependent on the effective octahedral shear stress. Haj-Ali et Muliana (2004) proposed that all nonlinearizing functions be polynomial functions of the effective octahedral shear stress. Sawant et Muliana (2008) proposed temperature-dependent nonlinearizing functions by assuming that g_0 was a linear function, while $\mathbf{G}_1$ and g_2 were exponential functions of the temperature while Muliana et Sawant (2009) assumed that all three functions were polynomial functions of temperature. However, to the knowledge of the authors, a model for the nonlinearizing functions depending on physical ageing has yet to be proposed.

4.4 Experimental method and data

4.4.1 Material

The material studied was the MVK-10 polyimide from Maverick Corporation. Panels were prepared using RTM and cured at a temperature slightly above MVK-10's T_g for approximately 4 hours before being subsequently post-cured at the same temperature for another 17 hours. 3 panels of 381mm $\times$ 317.5mm $\times$ 5.2mm and 1 panel of 381mm $\times$ 317.5mm $\times$ 12.7mm were available for this project.

The material's dry- and wet-glass transition temperatures, dry-T_g and wet-T_g, were investigated with a Dynamic Mechanical Analyzer (DMA) TA Q800 from TA Instruments and according to ASTM D7028 standard. Samples of 60mm $\times$ 6.75mm $\times$ 5.2mm were obtained by water jet cutting from the flat panels. Prior to testing, dry-T_g samples were left to dry for 48 hours in an oven at a temperature of 50°C before being cooled down and stored in a desiccator. Wet-T_g samples were fully saturated with water in an environmental chamber. Their masses were recorded regularly until no more gains were observed. Full saturation was achieved in approximately 11 days. The samples were subsequently loaded at a frequency of 1Hz under strain control while being heated at a constant rate of $5°\text{C} \cdot \text{min}^{-1}$. As is customary of aerospace applications, the T_g was determined as the intersection of the two slopes associated to the storage modulus E' for the glassy and rubbery states.

The wet-T_g was found to be more than 60°C lower than the dry-T_g. As per Federal Aviation Administration regulations, the service temperature of the polyimide was defined as wet-$T_g - 28°$C. While the actual value of the wet-T_g cannot be revealed for confidentiality reasons it was well in excess of 200°C.

4.4.2 Mechanical testing

Tensile as well as three-point bending testing was conducted with an MTS Insight 50kN electromechanical load frame equipped with a Lab-Temp LBO-series box environmental

chamber from Thermcraft Incorporated. The environmental chamber allows for testing at temperatures up to 425°C with a maximum heating rate of $10°C \cdot min^{-1}$. The chamber's temperature was manually set so as to ensure that a thermocouple directly attached to the specimen's gage section (tensile tests) or very close to it (bending tests) recorded the target temperature.

Tensile testing

Tensile tests were performed on non-aged samples at wet-$T_g - 28\,°C$ according to ASTM D638 standard and coupons were designed in compliance with ASTM D638 and ASTM D2990 standards for tensile and tensile creep testing of plastics, respectively. Some dimensions had to be adjusted to allow for proper gripping (see Figure 4.1a).

Strains were measured with Vishay WK-06-125TM-350 tee rosettes to measure axial and transverse strains. These rosettes were bonded with Vishay M-Bond 610 Adhesive on both sides of the samples to account for specimen bending or initial curvature.

Three tensile tests at wet-$T_g - 28\,°C$ were performed to evaluate the tensile stress up to failure (σ_{max}). The tests were conducted under displacement control at a rate of $5mm.min^{-1}$. The resulting standard deviation was less than 5% of σ_{max} mean value. Creep tests at wet-$T_g - 28\,°C$ were also performed under different stress levels to assess the material's linearity. The axial creep compliance $S(t)$ and Poisson's ratio $\nu(t)$ were computed as per:

$$S(t) = \frac{\varepsilon_l(t)}{\sigma_0} \tag{4.8a}$$

$$\nu(t) = -\frac{\varepsilon_t(t)}{\varepsilon_l(t)} \tag{4.8b}$$

where σ_0 is the creep stress, $\varepsilon_l(t)$ and $\varepsilon_t(t)$ are the axial and transverse strains, respectively. Figures 4.2 and 4.3 plot the normalized [1] creep compliances and Poisson's ratio computed for different values of σ_0. The results show that the stress level had a negligible impact on the creep compliance and the viscoelastic Poisson's ratio at wet-$T_g - 28\,°C$. Tensile tests could not be performed at higher temperatures since strain gages were not rated for such temperatures. Therefore, the effect of stress on the creep compliance was further investigated with three-point bending tests. The viscoelastic Poisson's ratio was considered to be stress-independent for all temperatures.

1. All the data reported in this work was normalized for confidentiality reasons.

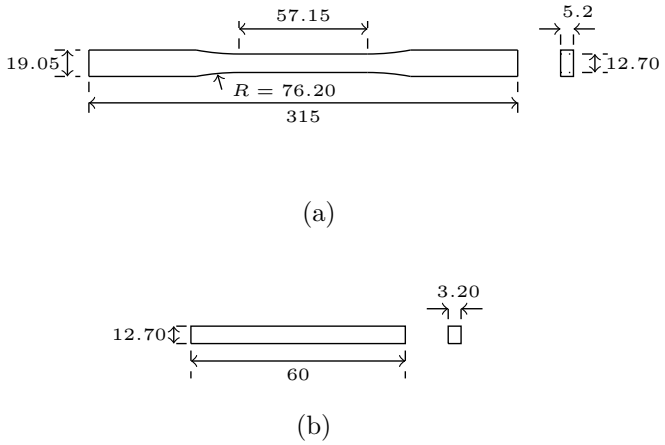

Figure 4.1: Dimensions in mm of the samples used: a)ASTM Type I specimen for tensile testing, b) ASTM D638 specimen for three-point bending testing.

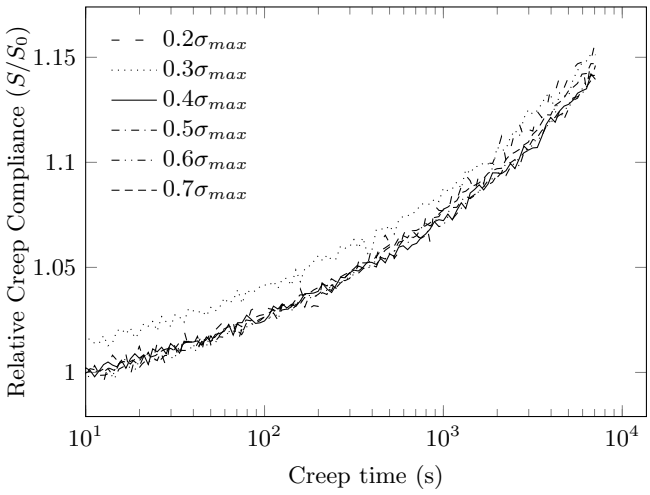

Figure 4.2: Impact of stress level on the normalized creep compliance at wet-$T_g - 28\,^{\circ}C$

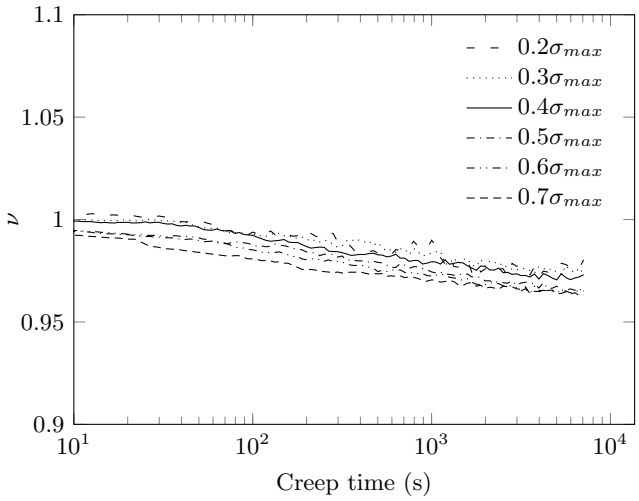

Figure 4.3: Impact of stress level on the normalized Poisson's ratio at wet-$T_g - 28\,°C$

Three-point bending testing

Owing to its cost, only a limited number of MVK-10 panels were available. Three-point bending testing was used to study the effect of ageing since it required much smaller samples than tensile testing. The tests were performed at temperatures ranging from wet-$T_g - 28\,°C$ to wet-$T_g + 37\,°C$. A homemade fixture was designed in compliance with ASTM D790 and ASTM D2990 standards. The loading nose and supports had cylindrical surfaces with radii of 5.0mm. The span between the two supports was of 50mm. The loading nose was attached to a 1kN loadcell whose crosshead was controlled by MTS TestWorks 4 software. The load cell allowed for measuring loads at ±0.1N and the crosshead's displacement was evaluated with an accuracy of 0.01mm. Rectangular samples, designed in compliance with ASTM D2990 standard (Figure 4.1b), were cut with a high precision low speed saw equipped with a diamond wafering blade.

The maximum deflection D at the middle of the sample was directly obtained from the crosshead's displacement. The flexural stress σ and strain ε were computed according to the well known formulas:

$$\sigma = \frac{3PL}{2wd^2} \tag{4.9a}$$

$$\varepsilon = \frac{6dD}{L^2} \tag{4.9b}$$

where P is the applied load, L is the span between the supports and w and d are respectively the sample's width and thickness.

Series of creep tests were performed at various temperatures using the methodology pro-

posed by Struik (1978) for short-term isothermal ageing tests to investigate the dependence of the polymer's mechanical properties to temperature, stress and physical ageing. The material was first heated to the testing temperature and then a series of creep and recovery tests were performed at increasing time intervals, with the duration of each creep tests being equal to 10% of the total ageing time (for physical ageing to be considered as constant during a creep test). It should be noted Struik recommends to initiate each test by a so-called rejuvenation period in which the material is heated slightly above its glass transition temperature for a few minutes to erase all previous ageing histories. However, such rejuvenation periods led to a severe thermal degradation for the material investigated in this study. Therefore, samples were directly heated to the test temperature without any rejuvenation period, for all tests. All the three-point bending samples were cut from the same panel and thus had the same ageing history. Furthermore, the ageing history prior to testing was assumed to have a negligible effect on mechanical properties since the panels were stored at room temperature, which is much lower than wet-$T_g - 28\,°C$.

Physical ageing was investigated at 5 temperatures, namely, wet-$T_g - 28\,°C$, wet-$T_g - 3\,°C$, wet-$T_g + 7\,°C$, wet-$T_g + 22\,°C$ and wet-$T_g + 37\,°C$. For each temperature, the tests were repeated at three stress levels, namely, $0.1\sigma_{max}$, $0.25\sigma_{max}$ and $0.5\sigma_{max}$ where σ_{max} is the ultimate stress at wet-$T_g - 28\,°C$ (obtained from the tensile tests). Each test was performed once.

The three-point bending setup and sample intrinsic thermal expansions were measured to isolate the deflection only associated to mechanical loading. Correction tests were performed at each testing temperature by submitting a sample to a small contact load of 1N. Data from one such correction test can be found in Figure 4.4. The figure shows that the initial increase in temperature is accompanied by an overall thermal expansion of the setup (which is represented by a negative crosshead's displacement). Once the test temperature was achieved, the crosshead's displacement reached a minimum before starting to increase. This increase in the crosshead's displacement can be explained by three phenomena: *i*) a creep behavior induced by the contact load of 1N; *ii*) a contraction of the polymer sample due to physical ageing as the polymer evolves towards its thermodynamic equilibrium; *iii*) a thermal expansion creep.

The correction data was subtracted from the creep and recovery data to obtain the samples deflections due to mechanical loading, leading to displacement data like that reported in Figure 4.5. It should be noted that this correction removes the crosshead's displacement due to the three phenomena explained above. In particular, it removed the volume contraction due to physical ageing. However, it does not remove the impact of physical ageing on the material's mechanical properties. This was possible since the material exhibited a linearly viscoelastic behavior in the testing range. It can be seen that increasing the test temperature leads to a much more compliant material. It can also be seen that the material does not fully

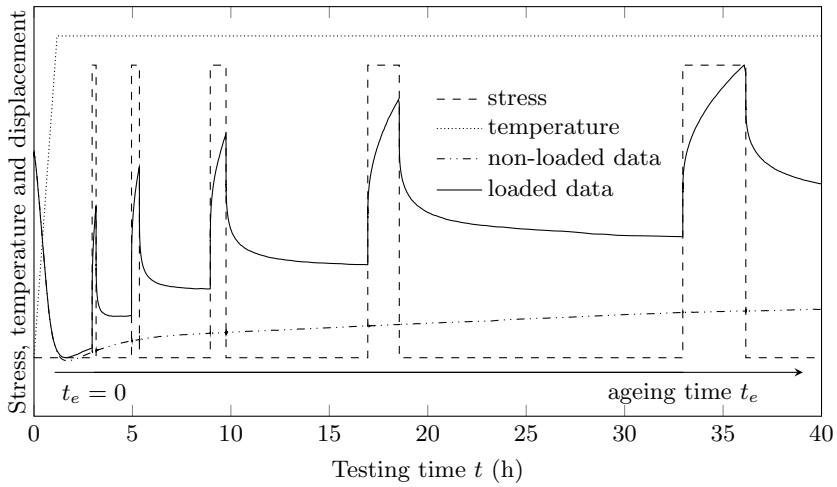

Figure 4.4: Temperature and loading histories applied to the three-point bending samples. The material was first heated at the ageing temperature, then a series of creep and recovery tests was performed at increasing time intervals. The first creep test began two hours ($t_e =$ 2h) after the ageing temperature was reached. Subsequent creep and recovery tests began at $t_e = 4$h, $t_e = 8$h, $t_e = 16$h and $t_e = 32$h. Non-loaded data, i. e. crosshead's displacement for a constant load of 1N, are used as baseline. Physical ageing was assumed to start when the testing temperature was reached inside the environmental chamber (It is denoted by $t_e = 0$ on the graph).

recover between two creep tests for higher test temperatures. Since the creep compliances are independent of the stress level, even at the higher temperatures, this phenomenon is not due to plasticity nor viscoplasticity. It can however be explained by the general increase in the material's stiffness due to physical ageing. For example, assume a viscoelastic material with one inverted retardation time λ_1 aged at constant temperature and with an ageing shift rate $\mu = 1$. The material is submitted to a creep-recovery test. The creep duration is t_1. Then, it can be shown that the recovery strain is:

$$\begin{aligned} \boldsymbol{\varepsilon}\left(t > t_1\right) &= \bar{\mathbf{S}}^{(1)} : \boldsymbol{\sigma} \exp\left(-\lambda_1 \bar{t_e}\left[\ln t - \ln t_1\right]\right)\left[1 - \exp\left(-\lambda_1 \bar{t_e}\left[\ln t_1 - \ln 0\right]\right)\right] \\ &\approx \bar{\mathbf{S}}^{(1)} : \boldsymbol{\sigma} \exp\left(-\lambda_1 \bar{t_e}\left[\ln t - \ln t_1\right]\right) \end{aligned} \tag{4.10}$$

Therefore, the smaller the quantity $\lambda_1 \bar{t_e}$ is, the longer the recovery strain requires to dissipate. As physical ageing increases, λ decreases, which explains why at higher temperatures, the material needs longer times to recover and residual strains build-up.

Figure 4.6 shows the creep compliance curves for the material for an ageing time of 32h at wet-$T_g + 37\,°$C and the three stress levels. This result is typical of what was obtained after various ageing times and at various temperature, and confirms that, in the range of stress

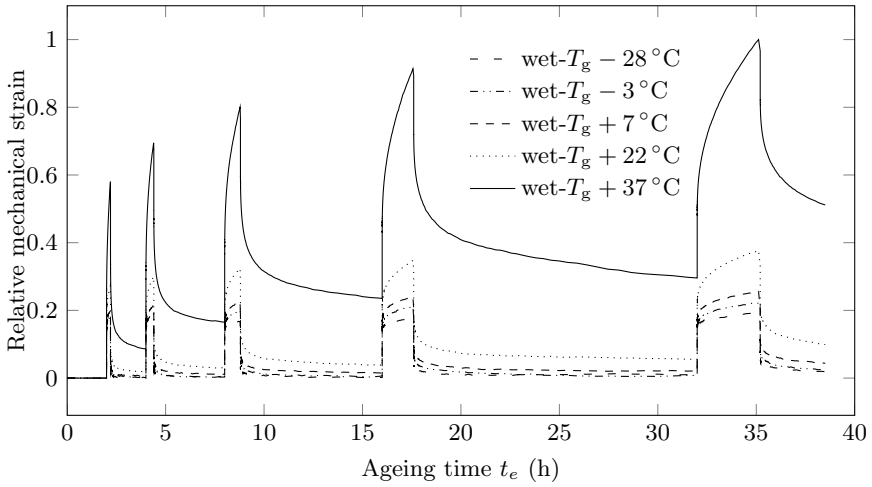

Figure 4.5: Corrected creep and recovery data, i. e. thermal strains have been removed using the correction data, for the five testing temperatures. The first creep test begins two hours ($t_e = 2$h) after the ageing temperature is reached. Subsequent creep and recovery tests begin at $t_e = 4$h, $t_e = 8$h, $t_e = 16$h and $t_e = 32$h.

and temperature used in the three-point bending tests, the material can be considered as linearly viscoelastic.

4.5 Results analysis

4.5.1 Model developments

Experimental data from tensile as well as three-point bending tests have shown that the material is linearly viscoelastic (with respect to stresses) and that its Poisson's ratio ν can be assumed as time-independent. Therefore, the three-dimensional compliance $\bar{\mathbf{S}}(t)$ can be reduced to:

$$\bar{\mathbf{S}}(t) = \bar{S}(t) \begin{pmatrix} 1 & -\nu & -\nu & 0 & 0 & 0 \\ -\nu & 1 & -\nu & 0 & 0 & 0 \\ -\nu & -\nu & 1 & 0 & 0 & 0 \\ 0 & 0 & 0 & 1+\nu & 0 & 0 \\ 0 & 0 & 0 & 0 & 1+\nu & 0 \\ 0 & 0 & 0 & 0 & 0 & 1+\nu \end{pmatrix} \tag{4.11}$$

Since the material is considered as linearly viscoelastic, $\frac{\mathrm{d}\gamma(t)}{\mathrm{d}\boldsymbol{\sigma}} = 0$ in Equation (4.7). Therefore, $\gamma(t)\mathbf{I}$ can be reduced to a scalar and the fourth order tensor $\mathbf{G}_1$ becomes the scalar g_1 and the three-dimensional constitutive theory of Equation (4.4) can be reduced to an unidimensional expression. Furthermore, Bradshaw et Brinson (1999) showed that, in the case of a linearly

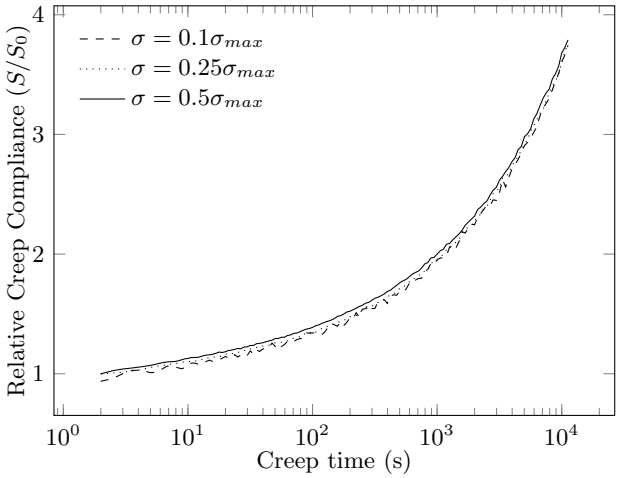

Figure 4.6: Relative creep compliance curves for the material for an ageing time of 32h at wet-$T_g + 37\,°C$ and three stress levels.

viscoelastic material submitted only to temperature and physical ageing, g_0 and g_1 could be set as equal and g_2 could be set to unity. Previous studies (Sullivan *et al.*, 1993; Bradshaw et Brinson, 1999) have shown that g_0 could generally be considered as independent of physical ageing without any loss of accuracy. All those considerations led to the following model for the material studied:

$$\varepsilon(t) = g_0(T)\left[\bar{S}^{(0)}\sigma(t) + \sum_{n=1}^{N}\bar{S}^{(n)}\int_0^t\left(1-\exp\left[-\bar{\lambda}_n(\Omega-\Omega')\right]\right)\frac{\mathrm{d}\sigma(\tau)}{\mathrm{d}\tau}\mathrm{d}\tau\right] \tag{4.12}$$

where

$$\Omega = \int_0^t \frac{\mathrm{d}t'}{a_T a_{t_e}} \tag{4.13}$$

The challenge lies in the determination of the temperature and physical ageing dependence of the nonlinearizing functions g_0, a_T and a_{t_e}.

4.5.2 Optimization algorithm

The optimization made use of the three point bending short-term isothermal ageing test data at different temperatures. The reference state was chosen as $\bar{T}$ = wet-$T_g + 37\,°C$ and $\bar{t_e} = 32$h. The inverted relaxation times were fixed prior to the optimization with one time by decade on a logarithmic scale as:

$$\bar{\lambda}_n \in \left\{10^{-6}\mathrm{s}^{-1}, ..., 10^{1}\mathrm{s}^{-1}\right\} \tag{4.14}$$

The optimization of the material's properties was performed using the minimization algorithm `fmincon` from Matlab's optimization toolbox. The optimization problem solved by this function can be written as:

$$\min_{x} \left(\sum_{i=1}^{I} \sum_{j=1}^{N_i} \left[F_{i,j} - \varepsilon_{i,j}(x) \right]^2 \right) \tag{4.15}$$

where $F_{i,j}$ and $\varepsilon_{i,j}$ are the experimental and predicted values for the j^{th} data-point from the i^{th} data-set, respectively. N_i is the number of data-points for the i^{th} data-set, I is the number of data-sets (one for each temperature tested) and x is the set of material's parameters to be optimized.

Numerical implementation

The predicted values $\varepsilon_{i,j}(x)$ of the model presented in Equation (4.12) were computed using the differential approach proposed by Crochon *et al.* (2010). This approach relies on the differential equations that are at the root of Schapery's hereditary integral and solves them with a Backward-Euler finite-difference scheme. Adapted to Equation (4.12), this approach leads to:

$$\varepsilon_{i,j+1} = g_{0_{i,j+1}} \left[S^{(0)} \sigma_{i,j+1} - \boldsymbol{A}^{(2)} \cdot \boldsymbol{\xi}_{i,j+1} \right] \tag{4.16}$$

where $\boldsymbol{\xi}$ is the tensor of internal variables defined as

$$\boldsymbol{\xi}_{i,j+1} = \left[\boldsymbol{I} + \frac{\Delta t_{i,j}}{a_{T_{i,j+1}} a_{t_{e_{i,j+1}}}} \boldsymbol{A}^{(3)} \right]^{-1} \cdot \left[\boldsymbol{\xi}_{i,j} - \frac{\Delta t_{i,j}}{a_{T_{i,j+1}} a_{t_{e_{i,j+1}}}} \sigma_{i,j+1} \boldsymbol{A}^{(2)} \right] \tag{4.17}$$

where $\boldsymbol{A}^{(2)}$ is the $1 \times N$ matrix $\left[\sqrt{\lambda_1 S^{(1)}}, ..., \sqrt{\lambda_n S^{(n)}}, ..., \sqrt{\lambda_N S^{(N)}} \right]$, $\boldsymbol{A}^{(3)}$ is the $N \times N$ matrix

$$\boldsymbol{A}^{(3)} = \begin{pmatrix} \lambda_1 & & & \\ & ... & & \\ & \lambda_n & & \\ & & ... & \\ & & & \lambda_N \end{pmatrix} \tag{4.18}$$

and $\boldsymbol{I}$ is the $N \times N$ identity matrix. $\Delta t_{i,j}$ is the time interval between j^{th} and $j+1^{\text{th}}$ data-points.

Extension to non-isothermal ageing

Non-isothermal ageing histories were accounted for by computing an equivalent ageing time, t_e^{equ}, used to obtain the ageing shift factor following the relationship:

$$a_{t_{e_{i,j}}} = \left(\frac{t_{e_{i,j}}^{equ}}{\bar{t}_e} \right)^{\mu_{i,j}} \tag{4.19}$$

where t_e^{equ} represents the time the material needs to spend under isothermal conditions to achieve the same ageing shift factor a_{t_e} as in the complex thermal history. For example, if a material is aged for a time t_1 at a temperature T_1 before being aged for a time t_2 at a temperature T_2, t_e^{equ} is the time the material would have to be isothermally aged at temperature T_2 to achieve the same ageing shift factor a_{t_e}. In this simple case, t_e^{equ} can be decomposed into two parts:

$$t_{e_{i,j}}^{equ} = t_{T_1 \to T_2} + t_{i,j} - t_1 \tag{4.20}$$

where $t_{T_1 \to T_2}$ is the time the material would have to spend at temperature T_2 to achieve the same amount of ageing as when aged at temperature T_1 for a time t_1. Since, the ageing shift rate μ is considered as temperature-independent, $t_{T_1 \to T_2}$ can be easily computed according to:

$$t_{T_1 \to T_2} = \frac{\mu(T_1)}{\mu(T_2)} t_1 \tag{4.21}$$

If a more complex thermal history was considered, for example the material was maintained at temperature T_0 for a time t_0 before being suddenly heated to temperature T_1 (the time to heat the material from T_0 to T_1 is considered negligible), then an equivalent time would have to be computed for t_1 in Equation (4.21). Therefore, if a material was submitted to N consecutive thermal steps, its equivalent ageing time can be computed using the following relationship:

$$t_e^{equ} = t_{T_{N-1} \to T_N} + t_{i,j} - t_{N-1} \tag{4.22}$$

where t_{N-1} is the time elapsed before the material was heated at the final temperature T_N ($t_{i,j} - t_{N-1}$ is the time elapsed since the last temperature jump) and $t_{T_{N-1} \to T_N}$ is defined following Equation (4.21). This procedure was use in conjunction with Equation (4.17) to predict the material's response under non-isothermal ageing histories.

Optimization results

A first optimization was performed in which the horizontal shift factor a_{t_e} was defined following the definition proposed in Equation (4.3). In this case, the material's parameters to be optimized were the reference viscoelastic parameters, $\bar{S}^{(0)}$, $\bar{S}^{(n)}$ and $\bar{\lambda}_n$ and the discrete

values of $\mu(T)$, $a_T(T)$ and $g_0(T)$

The results of this first optimization can be found in Figures 4.7 to 4.10. An excellent agreement between predicted and experimental data was obtained for the creep and the recovery phases, for all temperatures. Those results support the assumption of g_0 being independent of physical ageing. Analysis of the results shows that, in the range of temperature investigated, the shift rate linearly increases with temperature. Furthermore, the optimization led to $\mu = 0$ at the lowest temperature, meaning that no physical ageing is occuring that far from the glass transition temperature. Simultaneously, the shift factor a_T exhibits an exponential shape while g_0 is constant for the lowest temperatures before abruptly increasing.

The second step of the optimization process aimed at determining the temperature-dependent functions for μ, a_T and g_0. Based on the punctual values obtained in the first optimization run, the following functions

$$\mu(T) = \mu_0 + \mu_1 \left(T - \bar{T}\right) \tag{4.23a}$$

$$a_T(T) = \exp\left[-a_0 \left(T - \bar{T}\right)^{a_1}\right] \tag{4.23b}$$

$$g_0(T) = 1 + b_0 \mathrm{atan}\left[b_1 \left(T - \bar{T}\right)\right] \tag{4.23c}$$

where μ_1, a_0, a_1, b_0 and b_1 are material parameters, were postulated and whose parameters were optimized with the same procedure as before. μ_0 was defined such as $\mu(\text{wet-}T_\text{g}+37\,^\circ\text{C})= 0$. The choice of the arctangent function to represent the temperature dependence of g_0 was motivated by the fact that it best represents the temperature-dependent behaviour of polymers since it is bounded for arguments converging towards $\pm\infty$, i.e. for temperatures far from the glass transition temperature, while also exhibiting a monotonic behaviour.

The results of this second step in the optimization process can be found in Figures 4.7 to 4.10 and the parameters are recapitulated in Tables 4.1 and 4.2. In overall, every function fits the results of the initial optimization.

4.5.3 Validation of the model with a complex thermo-mechanical history

The model proposed above was validated by submitting the material to complex thermo-mechanical histories and comparing the experimental data to the model predictions. The

Table 4.1: Values of the normalized viscoelastic parameters.

n	0	1	2	3	4	5	6	7	8
$\lambda_n(\text{s}^{-1})$	–	10^{-6}	10^{-5}	10^{-4}	10^{-3}	10^{-2}	10^{-1}	10^{0}	10^{1}
$S^{(n)}$	1	31.9191	10.5949	1.0544	0.7931	0.2653	0.1737	0.0470	0.0416

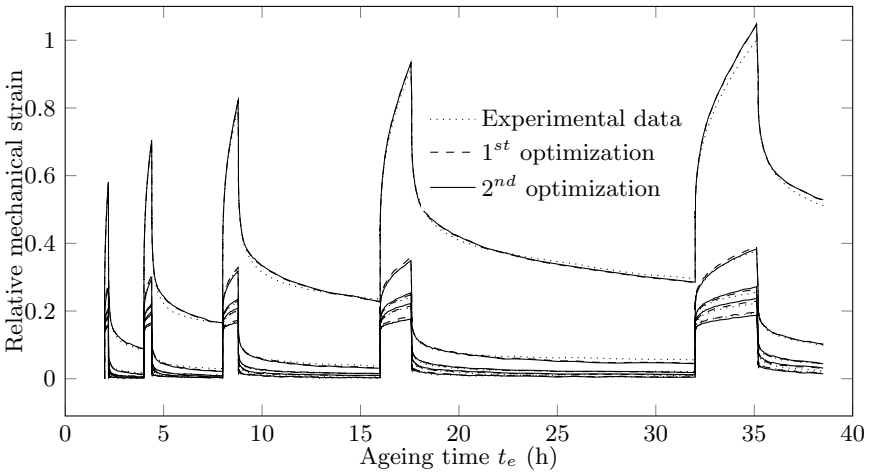

Figure 4.7: Modeling of the material behaviour using a Schapery-type constitutive theory with nonlinearizing functions depending on temperature and physical ageing. The model shows an excellent fit with the experimental data for each temperature. The experimental data is represented with dotted lines, predictions of the 1^{st} optimization with dashed lines and predictions of the 2^{nd} optimization with solid lines.

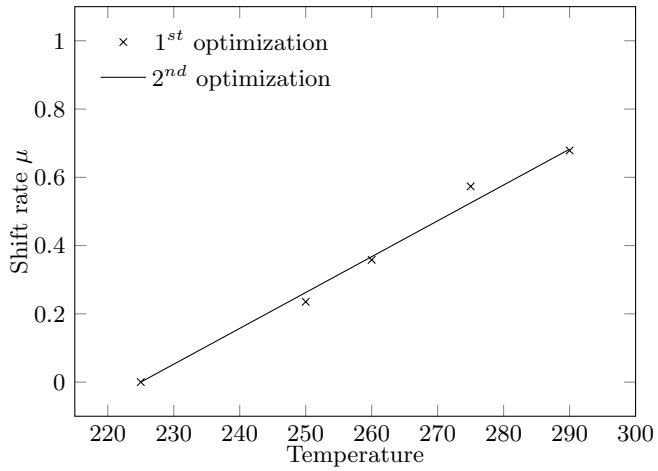

Figure 4.8: Evolution of the shift rate μ with respect to ageing temperature and physical ageing time. 1^{st} optimization values represent the results obtained without representing μ as a function while 2^{nd} optimization represents the results obtained for Equation (4.23a).

Table 4.2: Values of the material parameters for μ, a_T and g_0 obtained after the 2^{nd} optimization.

μ_0	μ_1	a_0	a_1	b_0	b_1
0.6825	0.0105	0.4631	0.6316	0.1285	−0.0661

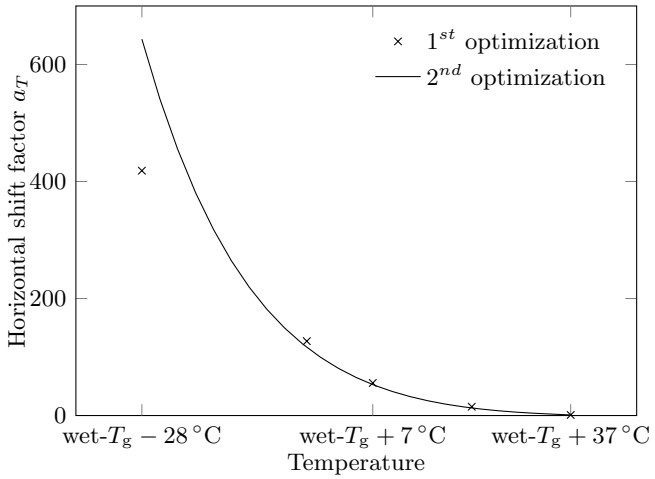

Figure 4.9: Evolution of the temperature-dependent horizontal shift factor a_T. 1^{st} optimization values represent the results obtained without representing a_T as a function while 2^{nd} optimization represents the results obtained for Equation (4.23b). $\bar{T}$ =wet-$T_g + 37\,°C$, therefore a_T(wet-$T_g + 37\,°C$)= 1

.

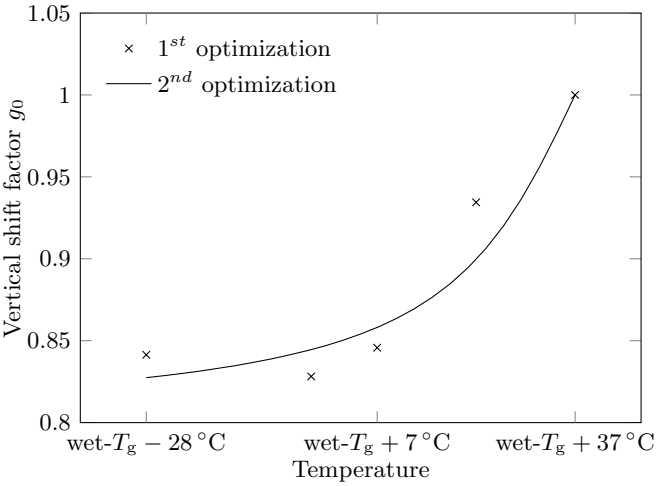

Figure 4.10: Evolution of the temperature-dependent vertical shift factor g_0. 1^{st} optimization values represent the results obtained without representing g_0 as a function while 2^{nd} optimization represents the results obtained for Equation (4.23c)

material was submitted to series of temperature up- and down-jumps, as well as three-point bending creep tests (see Figure 4.11). As for the isothermal tests, initial tests with only the thermal histories and a constant load were performed. The results of these tests were subtracted to the results of the tests with the loading histories.

Figure 4.11 shows the two complex thermo-mechanical histories imposed on the samples, while Figure 4.12 reports the experimental as well as the predicted strains. The predicted strains were represented for 4 different models: *i*) a simple viscoelastic model; *ii*) a viscoelastic model including temperature effects; *iii*) a viscoelastic model including ageing effects; *iv*) a viscoelastic model including temperature and physical ageing effects. Figure 4.12 shows that the model including temperature and physical ageing effects predicts the experimental data the best for the two independent thermo-mechanical load histories. In particular, the model predicts two behaviors related to temperature changes in Figure 4.12a: *i*) at $t \sim 13.5$h, the temperature was increased from wet-$T_g - 28\,^\circ$C to wet-$T_g + 37\,^\circ$C, which led to an increased compliance and full recovery of the remaining strain; *ii*) at $t \sim 16$h, the temperature was decreased from wet-$T_g + 37\,^\circ$C to wet-$T_g - 3\,^\circ$C while the creep stress was maintained. The material became much stiffer and the creep strain did not increase anymore. Both phenomena are very well predicted by the model. For the second complex thermo-mechanical history of Figure 4.12b, the results do not fit the experimental data with as good accuracy as in Figure 4.12a for the lower temperatures. However, the overall fit remains very good and the main features are captured.

4.6 Conclusions

The main objective of this work was to propose a model for representing the effect of physical ageing on the viscoelastic behaviour of MVK-10 polymide over a wide range of temperatures. The material was submitted to a series of creep and recovery tests at various temperatures. The model proposed is based on the constitutive theories proposed by Schapery. The principal conclusions are as follows:

1. The material was found to be linearly viscoelastic with respect to stress over the range of temperatures, ageing times and creep stresses studied.
2. The Poisson's ratio was found to be independent of time. Therefore, the 3D viscoelastic model could be simplified to a 1D model with a constant Poisson's ratio.
3. The model led to an excellent fit of the isothermal creep data at various temperatures. Moreover, the model was validated with complex thermo-mechanical histories. An equivalent ageing time was defined to account for the non-isothermal histories. The predicted data fitted the experimental data very well.

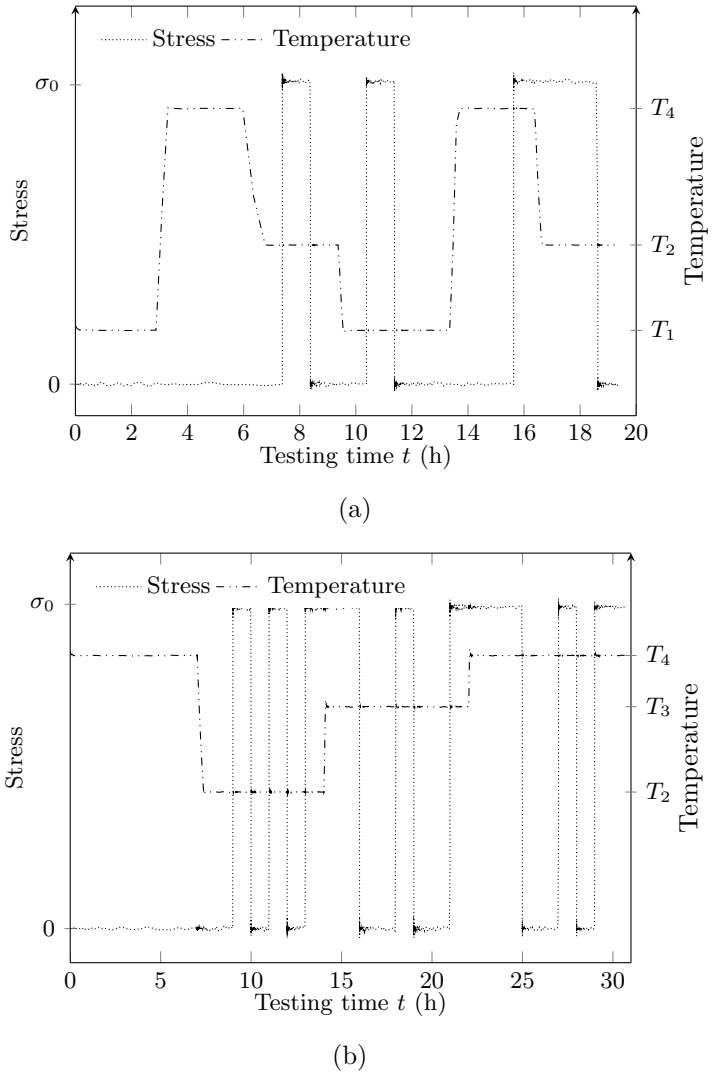

Figure 4.11: Complex thermo-mechanical histories used to validate the model. The material is submitted to series of temperature up- and -down-jumps as well as creep tests. Temperatures T_1, T_2, T_3 and T_4 correspond to wet-$T_g - 28\,°C$, wet-$T_g - 3\,°C$, wet-$T_g + 22\,°C$ and wet-$T_g + 37\,°C$, respectively.

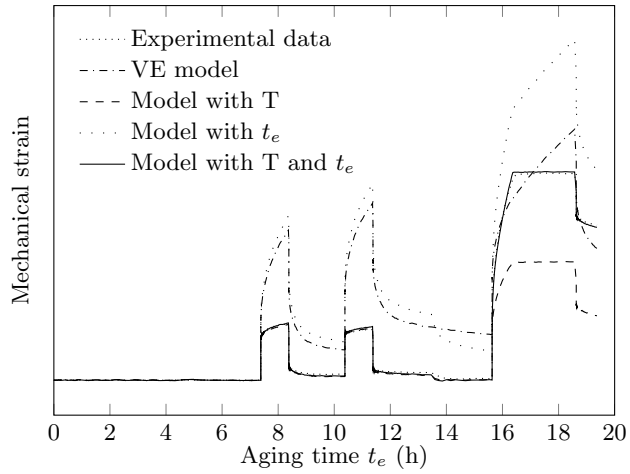

(a)

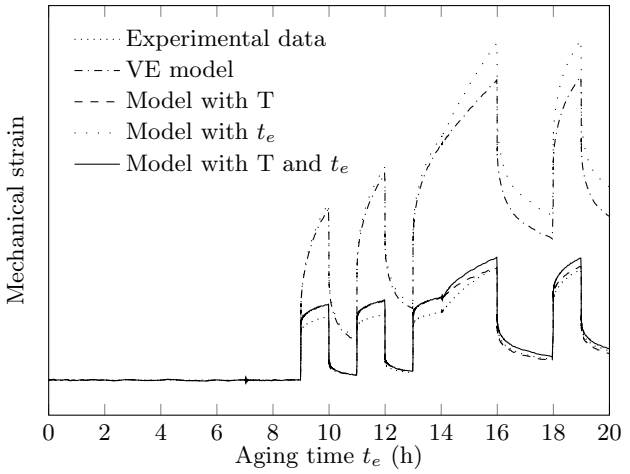

(b)

Figure 4.12: Experimental data and model predictions for the mechanical strains obtained with the complex thermo-mechanical histories presented in Figure 4.11. VE model, Model with T, Model with t_e and Model with T and t_e represents the model predictions with a simple viscoelastic model, a viscoelastic model including temperature effects, a viscoelastic model with physical ageing effects and a viscoelastic model including temperature and physical ageing effects, respectively.

CHAPTER 5

ARTICLE 3: On finite-element implementation strategies of Schapery-type constitutive theories

T. Crochon, T. Schönherr, C. Li, M. Lévesque (2010). *Mechanics of Time-Dependent materials* 14, pp. 359 - 387.

5.1 Abstract

This paper presents two new strategies for implementing Schapery-type nonlinearly viscoelastic constitutive theories into finite element codes. The first strategy uses the original differential equations that lead to the integral formulation of Schapery-type constitutive theories and Finite Difference (FD) schemes. This strategy is quite different from all the other strategies found in the literature. The second strategy is an improvement of recursive strategies, used by many authors, based on the integral formulation of the constitutive theory. The performances of the new algorithms are compared with those of existing strategies for various load histories and nonlinearities. It is shown that the newly developed strategy based on FD schemes can exhibit quadratic convergence rate when one time step is stored and 4th order convergence rate when two time steps are stored, which is a major improvement over the recursive strategies.

5.2 Introduction

Since their first introduction, Schapery's constitutive theories (Schapery, 1964) have become widely used in the scientific literature to model the response of a time-dependent material. These theories, based upon the thermodynamics of irreversible processes, have been developed for fully anisotropic nonlinearly viscoelastic materials in a number of journal papers over the last forty years. The last revision and update can be found in Schapery (1997).

Although developed as a set of differential equations in Schapery (1964), Schapery's constitutive theories have mainly been used in their hereditary integral shape that can be found in Schapery (1969b). Generally speaking, using an integral-type viscoelastic constitutive theory into a Finite Element (FE) package requires storage of the loading history for all time-steps, which can be prohibitive. A number of FE implementation strategies have been developed in order to bypass this difficulty. Expressing the compliance under the form of a

power law function [1] (Tuttle et Brinson, 1986; Zhang et Tsai, 1994) or Prony series (Taylor *et al.*, 1970; Henriksen, 1984; Lai et Bakker, 1996; Beijer et Spoormaker, 2002; Haj-Ali et Muliana, 2004) and introducing a recursive expression to numerically solve the hereditary integral (aka: recursive strategies) or going back to a set of differential equations (Touati et Cederbaum, 1998; Poon et Ahmad, 1998, 1999) and using a Finite-Difference (FD) scheme (aka: differential strategies) are two different strategies that have been studied for the linearly and nonlinearly viscoelastic materials alike. These approaches result in the development of incremental models, meaning that a relationship is defined between the solutions of the constitutive theories at successive time-steps. These incremental models only requires that some variables computed at a finite number of time-steps be stored instead of the whole load history, which is a major improvement.

Most of the strategies quoted above have been developed for isotropic materials (Henriksen, 1984; Lai et Bakker, 1996; Beijer et Spoormaker, 2002; Haj-Ali et Muliana, 2004). However, some authors have developed strategies for more complex material symmetries. Zocher et Groves (1997) and Sawant et Muliana (2008) used orthotropic media while Poon et Ahmad (1998, 1999) developed their method for fully anisotropic materials.

To the knowledge of the authors, all the FE implementation strategies developed in the literature were derived from the hereditary integral shape of Schapery's constitutive theories (even differential strategies such as the strategy of Poon et Ahmad (1998, 1999). In this paper, a completely new differential strategy is introduced. This strategy is based on the set of differential equations (Schapery, 1964, 1966a, 1997) - that has been overlooked for many decades - leading to the integral shape (Schapery, 1969b). This strategy leads to an incremental formulation developed from FD schemes such as the Backward-Euler or Crank-Nicolson schemes.

This paper is organized as follows: Section 5.3 recalls the developments of Schapery's constitutive theories and of the various FE implementation strategies that can be found in the literature; Section 5.4 introduces a new FE implementation strategy developed from Schapery's differential equations. Furthermore, a new recursive algorithm is proposed as well. Since Schapery's constitutive theories have been developed for any kind of material symmetry, the strategies proposed in this paper can be applied to fully anisotropic materials. The performances of these two new strategies are compared with the performances of other strategies and the results are analyzed in section 5.5.

In this paper, the summation of repeated indices is adopted, unless otherwise specified. Stresses or strains and stiffnesses or compliances are represented as vectors and matrices,

1. We recall that a power law can be obtained when the retardation times are in fact a continuous spectrum (See Bouleau (1992) for details).

according to the modified Voigt notation that is recalled in Lévesque *et al.* (2008). A vector is denoted by a boldfaced lower case letter, i.e., $\boldsymbol{a}$ and $\boldsymbol{\alpha}$) and a matrix is denoted by a boldfaced capital Roman letter, i.e., $\mathbf{A}$.

5.3 Background

5.3.1 On the development of Schapery's constitutive theories

This section recalls the main equations of Schapery's constitutive theories. The reader can find the complete development that leads to Schapery's theories in Schapery (1997) or Lévesque *et al.* (2008).

In thermodynamics, it is assumed that the state of a material can be fully characterized by state functions of state variables. State variables can be divided into observable variables which can be measured by experiments (mass, volume,...) and hidden variables which are associated with immeasurable phenomena (atomic structure, cracks,...).

Schapery's theories have been developed for cases where strains are applied and stresses obtained (Schapery, 1966a,b) and vice versa (Schapery, 1969a). If it is assumed that strains $\boldsymbol{\varepsilon}$ (or stresses $\boldsymbol{\sigma}$ in the case of a stress-based constitutive theory) are the observable state variables whereas $\boldsymbol{\chi}$ (or $\boldsymbol{\xi}$) represents the hidden state variables, then the application of the first and second principles of thermodynamics [2] leads to the differential equations

$$p_1(\boldsymbol{\varepsilon})B_{rs}^{(\chi)}\dot{\chi}_s + p_2(\boldsymbol{\varepsilon})L_{rs}^{(3)}\chi_s + p_3(\boldsymbol{\varepsilon})L_{jr}^{(2)}\varepsilon_j = 0 \tag{5.1a}$$

$$a_1(\boldsymbol{\sigma})B_{rs}^{(\xi)}\dot{\xi}_s + a_2(\boldsymbol{\sigma})A_{rs}^{(3)}\xi_s + a_3(\boldsymbol{\sigma})A_{jr}^{(2)}\sigma_j = 0 \tag{5.1b}$$

and to the constitutive equations

$$\sigma_i(t) = p_4(\boldsymbol{\varepsilon})L_{ij}^{(1)}\varepsilon_j + \left(\frac{\partial p_3(\boldsymbol{\varepsilon})}{\partial \varepsilon_i}L_{js}^{(2)}\varepsilon_j + p_3(\boldsymbol{\varepsilon})L_{is}^{(2)}\right)\chi_s \tag{5.2a}$$

$$\varepsilon_i(t) = -a_4(\boldsymbol{\sigma})A_{ij}^{(1)}\sigma_j - \left(\frac{\partial a_3(\boldsymbol{\sigma})}{\partial \sigma_i}A_{js}^{(2)}\sigma_j + a_3(\boldsymbol{\sigma})A_{is}^{(2)}\right)\xi_s \tag{5.2b}$$

where $a_z(\boldsymbol{\sigma}) > 0$ and $p_z(\boldsymbol{\varepsilon}) > 0$ are nonlinearizing functions implicitly introduced in Schapery (1964). $\mathbf{B}^{(\chi)}$ and $\mathbf{B}^{(\xi)}$ are positive semi-definite matrices defined by

$$\frac{\partial \Psi}{\partial \chi_r} = -p_1(\boldsymbol{\varepsilon})B_{rs}^{(\chi)}\dot{\chi}_s \tag{5.3a}$$

2. In this work, for simplification purposes, the loading history is assumed to be isothermal and adiabatic.

$$\frac{\partial G}{\partial \xi_r} = -a_1(\boldsymbol{\sigma}) B_{rs}^{(\xi)} \dot{\xi}_s \tag{5.3b}$$

where Ψ and G are Helmholtz's and Gibbs' free energies. The internal matrices $\mathbf{A}^{(1)}$, $\mathbf{A}^{(2)}$ and $\mathbf{A}^{(3)}$ are obtained using a Taylor expansion of G around its reference state (Lévesque *et al.*, 2008) and

$$\mathbf{A}^{(1)} = A_{ij}^{(1)} = \frac{\partial^2 G}{\partial \sigma_i \partial \sigma_j} \tag{5.4a}$$

$$\mathbf{A}^{(2)} = A_{ir}^{(2)} = \frac{\partial^2 G}{\partial \sigma_i \partial \xi_r} \tag{5.4b}$$

$$\mathbf{A}^{(3)} = A_{rs}^{(3)} = \frac{\partial^2 G}{\partial \xi_r \partial \xi_s} \tag{5.4c}$$

Similarly, $\mathbf{L}^{(1)}$, $\mathbf{L}^{(2)}$ and $\mathbf{L}^{(3)}$ are obtained using a Taylor expansion of Ψ around its reference state.

Equations (5.1a) and (5.2a) are strain-based since strains are applied and stresses obtained whereas Equations (5.1b) and (5.2b) are stress-based. Equations (5.1) are called evolution equations and solving for $\boldsymbol{\chi}$ and $\boldsymbol{\xi}$ leads to the explicit constitutive theories in Equations (5.2).

In order to solve Equations (5.1), Schapery (1964) has introduced the so-called reduced-times

$$\Phi = \int_0^t \frac{p_2(\tau)}{p_1(\tau)} \mathrm{d}\tau = \int_0^t \frac{1}{p_\varepsilon(\tau)} \mathrm{d}\tau \tag{5.5a}$$

$$\Omega = \int_0^t \frac{a_2(\tau)}{a_1(\tau)} \mathrm{d}\tau = \int_0^t \frac{1}{a_\sigma(\tau)} \mathrm{d}\tau \tag{5.5b}$$

After some mathematical manipulations (more details can be found in Lévesque *et al.* (2008)), the constitutive theories (5.2) for nonlinearly viscoelastic materials can be expressed as the hereditary integrals

$$\sigma_i(t) = \frac{\partial \phi}{\partial \varepsilon_i} + \left(\frac{\partial p_3}{\partial \varepsilon_i} \varepsilon_j + p_3 \delta_{ij} \right) \int_0^t \Delta C_{jk} \left(\Phi - \Phi' \right) \frac{\mathrm{d}}{\mathrm{d}\tau} \left[\frac{p_3(\tau)}{p_2(\tau)} \varepsilon_k(\tau) \right] \mathrm{d}\tau \tag{5.6a}$$

$$\varepsilon_i(t) = \frac{\partial \varphi}{\partial \sigma_i} + \left(\frac{\partial a_3}{\partial \sigma_i} \sigma_j + a_3 \delta_{ij} \right) \int_0^t \Delta S_{jk} \left(\Omega - \Omega' \right) \frac{\mathrm{d}}{\mathrm{d}\tau} \left[\frac{a_3(\tau)}{a_2(\tau)} \sigma_k(\tau) \right] \mathrm{d}\tau \tag{5.6b}$$

where δ_{ij} is Kronecker's delta and ϕ and φ are respectively the strain and stress energy functions associated with nonlinearly elastic materials. $\Delta\mathbf{C}$ and $\Delta\mathbf{S}$ are the transient stiffness

and compliance matrices which can be expressed as

$$\Delta C_{jk}(t) = \sum_{m=1}^{M} C_{jk}^{(m)} \exp\left[-\omega_m t\right] \tag{5.7a}$$

$$\Delta S_{jk}(t) = \sum_{m=1}^{M} S_{jk}^{(m)} \left(1 - \exp\left[-\lambda_m t\right]\right) \tag{5.7b}$$

where ω_m are the so-called inverted relaxation times and λ_m are the so-called inverted retardation times. $\mathbf{C}^{(m)}$ and $\mathbf{S}^{(m)}$ are positive definite and symmetric matrices.

It is important to note that the equations introduced above are not restricted to any material symmetry or nonlinearizing functions shapes. Moreover, they have been developed for uni-dimensional, bi-dimensiomal as well as for three-dimensional representations. In literature, however, some three-dimensional equations were directly derived from the well-known stress-based uni-dimensional Schapery's constitutive theory (Schapery, 1969b)

$$\varepsilon(t) = g_0 S^{(0)} \sigma(t) + g_1 \int_0^t \Delta S \left(\Omega - \Omega'\right) \frac{\mathrm{d}}{\mathrm{d}\tau} \left[g_2 \sigma(\tau)\right] \mathrm{d}\tau \tag{5.8}$$

by introducing tensors instead of scalars for the elastic and linearly viscoelastic properties

$$\varepsilon_i(t) = g_0 S_{ij}^{(0)} \sigma_j(t) + g_1 \int_0^t \Delta S_{ij} \left(\Omega - \Omega'\right) \frac{\mathrm{d}}{\mathrm{d}\tau} \left[g_2 \sigma_j(\tau)\right] \mathrm{d}\tau \tag{5.9}$$

where g_0, g_1 and g_2 are nonlinearizing functions and $\mathbf{S}^{(0)}$ is the elastic compliance matrix.

The difference between the three-dimensional theories (5.6b) and the constitutive theory (5.9) is that the nonlinearizing function in front of the integral is a matrix in (5.6b) and a scalar in (5.9) respectively. This generalization is done without any thermodynamics backing and does not guarantee that the thermodynamics principles are met for all loading histories. Therefore, the strategies developed in this paper are only developed for thermodynamically admissible three-dimensional constitutive theories.

5.3.2 On the problem of FE implementation

As introduced in Section 5.2, incremental models have to be developed in order to implement Schapery's constitutive theories into FE software. Using an incremental model requires the time-interval $[0, T]$ in which the material behavior is studied to be discretized into a finite number N of time-steps named t^n (which leads to $t^0 = 0$ and $t^N = T$). A time-increment $\Delta t^n = t^{n+1} - t^n$ can then be defined between two consecutive time-steps.

Two strategies to obtain incremental models stand out in the scientific literature. The

first strategy consists of numerically solving the hereditary integrals in Equations (5.6) by establishing a recursive relationship between two successive time-steps while the second strategy lies in differentiating the integral in order to find a set of differential equations that can be solved using FD schemes.

On recursive strategies

To the knowledge of the authors, Taylor *et al.* (1970) were the first to have used a recursive strategy to compute the solution of linearly viscoelastic constitutive theories expressed as hereditary integrals. To achieve that, Taylor *et al.* (1970) assumed that the load history varied linearly over the time-interval Δt^n and then divided the hereditary integral into recursive parts, thus establishing a recursive relationship between successive time-steps. Henriksen (1984) used a similar method for Schapery's constitutive theories.

To obtain these recursive relationships, Henriksen (1984) expressed the transient compliance matrix (or transient stiffness matrix) as Equation (5.7b). Equation (5.8) [3] becomes

$$\varepsilon(t^{n+1}) = \varepsilon^{n+1} = g_0^{n+1} S^{(0)} \sigma^{n+1} + g_1^{n+1} \sum_{m=1}^{M} S^{(m)} \left\{ g_2^{n+1} \sigma^{n+1} - g_2^0 \sigma^0 - q_m^{n+1} \right\} \tag{5.10}$$

where

$$q_m^{n+1} = \int_0^{t^{n+1}} \exp\left[-\lambda_m \left(\Omega^{n+1} - \Omega\right)\right] \frac{\mathrm{d}}{\mathrm{d}\tau} \left[g_2 \sigma\right] \mathrm{d}\tau \tag{5.11}$$

The hereditary integral in Equation (5.11) can be decomposed into two parts as:

$$\begin{aligned} q_m^{n+1} = & \int_0^{t^n} \exp\left[-\lambda_m \left(\Omega^{n+1} - \Omega\right)\right] \frac{\mathrm{d}}{\mathrm{d}\tau} \left[g_2 \sigma\right] \mathrm{d}\tau \\ & + \int_{t^n}^{t^{n+1}} \exp\left[-\lambda_m \left(\Omega^{n+1} - \Omega\right)\right] \frac{\mathrm{d}}{\mathrm{d}\tau} \left[g_2 \sigma\right] \mathrm{d}\tau \end{aligned} \tag{5.12}$$

As in the linearly viscoelastic case (Taylor *et al.*, 1970), two simplifying hypotheses are necessary to develop a recursive relationship from Equation (5.12). The quantity $g_2\sigma$ and the reduced-time Ω must be assumed to vary linearly with respect to τ over the time-interval Δt^n (Henriksen, 1984; Haj-Ali et Muliana, 2004). Then, Equation (5.12) leads to the recursive relationship and incremental model

$$q_m^{n+1} = q_m^n \exp\left[-\lambda_m \Delta\Omega^{n+1}\right] + \left(g_2^{n+1} \sigma^{n+1} - g_2^n \sigma^n\right) \Gamma_m^{n+1} \tag{5.13}$$

3. In this section, the constitutive theory used is expressed as per its 1D expression for simplicity. The developments presented here can be applied to 3D constitutive theories (5.6b) without difficulty. Similarly, the equations developed in this section can be adapted to the strain-based theory, assuming the same kind of simplifications.

where

$$\Delta\Omega^{n+1} = \Omega^{n+1} - \Omega^n \tag{5.14}$$

is the reduced-time increment and

$$\Gamma_m^{n+1} = \frac{1 - \exp\left[-\lambda_m \Delta\Omega^{n+1}\right]}{\lambda_m \Delta\Omega^{n+1}} \tag{5.15}$$

As for the reduced-time increment defined in (5.14), it should be noted that the hypothesis of linear variation over the time-increment Δt^n leads to the conclusion that the nonlinearizing function a_σ has to be time-independent, i.e., constant, over this time-increment (Haj-Ali et Muliana, 2004) and, therefore, Equation (5.14) becomes (for example)

$$\Delta\Omega^{n+1} = \frac{1}{a_\sigma^{n+1}}\Delta t = \frac{a_2^{n+1}}{a_1^{n+1}}\Delta t^n \tag{5.16}$$

Other similar methods can be developed with different hypotheses for the behavior of the quantity $g_2\sigma$ over the time-increment Δt. For example, Lai et Bakker (1996) only took σ as linear and considered g_2 to be constant over the time-interval which leads to

$$q_m^{n+1} = q_m^n \exp\left[-\lambda_m \Delta\Omega^{n+1}\right] + g_2^{n+1}\left(\sigma^{n+1} - \sigma^n\right)\Gamma_m^{n+1} \tag{5.17}$$

while Beijer et Spoormaker (2002) considered g_2 and σ as being both piecewise constant. Beijer et Spoormaker (2002) approach leads to

$$q_m^{n+1} = \left(q_m^n \exp\left[-\lambda_m \Delta t^n \frac{\alpha}{a_\sigma^n}\right] + g_2^{n+1}\sigma^{n+1} - g_2^n\sigma^n\right)\exp\left[-\lambda_m \Delta t^n \frac{1-\alpha}{a_\sigma^{n+1}}\right] \tag{5.18}$$

where $\alpha \in [0, 1]$.

On differential strategies

The second main strategy to the problem of Schapery-type constitutive theories implementation is to transform the hereditary integrals into a set of first order differential equations before solving them with a FD scheme. The FD scheme can range from a simple Euler Method (Zienkiewicz *et al.*, 1968; Greenbaum et Rubinstein, 1968; Poon et Ahmad, 1998, 1999) to a higher-order FD scheme such as Runge-Kutta's methods (Carpenter, 1972; Bažant, 1972).

Poon et Ahmad (1999) developed their method for the strain-based constitutive theory in the case of an anisotropic nonlinear material. Here, for the sake of consistency, their results are presented for a one-dimensional stress-based constitutive theory and for an isotropic nonlinear material. To determine their set of differential equations, Poon et Ahmad (1998,

1999) differentiated the hereditary integral

$$y^t = \int_0^t f^{t,\tau} d\tau \tag{5.19}$$

where $f^{t,\tau} = f(t,\tau)$. Using δt to note an infinitesimal variation in time, Poon et Ahmad (1999) obtained the differentiation formula

$$y^{t+\delta t} - y^t \approx f^{t,t}\delta t + \frac{\partial}{\partial t} f^{t,t}(\delta t)^2 + \delta t \int_0^t \frac{\partial}{\partial t} f^{t,\tau} \mathrm{d}\tau \tag{5.20}$$

leading to

$$\begin{aligned} \frac{\mathrm{d}y}{\mathrm{d}t} &= \lim_{\delta t \to 0} \frac{y^{t+\delta t} - y^t}{\delta t} \\ &= f^{t,t} + \int_0^t \frac{\partial}{\partial t} f^{t,\tau} \mathrm{d}\tau \end{aligned} \tag{5.21}$$

Poon et Ahmad (1999) introduced the hidden state variables y_m and defined them as

$$y_m^t = \int_0^t S^{(m)} \left(1 - \exp\left[-\lambda\left(\Omega^{t+\Delta t} - \Omega^t\right)\right]\right) \frac{\mathrm{d}}{\mathrm{d}\tau}\left[g_2^\tau \sigma^\tau\right] \mathrm{d}\tau \tag{5.22}$$

Therefore, Equation (5.22) leads to

$$f^{t,t} = 0 \tag{5.23a}$$

$$\frac{\partial}{\partial t} f^{t,\tau} = \frac{\lambda}{a_\sigma} S^{(m)} \left(\exp\left[-\lambda\left(\Omega^{t+\Delta t} - \Omega^t\right)\right]\right) \frac{\mathrm{d}}{\mathrm{d}\tau}\left[g_2^\tau \sigma^\tau\right] \tag{5.23b}$$

and

$$\begin{aligned} \frac{\mathrm{d}}{\mathrm{d}t} y_m^t &= \int_0^t \frac{\lambda}{a_\sigma} S^{(m)} \left(\exp\left[-\lambda\left(\Omega^{t+\Delta t} - \Omega^t\right)\right]\right) \frac{\mathrm{d}}{\mathrm{d}\tau}\left[g_2^\tau \sigma^\tau\right] \mathrm{d}\tau \\ &= \frac{\lambda}{a_\sigma} \int_0^t S^{(m)} \left[1 - \left(1 - \exp\left[-\lambda\left(\Omega^{t+\Delta t} - \Omega^t\right)\right]\right)\right] \frac{\mathrm{d}}{\mathrm{d}\tau}\left[g_2^\tau \sigma^\tau\right] \mathrm{d}\tau \\ &= \frac{\lambda}{a_\sigma} \left[S^{(m)}\left(g_2^t \sigma^t - g_2^0 \sigma^0\right) - y_m^t\right] \end{aligned} \tag{5.24}$$

The differential Equation (5.24) can be solved for y_m using a FD scheme, leading to an expression for y_m^{n+1}.

5.4 A new strategy to implement Schapery's constitutive theories using Schapery's differential equations

The objective in this section is to introduce a new strategy to implement Schapery-type constitutive theories for fully anisotropic nonlinearly viscoelastic material into FE packages. This strategy is based on the set of differential Equations (5.1) and constitutive Equations (5.2). It is developed here for the stress-based theory but can be easily developed for the strain-based theory as well (see Appendix 5.6). This strategy requires the full determination of the set of internal matrices introduced in Equations (5.1b) and (5.2b) using the material properties. Then a FD scheme can be used to solve the differential equations.

5.4.1 On the determination of a material's internal matrices

The objective in this subsection is to determine the aforementioned internal matrices from the material parameters. These parameters allow the compliance matrix to be expressed as Prony series (5.7).

Since, for small stresses, a material can be considered to have a linearly viscoelastic behavior, the internal matrices can be determined while considering the nonlinearizing functions as $a_z = 1$ (for $z = 1, 2, 3, 4$). The differential Equation (5.1b) becomes

$$B_{rs}^{(\xi)}\dot{\xi}_s + A_{rs}^{(3)}\xi_s + A_{jr}^{(2)}\sigma_j = 0 \tag{5.25}$$

while the constitutive Equation (5.2b) can be written

$$\varepsilon_i(t) = -A_{ij}^{(1)}\sigma_j - A_{is}^{(2)}\xi_s \tag{5.26}$$

By applying the Laplace transform [4], Equation (5.25) becomes

$$\left(pB_{rs}^{(\xi)} + A_{rs}^{(3)}\right)\widetilde{\xi}_s + A_{jr}^{(2)}\widetilde{\sigma}_j = 0 \tag{5.27}$$

$\mathbf{B}^{(\xi)}$ is a positive semi-definite and symmetric matrix and $\mathbf{A}^{(3)}$ is a positive definite symmetric matrix (Schapery, 1997; Lévesque *et al.*, 2008), therefore $p\mathbf{B}^{(\xi)} + \mathbf{A}^{(3)}$ admits an inverse matrix and reorganizing Equation (5.27) leads to

$$\widetilde{\xi}_s = -\left(pB_{rs}^{(\xi)} + A_{rs}^{(3)}\right)^{-1} A_{jr}^{(2)}\widetilde{\sigma}_j \tag{5.28}$$

4. $\widetilde{f}(p) = \mathcal{L}\left[f(t)\right] = \int_{-\infty}^{\infty} \exp\left(-pt\right) f(t)dt$

This expression of the hidden state variables can then be introduced into (5.26) which becomes

$$\widetilde{\varepsilon}_i = \left[-A_{ij}^{(1)} + A_{is}^{(2)} \left(pB_{rs}^{(\xi)} + A_{rs}^{(3)}\right)^{-1} A_{jr}^{(2)}\right] \widetilde{\sigma}_j \tag{5.29}$$

For a constant loading $\boldsymbol{\sigma}^{(0)}$, it can be shown from Equation (5.6b) that the creep response can be expressed as

$$\varepsilon_i(t) = \left[S_{ij}^{(0)} + \Delta S_{ij}\right] \sigma_j^{(0)} \tag{5.30}$$

where $\mathbf{S}^{(0)}$ is the initial compliance matrix and $\boldsymbol{\Delta}\mathbf{S}$ is the transient compliance matrix. The transient compliance matrix is written as in Equation (5.7b). By applying the Laplace transform to $\boldsymbol{\Delta}\mathbf{S}$, Equation (5.30)can be written as

$$\Delta\widetilde{S}_{ij}(p) = \mathcal{L}\left[\Delta S_{ij}(t)\right] = \frac{1}{p}\sum_{m}^{M} \frac{\lambda_m S_{ij}^{(m)}}{\lambda_m + p} \tag{5.31}$$

Applying the Laplace transform to Equation (5.30) and using Equation (5.31) lead to

$$\widetilde{\varepsilon}_i = \frac{1}{p}\left[S_{ij}^{(0)} + \sum_{m}^{M} \frac{\lambda_m S_{ij}^{(m)}}{\lambda_m + p}\right] \widetilde{\sigma}_j^{(0)} \tag{5.32}$$

For a constant loading, Equation (5.29) becomes

$$\widetilde{\varepsilon}_i = \frac{1}{p}\left[-A_{ij}^{(1)} + A_{is}^{(2)} \left(pB_{rs}^{(\xi)} + A_{rs}^{(3)}\right)^{-1} A_{jr}^{(2)}\right] \widetilde{\sigma}_j^{(0)} \tag{5.33}$$

Therefore, comparing the terms of Equation (5.32) with the terms of (5.33) leads to

$$A_{ij}^{(1)} = -S_{ij}^{(0)} \tag{5.34}$$

and

$$A_{is}^{(2)} \left(pB_{rs}^{(\xi)} + A_{rs}^{(3)}\right)^{-1} A_{jr}^{(2)} = \sum_{m}^{M} \frac{\lambda_m S_{ij}^{(m)}}{\lambda_m + p} \tag{5.35}$$

Each matrix $\lambda_m \mathbf{S}^{(m)}$ is a 6×6 positive semi-definite, symmetric matrix and admits the Cholesky decomposition

$$\lambda_m S_{ij}^{(m)} = T_{ir}^{(m)} T_{jr}^{(m)} \tag{5.36}$$

where $\mathbf{T}^{(m)}$ is a 6×6 lower triangular matrix.

It is assumed that a basis exists in which $\mathbf{A}^{(2)}$ is the $6 \times 6M$ block matrix

$$\mathbf{A}^{(2)} = \left(\mathbf{T}^{(1)}\middle|\, \mathbf{T}^{(2)}\middle|\, ... \,\middle|\mathbf{T}^{(m)}\middle|\, ... \,\middle|\mathbf{T}^{(M)}\right) \tag{5.37}$$

where M is the number of so-called inverted retardation times considered in Equation (5.7b) and where each block $\mathbf{T}^{(m)}$ is defined as in Equation (5.36) and

$$p\mathbf{B}^{(\xi)} + \mathbf{A}^{(3)} = \begin{pmatrix} [p+\lambda_1]_6 & & & & & \\ & [p+\lambda_2]_6 & & & & \\ & & \cdots & & & \\ & & & [p+\lambda_m]_6 & & \\ & & & & \cdots & \\ & & & & & [p+\lambda_M]_6 \end{pmatrix} \tag{5.38}$$

where the subscript 6 points out that $[p+\lambda_m]_6$ is a 6×6 diagonal matrix whose diagonal terms are $(p+\lambda_m)$.

If such a basis exists then Equations (5.37) and (5.38) lead to

$$\begin{aligned} A_{is}^{(2)} \left(pB_{rs}^{(\xi)} + A_{rs}^{(3)}\right)^{-1} A_{jr}^{(2)} &= \sum_m^M T_{is}^{(m)} \left(p+\lambda_m\right)_{rs}^{-1} T_{jr}^{(m)} \\ &= \sum_m^M \frac{1}{p+\lambda_m} T_{is}^{(m)} \delta_{rs} T_{jr}^{(m)} \\ &= \sum_m^M \frac{\lambda_m S_{ij}^{(m)}}{\lambda_m + p} \end{aligned} \tag{5.39}$$

which complies with Equation (5.35), thus validating the existence of the basis as well as the expressions of $p\mathbf{B}^{(\xi)} + \mathbf{A}^{(3)}$ and $\mathbf{A}^{(2)}$ assumed above.

Finally, decomposing Equation (5.38) leads to

$$\mathbf{A}^{(3)} = \begin{pmatrix} [\lambda_1]_6 & & & & & \\ & [\lambda_2]_6 & & & & \\ & & \cdots & & & \\ & & & [\lambda_m]_6 & & \\ & & & & \cdots & \\ & & & & & [\lambda_M]_6 \end{pmatrix} \tag{5.40}$$

and $\mathbf{B}^{(\xi)}$ is the $6M \times 6M$ identity matrix.

It should be noted that no hypothesis of any kind of material symmetry is necessary in order to obtain the internal matrices with the method introduced in this section. Internal matrices and compliance matrices are symmetric matrices for any kind of material symmetry. Therefore, any of the previous operations are valid for isotropic materials as well as for

anisotropic materials.

5.4.2 Notes on the differential strategies

In this paper, two differential strategies have been introduced. The strategy of Poon et Ahmad (1999), developed in Section 5.3.2, starts from Schapery's hereditary integral. A state variable, consisting of the integral, is defined and then differentiated in order to obtain a set of differential equations which can be solved using a FD scheme.

On the other hand, the strategy developed in this paper uses Schapery's differential equations introduced by Schapery (1964) and from which the hereditary integral is derived.

It can be shown that these two differential strategies give similar results. However, the method by which they are obtained is quite different. The model of Poon et Ahmad (1999) is obtained from an integral while the new model presented in this article is obtained from differential equations by defining the internal matrices. Therefore, the second strategy is a more natural differential strategy to obtain an incremental model from Schapery's constitutive theories since it originates from the basic equations that lead to the integral form. In addition, that kind of formulation is very similar to that of other nonlinear materials (plasticity, viscoplasticity, ...).

5.4.3 On the development of an incremental model

Once the internal matrices $\mathbf{B}^{(\xi)}$, $\mathbf{A}^{(1)}$, $\mathbf{A}^{(2)}$ and $\mathbf{A}^{(3)}$ have been determined, numerical constitutive models can be built using FD schemes such as Backward-Euler or Crank-Nicolson schemes. Higher order schemes such as the 4^{th} Runge-Kutta scheme can also be used, but at the expense of storing more history data.

On the Backward-Euler and Crank-Nicolson schemes

If a time interval is decomposed into N intervals ($t^0 = 0$) then (Zienkiewicz et Taylor, 1991; Beijer et Spoormaker, 2002)

$$\xi_s^{n+1} = \xi_s^n + \Delta\xi_s^n = \xi_s^n + \Delta t^n \left((1-\beta) \left.\frac{\partial \xi_s}{\partial t}\right|_n + \beta \left.\frac{\partial \xi_s}{\partial t}\right|_{n+1} \right) \tag{5.41}$$

where the value of β determines which method is used. If $\beta = 0$ the Forward-Euler scheme is used (which is not used in this paper since it is inaccurate and unstable). If $\beta = 1$ the Backward-Euler scheme is used and if $\beta = 0.5$ then the Crank-Nicolson scheme is used.

At the n^{th} step, Equation (5.1b) becomes

$$a_1^n B_{rs}^{(\xi)} \left.\frac{\partial \xi_s}{\partial t}\right|_n + a_2^n A_{rs}^{(3)} \xi_s^n + a_3^n A_{jr}^{(2)} \sigma_j^n = 0 \tag{5.42}$$

while at the $n^{\text{th}} + 1$ step, Equation (5.1b) becomes

$$a_1^{n+1} B_{rs}^{(\xi)} \left.\frac{\partial \xi_s}{\partial t}\right|_{n+1} + a_2^{n+1} A_{rs}^{(3)} \xi_s^{n+1} + a_3^{n+1} A_{jr}^{(2)} \sigma_j^{n+1} = 0 \tag{5.43}$$

where $a_z^n = a_z(\boldsymbol{\sigma}^n)$.

Since $\mathbf{B}^{(\xi)}$ is the identity matrix, Equations (5.42) and (5.43) become

$$\left.\frac{\partial \xi_s}{\partial t}\right|_n = -\frac{1}{a_1^n}\left(a_2^n A_{rs}^{(3)} \xi_s^n + a_3^n A_{jr}^{(2)} \sigma_j^n\right) \tag{5.44a}$$

$$\left.\frac{\partial \xi_s}{\partial t}\right|_{n+1} = -\frac{1}{a_1^{n+1}}\left(a_2^{n+1} A_{rs}^{(3)} \xi_s^{n+1} + a_3^{n+1} A_{jr}^{(2)} \sigma_j^{n+1}\right) \tag{5.44b}$$

Inserting Equations (5.44) into Equation (5.41), $\boldsymbol{\xi}^{n+1}$ can be expressed as

$$\begin{aligned} \xi_r^{n+1} = \left(\delta_{rs} + \beta \Delta t^n \frac{a_2^{n+1}}{a_1^{n+1}} A_{rs}^{(3)}\right)^{-1} \Bigg[& \left(\delta_{sv} - (1-\beta)\Delta t^n \frac{a_2^n}{a_1^n} A_{sv}^{(3)}\right) \xi_v^n \\ & - (1-\beta)\Delta t^n \frac{a_3^n}{a_1^n} A_{js}^{(2)} \sigma_j^n - \beta \Delta t^n \frac{a_3^{n+1}}{a_1^{n+1}} A_{js}^{(2)} \sigma_j^{n+1} \Bigg] \end{aligned} \tag{5.45}$$

Incremental scheme is obtained as follows by inserting Equation (5.45) into the constitutive theory (5.2b)

$$\varepsilon_i^{n+1} = -a_4^{n+1} A_{ij}^{(1)} \sigma_j^{n+1} - \left(\frac{\partial a_3^{n+1}}{\partial \sigma_i^{n+1}} A_{js}^{(2)} \sigma_j^{n+1} + a_3^{n+1} A_{is}^{(2)}\right) \xi_s^{n+1} \tag{5.46}$$

Therefore, in order to determine $\boldsymbol{\varepsilon}^{n+1}$, only the quantities $\boldsymbol{\sigma}^n$, $\boldsymbol{\sigma}^{n+1}$, $\boldsymbol{\varepsilon}^n$ and $\boldsymbol{\xi}^n$ need to be stored.

On the 4^{th} order Runge-Kutta scheme

Backward-Euler is a first order scheme and Crank-Nicolson is a second order scheme. However, a higher order scheme such as the 4^{th} Runge-Kutta scheme can be obtained by solving an ordinary differential equation with the FD method. Equation (5.1b) can be written

as

$$\begin{aligned}\frac{\partial \xi_r}{\partial t} &= F(\xi_s, t) \\ &= -\frac{1}{a_1(\boldsymbol{\sigma})}\left[a_2(\boldsymbol{\sigma})A^{(3)}_{rs}\xi_s + a_3(\boldsymbol{\sigma})A^{(2)}_{jr}\sigma_j\right]\end{aligned} \tag{5.47}$$

Applying the explicit 4^{th} order Runge-Kutta scheme to Equation (5.47) leads to the incremental formulation of the hidden state variables

$$\xi_s^{n+1} = \xi_s^n + \frac{\Delta t}{6}\left(k^n_{1,s} + 2k^n_{2,s} + 2k^n_{3,s} + k^n_{4,s}\right) \tag{5.48}$$

where

$$\begin{aligned}k^n_{1,s} &= F(\xi^n_s, t^n) \\ &= -\frac{1}{a_1^n}\left[a_2^n A^{(3)}_{rs}\xi^n_s + a_3^n A^{(2)}_{jr}\sigma^n_j\right]\end{aligned} \tag{5.49a}$$

$$\begin{aligned}k^n_{2,s} &= F(\xi^n_s + \frac{\Delta t}{2}k^n_{1,s}, t^{n+\frac{1}{2}}) \\ &= -\frac{1}{a_1^{n+\frac{1}{2}}}\left[a_2^{n+\frac{1}{2}} A^{(3)}_{rs}\left(\xi^n_s + \frac{\Delta t}{2}k^n_{1,s}\right) + a_3^{n+\frac{1}{2}} A^{(2)}_{jr}\sigma^{n+\frac{1}{2}}_j\right]\end{aligned} \tag{5.49b}$$

$$\begin{aligned}k^n_{3,s} &= F(\xi^n_s + \frac{\Delta t}{2}k^n_{2,s}, t^{n+\frac{1}{2}}) \\ &= -\frac{1}{a_1^{n+\frac{1}{2}}}\left[a_2^{n+\frac{1}{2}} A^{(3)}_{rs}\left(\xi^n_s + \frac{\Delta t}{2}k^n_{2,s}\right) + a_3^{n+\frac{1}{2}} A^{(2)}_{jr}\sigma^{n+\frac{1}{2}}_j\right]\end{aligned} \tag{5.49c}$$

$$\begin{aligned}k^n_{4,s} &= F(\xi^n_s + \Delta t k^n_{3,s}, t^{n+1}) \\ &= -\frac{1}{a_1^{n+1}}\left[a_2^{n+1} A^{(3)}_{rs}\left(\xi^n_s + \Delta t k^n_{3,s}\right) + a_3^{n+1} A^{(2)}_{jr}\sigma^{n+1}_j\right]\end{aligned} \tag{5.49d}$$

and $a_z^{n+\frac{1}{2}} = a_z(\sigma^{n+\frac{1}{2}})$. Then the incremental form of the hidden state variables can be introduced into Equation (5.46), leading to incremental model that can be introduced into a FE software.

5.4.4 Remarks on recursive strategies

Usage of a differential strategy enables the possibility of using high-order FD schemes which leads to a high-order convergence rate of the computed solution. However, to the knowledge of the authors, no recursive strategy exhibiting a high-order convergence rate has been developed.

When developing a recursive strategy, hypotheses on the material behavior and on the loading history are introduced. These hypotheses have an effect on the convergence rate of the strategy. Since Henriksen (1984) assumed a_σ to be constant over a time increment, his strategy exhibits a linear convergence rate (see Section 5.5).

A strategy with a quadratic convergence rate can be developed by assuming the quantity a_σ to be piecewise constant. This hypothesis leads to

$$\begin{aligned} \Delta\Omega^{n+1} &= \Omega^{n+1} - \Omega^n \\ &= \frac{\Delta t}{2}\left(\frac{1}{a_\sigma^{n+1}} + \frac{1}{a_\sigma^n}\right) \end{aligned} \tag{5.50}$$

and Equation (5.12) becomes

$$q_m^{n+1} = q_m^n \exp\left[-\lambda_m \Delta\Omega^{n+1}\right] + \left(g_2^{n+1}\sigma^{n+1} - g_2^n\sigma^n\right)\Upsilon_m^{n+1} \tag{5.51}$$

where

$$\Upsilon_m^{n+1} = \exp\left[\frac{-\lambda_m \Delta t^n}{2a_\sigma^{n+1}}\right] \frac{1 - \exp\left[\frac{-\lambda_m \Delta t^n}{2a_\sigma^n}\right]}{\frac{\lambda_m \Delta t^n}{a_\sigma^n}} + \frac{1 - \exp\left[\frac{-\lambda_m \Delta t^n}{2a_\sigma^{n+1}}\right]}{\frac{\lambda_m \Delta t^n}{a_\sigma^{n+1}}} \tag{5.52}$$

The assumption of a piecewise constant a_σ over time-increment leads to a better approximation of the reduced-time increment than the constant hypothesis introduced in Henriksen (1984). Therefore, a higher order convergence rate can be obtained for this strategy than for recursive algorithms (5.13) or (5.17).

5.4.5 On the implementation of an incremental model into the FE software ABAQUS

The FE software ABAQUS was chosen for this section since it easily allows implementation of user-defined material behavior. The only requirement is to write, in FORTRAN, a user subroutine called UMAT. At the n^{th} time-step, the subroutine is provided with the state of the material at this time-step, i.e., $\boldsymbol{\sigma}^n$, $\boldsymbol{\varepsilon}^n$ and $\boldsymbol{\xi}^n$ as well as with the strain-increment $\Delta\boldsymbol{\varepsilon}^n$ and the time-increment Δt^n. The subroutine must provide

1. The incremental scheme to update the state variables and the stresses to their values at the end of the time-increment, i.e., $\boldsymbol{\xi}^{n+1}$ and $\boldsymbol{\sigma}^{n+1}$.
2. The material Jacobian matrix $\partial\Delta\boldsymbol{\sigma}^n/\partial\Delta\boldsymbol{\varepsilon}^n$ for the mechanical constitutive model.

Only the stress-based constitutive theories are considered here. The difficulty resides in the fact that the incremental model in Equation (5.46) is a function of the stresses at the end of the time-increment. An iterative method such as the Newton-Raphson method is therefore

required in order to determine the increment of the stresses. The algorithm is decomposed into the following steps:

1. As in Haj-Ali et Muliana (2004) the FD scheme is linearized by setting

$$a_i^{n+1} = a_i^n; \quad i = 1, 2, 3, 4 \tag{5.53}$$

in order to find a trial stress-increment $\Delta\boldsymbol{\sigma}^{n,tr}$ that serves as the initial guess for the stress-increment.

For example, using the incremental model for the lower order schemes developed in Section 5.4.3 leads to

$$\begin{aligned}\Delta\sigma_i^{n,tr} = &\left[-a_4^n A_{ij}^{(1)} + \beta\Delta t^n \frac{a_3^n}{a_1^n}\left(\frac{\partial a_3^n}{\partial\sigma_i^n}A_{rk}^{(2)}\sigma_r^n + a_3^n A_{ik}^{(2)}\right)\right.\\ &\left.\left(\delta_{kl} + \beta\Delta t^n \frac{a_2^n}{a_1^n}A_{kl}^{(3)}\right)^{-1} A_{lj}^{(2)}\right]^{-1}\\ &\left\{\varepsilon_j^{n+1} + \left(\frac{\partial a_3^n}{\partial\sigma_j^n}A_{rk}^{(2)}\sigma_r^n + a_3^n A_{jk}^{(2)}\right)\left(\delta_{kl} + \beta\Delta t^n \frac{a_2^n}{a_1^n}A_{kl}^{(3)}\right)^{-1}\right.\\ &\left.\left[\left(\delta_{lm} - (1-\beta)\Delta t^n \frac{a_2^n}{a_1^n}A_{lm}^{(3)}\right)\xi_v^n - (1-\beta)\Delta t^n \frac{a_3^n}{a_1^n}A_{lq}^{(2)}\sigma_q^n\right]\right\} - \sigma_i^n\end{aligned} \tag{5.54}$$

2. The trial stress-increment obtained in Equation (5.54) is inserted into Equation (5.46), leading to a first approximation of the value of the strains at the end of the increment. This approximation is called the trial strain and is noted $\boldsymbol{\varepsilon}^{n+1,tr}$. It is a function of the trial stress-increment and of the stresses and the hidden state variables at the end of the previous increment, i.e., $\Delta\boldsymbol{\sigma}^{n,tr}$, $\boldsymbol{\sigma}^n$ and $\boldsymbol{\xi}^n$.
3. A strain-residual function $\boldsymbol{R}^{(\varepsilon)}$ is defined and

$$R_i^{(\varepsilon)} = \Delta\varepsilon_i^{n,tr} - \Delta\varepsilon_i^n \tag{5.55}$$

4. If $\left|\left|\boldsymbol{R}^{(\varepsilon)}\right|\right| > \epsilon$ (ϵ is a coefficient set by the user in order to define the precision of the results, for example $\epsilon = 10^{-10}$.), the trial stress-increment is updated

$$\Delta\sigma_i^{n,tr} \leftarrow \Delta\sigma_i^{n,tr} + \left[J_{ij}^{n,tr}\right]^{-1} R_j^{(\varepsilon)} \tag{5.56}$$

where J is the Jacobian matrix (its determination in the case of the lower order schemes is detailed in Appendix 5.6)

$$J_{ij}^{n,tr} = \frac{\partial\Delta\varepsilon_i^{n,tr}}{\partial\Delta\sigma_j^{n,tr}} \tag{5.57}$$

and the algorithm goes back to step 2.

If $\left|\left|\boldsymbol{R}^{(\varepsilon)}\right|\right| \leq \epsilon$, a good approximation of the stress-increment $\Delta\boldsymbol{\sigma}^n$ on the current time-step has been found and the algorithm ends.

Finally, to complete the requirements of the user-subroutine, the material Jacobian matrix can be found using

$$\frac{\partial \Delta\sigma_i^n}{\partial \Delta\varepsilon_j^n} = \left[J_{ij}^n\right]^{-1} \tag{5.58}$$

In order to converge rapidly towards the solution, this algorithm requires the first trial stress-increment found in step 1 to be 'near enough' the 'real' stress-increment and therefore adequate time-steps have to be considered.

User-subroutines have been developed in `ABAQUS` for the low-order FD schemes presented in Section 5.4.3 for the three-dimensional case and tested for a cube shape meshed with a single element and submitted to various loading histories. The results obtained for this cube shape with `ABAQUS` have been found to be identical to the results obtained for the same cube in Matlab, thus validating the method. Therefore, more complex geometries have also been tried in `ABAQUS`.

Furthermore, for the low-order FD schemes, it has been found that, in order to find the stress-increment with the algorithm developed above, an average of two iterations of the Newton-Raphson method is necessary in the general case. That number rises when the size of the time-step or the level of nonlinearity increase.

Finally, it should be noted that when strain-based constitutive theories are used, this iterative method is not necessary anymore to implement the incremental model into the FE software, resulting in a greatly reduced computation time.

5.5 Example of application and comparisons of the convergence rate of the various incremental models

The incremental models obtained from the strategies introduced in Section 5.4 are implemented into the software Matlab. The accuracy and the convergence rate of these strategies are compared with the performances of the recursive algorithm developed in Equation (5.13).

5.5.1 Material considerations

The material considered in this section is polypropylene (semi-crystalline) supplied by the company RTP under the grade RTP100. The material properties have been identified by Lévesque *et al.* (2008) and are recalled in Table 5.1 in which α is the elastic axial compliance,

Table 5.1: Numerical values of the various material properties

n	0	1	2	3
$\lambda_n(\mathrm{s}^{-1})$	–	10^{-2}	10^{-3}	3.16×10^{-4}
S_n	5×10^{-4}	3.5×10^{-2}	1.65×10^{-3}	2.0×10^{-1}
ν	0.47			

ν is the Poisson's ratio, and α_i are the transient axial compliance associated with the inverted retardation times λ_i.

Since the objective of this study is to compare the performances of the various algorithms and not the overall accuracy of Schapery's constitutive theories for the modeling of a material mechanical behavior, the material is assumed to be isotropic and to have a constant Poisson's ratio.

In this paper, the nonlinearizing functions are defined in the same way as in Lévesque *et al.* (2008). The nonlinearizing functions are considered to be quadratic functions of the stresses and are developed in an isotropic manner, i.e., the nonlinearizing functions are invariant by rotation of the stress state. Therefore, the nonlinearizing functions are functions of the first and second stress invariants.

I_1 and I_2, the first and second stress invariants, are given by

$$I_1 = \sigma_1 + \sigma_2 + \sigma_3 \tag{5.59a}$$

$$I_2 = \sigma_1\sigma_2 + \sigma_1\sigma_3 + \sigma_2\sigma_3 - \frac{1}{2}\left(\sigma_4^2 + \sigma_5^2 + \sigma_6^2\right) \tag{5.59b}$$

and a scalar parameter

$$h^{(z)} = \frac{1}{2}\sigma_i Q_{ij}^{(z)} \sigma_j = \theta^{(z)} I_1^2 + \zeta^{(z)} I_2 \tag{5.60}$$

is defined, where z refers to a particular nonlinearizing function and θ and ζ control the weight of I_1 and I_2 on h. If it is assumed that $\mathbf{Q}^{(z)}$ is symmetric, then simple manipulations lead to

$$\mathbf{Q}^{(z)} = \alpha^{(z)} \begin{pmatrix} 1 & -\nu^{(z)} & -\nu^{(z)} & 0 & 0 & 0 \\ -\nu^{(z)} & 1 & -\nu^{(z)} & 0 & 0 & 0 \\ -\nu^{(z)} & -\nu^{(z)} & 1 & 0 & 0 & 0 \\ 0 & 0 & 0 & 1-\nu^{(z)} & 0 & 0 \\ 0 & 0 & 0 & 0 & 1-\nu^{(z)} & 0 \\ 0 & 0 & 0 & 0 & 0 & 1-\nu^{(z)} \end{pmatrix} \tag{5.61}$$

where $\alpha^{(z)}$ and $\nu^{(z)}$ are interpreted as material constants and $\mathbf{Q}^{(z)}$ is an isotropic matrix.

With these considerations taken into account, the stress energy function φ introduced in

Equation (5.6b) can be defined by

$$\varphi = \int_0^{h_4} a_4(h_4')d'h_4 \tag{5.62}$$

and, thus,

$$\frac{\partial \varphi}{\partial \sigma_i} = a_4(h_4)Q_{ij}^{(4)}\sigma_j \tag{5.63}$$

With this choice, the shape of the nonlinear elastic term of Equation (5.6b) is the same as the shape of the nonlinear elastic term of Equation (5.9) and $\mathbf{Q}^{(4)}$ is identical to the initial compliance matrix $\mathbf{S}^{(0)}$.

In this study, all the nonlinearizing functions are assumed to be functions of the same equivalent stress h, i.e., $\mathbf{Q}^{(1)} = \mathbf{Q}^{(2)} = \mathbf{Q}^{(3)} = \mathbf{Q}^{(4)} = \mathbf{S}^{(0)}$ and

$$a_z = a_0^{(z)} + \mu^{(z)}h; \quad z = 1, 2, 3, 4 \tag{5.64}$$

where $a_0^{(z)} = 1$ and $\mu^{(z)} = 0$ in the case of a linearly viscoelastic material [5] .

5.5.2 On the determination of the internal matrices for RTP100

The first step of the method proposed in Section 5.4.1 consists in determining the compliance matrix and the transient compliance matrices from the material properties given in Table 5.1. The general compliance matrix for an isotropic material can be written

$$\mathbf{S} = \alpha \begin{pmatrix} 1 & -\nu & -\nu & 0 & 0 & 0 \\ -\nu & 1 & -\nu & 0 & 0 & 0 \\ -\nu & -\nu & 1 & 0 & 0 & 0 \\ 0 & 0 & 0 & 1+\nu & 0 & 0 \\ 0 & 0 & 0 & 0 & 1+\nu & 0 \\ 0 & 0 & 0 & 0 & 0 & 1+\nu \end{pmatrix} \tag{5.65}$$

5. In this journal paper, the nonlinearizing functions are always considered such as $a_0^{(z)} = 1$.

which, considering the material properties given in Table 5.1 leads to

$$\mathbf{S}^{(0)} = 10^{-4} \begin{pmatrix} 5 & -2.35 & -2.35 & 0 & 0 & 0 \\ -2.35 & 5 & -2.35 & 0 & 0 & 0 \\ -2.35 & -2.35 & 5 & 0 & 0 & 0 \\ 0 & 0 & 0 & 7.35 & 0 & 0 \\ 0 & 0 & 0 & 0 & 7.35 & 0 \\ 0 & 0 & 0 & 0 & 0 & 7.35 \end{pmatrix} \tag{5.66}$$

for the compliance matrix of the RTP100 and to

$$\mathbf{S}^{(1)} = 10^{-2} \begin{pmatrix} 3.5 & -1.645 & -1.645 & 0 & 0 & 0 \\ -1.645 & 3.5 & -1.645 & 0 & 0 & 0 \\ -1.645 & -1.645 & 3.5 & 0 & 0 & 0 \\ 0 & 0 & 0 & 5.145 & 0 & 0 \\ 0 & 0 & 0 & 0 & 5.145 & 0 \\ 0 & 0 & 0 & 0 & 0 & 5.145 \end{pmatrix} \tag{5.67}$$

$$\mathbf{S}^{(2)} = 10^{-3} \begin{pmatrix} 1.65 & -0.7755 & -0.7755 & 0 & 0 & 0 \\ -0.7755 & 1.65 & -0.7755 & 0 & 0 & 0 \\ -0.7755 & -0.7755 & 1.65 & 0 & 0 & 0 \\ 0 & 0 & 0 & 2.4255 & 0 & 0 \\ 0 & 0 & 0 & 0 & 2.4255 & 0 \\ 0 & 0 & 0 & 0 & 0 & 2.4255 \end{pmatrix} \tag{5.68}$$

$$\mathbf{S}^{(3)} = 10^{-1} \begin{pmatrix} 2 & -0.94 & -0.94 & 0 & 0 & 0 \\ -0.94 & 2 & -0.94 & 0 & 0 & 0 \\ -0.94 & -0.94 & 2 & 0 & 0 & 0 \\ 0 & 0 & 0 & 2.94 & 0 & 0 \\ 0 & 0 & 0 & 0 & 2.94 & 0 \\ 0 & 0 & 0 & 0 & 0 & 2.94 \end{pmatrix} \tag{5.69}$$

for the transient compliances matrices. These matrices are the compliance matrices introduced in Schapery's hereditary integral in Equation (5.6b).

In the second step of the method, the internal matrices $\mathbf{B}^{(\xi)}$, $\mathbf{A}^{(1)}$, $\mathbf{A}^{(2)}$ and $\mathbf{A}^{(3)}$ are determined using Equations (5.34), (5.36), (5.37) and (5.40). The successive steps to determined the internal matrices from the compliance matrices are recalled below.

First, $\mathbf{A}^{(1)}$ is determined using (5.34). Therefore, $\mathbf{A}^{(1)}$ is the 6×6 block matrix

$$\mathbf{A}^{(1)} = -10^{-4} \begin{pmatrix} 5 & -2.35 & -2.35 & 0 & 0 & 0 \\ -2.35 & 5 & -2.35 & 0 & 0 & 0 \\ -2.35 & -2.35 & 5 & 0 & 0 & 0 \\ 0 & 0 & 0 & 7.35 & 0 & 0 \\ 0 & 0 & 0 & 0 & 7.35 & 0 \\ 0 & 0 & 0 & 0 & 0 & 7.35 \end{pmatrix} \tag{5.70}$$

The second matrix that can be computed is $\mathbf{A}^{(2)}$. Since three inverted retardation times ($M = 3$) have been computed for this material (see Table 5.1), $\mathbf{A}^{(2)}$ is a 6×18 block matrix where each block $\mathbf{T}^{(m)}$ is obtained from the Cholesky decomposition of the matrix $\lambda(m)\mathbf{S}^{(m)}$ as in Equation (5.36). Then each block $\mathbf{T}^{(m)}$ is introduced in Equation (5.37) which leads to

$$\mathbf{A}^{(2)} = -10^{-2} \left(\begin{array}{cccccc|ccc} 1.87 & 0 & 0 & 0 & 0 & 0 & 0.13 & 0 & 0 \\ -0.88 & 1.65 & 0 & 0 & 0 & 0 & -0.06 & 0.11 & 0 \\ -0.88 & -1.46 & 0.76 & 0 & 0 & 0 & -0.06 & -0.10 & 0.052 \\ 0 & 0 & 0 & 2.27 & 0 & 0 & 0 & 0 & 0 \\ 0 & 0 & 0 & 0 & 2.27 & 0 & 0 & 0 & 0 \\ 0 & 0 & 0 & 0 & 0 & 2.27 & 0 & 0 & 0 \end{array}\right.$$
$$\left.\begin{array}{ccc|ccccccc} 0 & 0 & 0 & 0.80 & 0 & 0 & 0 & 0 & 0 \\ 0 & 0 & 0 & -0.37 & 0.70 & 0 & 0 & 0 & 0 \\ 0 & 0 & 0 & -0.37 & -0.62 & 0.32 & 0 & 0 & 0 \\ 0.16 & 0 & 0 & 0 & 0 & 0 & 0.96 & 0 & 0 \\ 0 & 0.16 & 0 & 0 & 0 & 0 & 0 & 0.96 & 0 \\ 0 & 0 & 0.16 & 0 & 0 & 0 & 0 & 0 & 0.96 \end{array}\right) \tag{5.71}$$

The third matrix which is computed is $\mathbf{A}^{(3)}$. Three inverted retardation times are considered, therefore, $\mathbf{A}^{(3)}$ is a 18×18 diagonal matrix of repeated eigenvalues as in Equation (5.40). The eigenvalues are the retardation times λ_m, each repeated 6 times, which leads to

$$\mathbf{A}^{(3)} = \begin{pmatrix} \left[\frac{1}{100}\right]_6 & & \\ & \left[\frac{1}{1000}\right]_6 & \\ & & \left[\frac{1}{3162}\right]_6 \end{pmatrix} \tag{5.72}$$

Finally, $\mathbf{B}^{(\xi)}$ is the 18×18 identity matrix.

In this example, an isotropic material is considered. However, if an anisotropic material

where to be considered, this would not change the shapes of the internal matrices. $\mathbf{B}^{(\xi)}$ would still be the identity matrix and $\mathbf{A}^{(3)}$ would still be a diagonal matrix of repeated eigenvalues. $\mathbf{A}^{(2)}$ would be a block matrix in which each block is still a lower-triangular matrix but with less zero-values and $\mathbf{A}^{(1)}$ would be a 6×6 symmetric matrix with no zero-values.

5.5.3 Numerical integration

In order to compare the performances of the various algorithms, the exact value of the constitutive theory developed in Equation (5.6b) is computed for each time-step t^n. To achieve that, the Gauss-Legendre quadrature is used. The values obtained by this method are precise but at the cost of storing all the load history.

The performances of various strategies are tested:

1. Two recursive strategies are tested. The first one is the strategy (HEN) of Henriksen (1984) introduced in Equation (5.13). The second one (2RA) is the newly developed strategy in Equation (5.51).
2. The new differential strategy introduced in this paper with various FD schemes: Backward-Euler (BE), Crank-Nicolson (CN) and 4^{th} Runge-Kutta (4RK). Since the differential strategy developed by Poon et Ahmad (1999) leads to the similar differential equations, its performances are not studied here.

For the sake of simplicity, only the 1D case is considered in this section. The constitutive theory used for the recursive strategies is Equation (5.8) with the nonlinearizing functions

$$g_0(\sigma) = a_4; \quad g_1(\sigma) = \frac{\partial a_3}{\partial \sigma}\sigma + a_3; \quad g_2(\sigma) = \frac{a_3}{a_2}; \quad a_\sigma(\sigma) = \frac{a_1}{a_2}. \tag{5.73}$$

Furthermore, since the recursive algorithms use assumptions of simple loading, i.e., the loading history is supposed to be constant or have a constant evolution rate over a time-increment and simple material behavior, i.e., a_σ is constant or piecewise constant over a time-increment while the quantity $g_2\sigma$ is linear, two kinds of tensile loadings, represented on Fig. 5.1, are tested as well as various kinds of nonlinearly viscoelastic behavior.

The first tensile loading consists of a constant stress rate of 1 MPa.s^{-1} and therefore is consistent with the simple loading hypothesis of the recursive algorithm. The second tensile loading is a more complex exponentially-shape loading history and is described by equation

$$\sigma(t) = 1 - \exp(-10t) \tag{5.74}$$

The algorithms are compared by computing their relative errors with the solution obtained

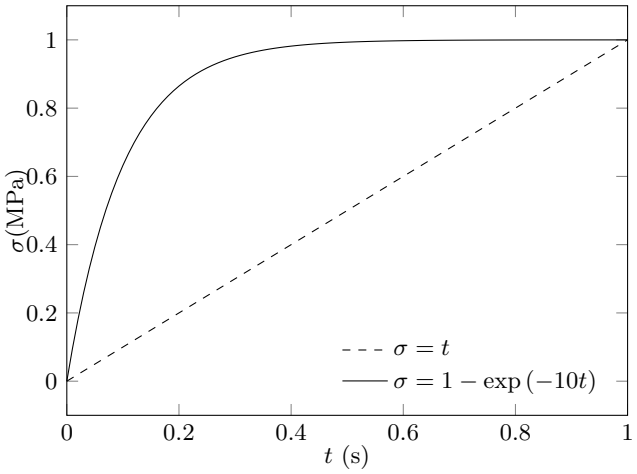

Figure 5.1: The two tensile loadings implemented into MATLAB.

by the Gauss-Legendre quadrature after one second of loading using

$$E_{\text{rel}}^{\text{1s}} = \frac{|\varepsilon_{\text{AL}}^{\text{1s}} - \varepsilon_{\text{GL}}^{\text{1s}}|}{|\varepsilon_{\text{GL}}^{\text{1s}}|} \cdot 100 \tag{5.75}$$

where $E_{\text{rel}}^{\text{1s}}$ is the relative error in percents after one second of loading, $\varepsilon_{\text{AL}}^{\text{1s}}$ and $\varepsilon_{\text{GL}}^{\text{1s}}$ are, respectively, strains computed by each algorithm and the Gauss-Legendre quadrature after one second of loading.

5.5.4 Results

Linearly viscoelastic case

The first comparison is done for the case of a linearly viscoelastic material, i.e., $a_0^{(z)} = 1$ and $\mu^{(z)} = 0$. The two kinds of tensile loadings introduced in Section 5.5.3 are considered.

In the case of the simple loading history, all the hypotheses of the recursive algorithms are respected and, therefore, the recursive algorithm should return the exact solution. However, in Fig. 5.2, it can be seen that the relative error of the recursive algorithms HEN and 2RA increases when the size of the time-step decreases. This can be explained by the fact that, in Equations (5.13) and (5.51), when the quantity $\lambda\Delta t$ is small the terms Γ and Υ suffer from cancellation errors (**?**). Therefore, when $\lambda\Delta t$ is small, it would in fact be better to use a series expansion. For example, Equation (5.15) would become

$$\Gamma_m^{n+1} = 1 - \frac{1}{2}\left(\frac{\lambda\Delta t}{a_\sigma^{n+1}}\right) + \frac{1}{6}\left(\frac{\lambda\Delta t}{a_\sigma^{n+1}}\right)^2 - \frac{1}{24}\left(\frac{\lambda\Delta t}{a_\sigma^{n+1}}\right)^3 + ... \tag{5.76}$$

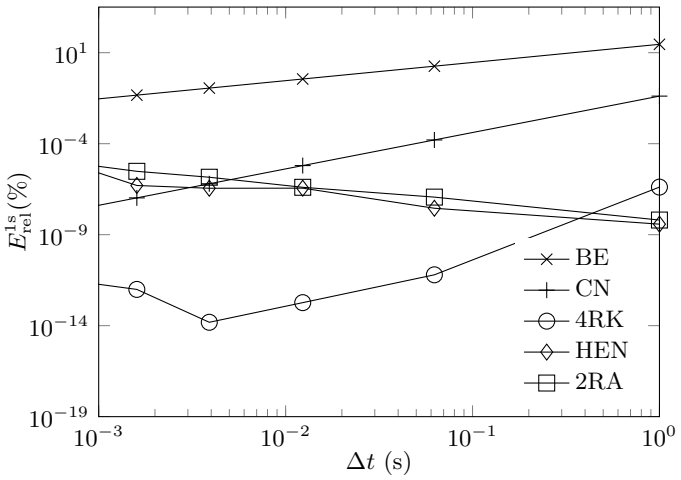

Figure 5.2: Performances of the various algorithms with respect to the size of the time-step in the case of a linearly viscoelastic material and a constant stress rate tensile loading.

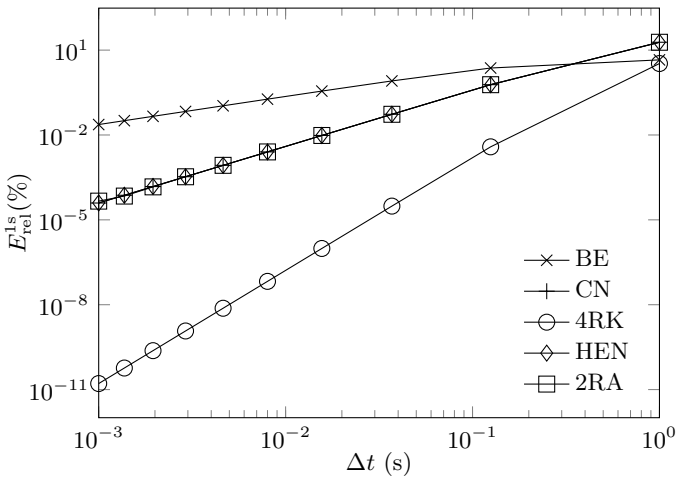

Figure 5.3: Performances of the various algorithms with respect to the size of the time-step in the case of a linearly viscoelastic material and a exponentially-shape load history. The curves of the three algorithms HEN, 2RA and CN are superimposed.

Furthermore, it can be seen in Fig. 5.2 that the Backward-Euler scheme BE exhibits a linear convergence rate, i.e., dividing the time-step by 10 reduced the relative error by a factor of 10, while the Crank-Nicolson scheme CN and the 4^{th} order Runge-Kutta scheme 4RK exhibit, respectively, a quadratic convergence rate and a 4^{th} order convergence rate which is consistent with the definition of these FD schemes. Finally, it can be seen that under a relative error of $10^{-11}\%$, the accuracy of the 4RK algorithm seems random. This can be explain by the fact that $\varepsilon_{\text{GL}}^{1\text{s}}$, in Equation (5.75), is computed with an accuracy of $10^{-12}\%$.

If instead of the constant stress rate tensile loading, the more complex loading history defined in Equation (5.74) is considered, the observed results are quite different. Fig. 5.3 shows that, now that the hypothesis of simple loading is no longer respected, the solutions given by the recursive algorithms HEN and 2RA and by the Crank-Nicolson scheme CN are now similar and exhibit a quadratic convergence rate. This can be explained by the fact that, in the recursive strategies, the term $\mathrm{d}\sigma/\mathrm{d}\tau$ is computed using the trapezoidal rule which is a second order approximation.

Nonlinearly viscoelastic case

The second hypothesis of the recursive algorithms is that the studied material exhibits a simple material behavior. This hypothesis is used to simplify the computation of the reduced-time increment defined in Equation (5.14) and in the trapezoidal approximation of the term $\mathrm{d}\left[g_2\sigma\right]/\mathrm{d}\tau$ in Equation (5.12).

Therefore the impact of the nonlinearizing functions a_z on the convergence rate of the various strategies is tested. To that end, each nonlinearizing functions is taken into account subsequently.

It should be noted that since the material is submitted to an uniaxial tensile loading, the nonlinearizing functions can be further simplified and Equation (5.77) becomes

$$a_z = a_0^{(z)} + \frac{1}{2}\mu^{(z)}\alpha\sigma^2; \quad z = 1, 2, 3, 4 \tag{5.77}$$

where $a_0^{(z)} = 1$ and α is the elastic axial compliance as defined in Table 5.1. Therefore, if the material is, for example, submitted to a stress of 1 MPa while $\mu^{(z)} = 1000$, then the nonlinearizing functions would take the value $a_z = 1.25$.

First, the impact of the nonlinearizing function a_3 on the convergence rate of the various algorithms is tested. In order to achieve that, the nonlinear coefficient $\mu^{(3)}$ introduced in Equation (5.77) is given a non-zero value while $\mu^{(z)} = 0$ for $z = 1, 2, 3, 4$. The nonlinearizing

functions given in Equations (5.73) become

$$g_0(\sigma) = 1; \quad g_1(\sigma) = \frac{\partial a_3}{\partial \sigma}\sigma + a_3; \quad g_2(\sigma) = a_3; \quad a_\sigma(\sigma) = 1. \tag{5.78}$$

In Equations (5.78), it can be seen that introducing the nonlinearizing functions a_3 results in functions g_1 and g_2 being nonlinear and therefore the impact of assuming $g_2\sigma$ to be linear on the recursive strategies' convergence rate is tested.

The second nonlinearizing function introduced is a_1. The nonlinear coefficient $\mu^{(1)}$ introduced in Equation (5.77) is given a non-zero value while $\mu^{(z)} = 0$ for $z = 2, 3, 4$. Thus, the nonlinearizing functions given in Equations (5.73) become

$$g_0(\sigma) = 1; \quad g_1(\sigma) = 1; \quad g_2(\sigma) = 1; \quad a_\sigma(\sigma) = a_1. \tag{5.79}$$

In Equations (5.79), it can be seen that introducing the nonlinearizing functions a_1 results in the function a_σ being nonlinear. Therefore the impact of the hypothesis made on the behavior of a_σ is tested.

The third and last nonlinearizing function introduced is a_2. The nonlinear coefficient μ_3 is given a non-zero value leading to

$$g_0(\sigma) = 1; \quad g_1(\sigma) = 1; \quad g_2(\sigma) = \frac{1}{a_2}; \quad a_\sigma(\sigma) = \frac{1}{a_2}. \tag{5.80}$$

In Equations (5.80), both a_σ and g_2 are nonlinear and the impact of the two hypotheses of the recursive strategies can be tested simultaneously.

Fig. 5.4 shows that the convergence rates of the CN strategy and the recursive algorithms HEN and 2RA are quadratic when the kind of nonlinearity introduced in Equation (5.78) is considered. This is due to the fact that the quantity $\mathrm{d}[g_2\sigma]/\mathrm{d}\tau$ is approximate by the trapezoidal rule.

Furthermore, Fig. 5.5, 5.7 and 5.9 show that, for a fixed size of the time-step ($\Delta t = 0.1s$) the impact of the nonlinearizing function a_z is similar for the differential strategies CN and 4RK and recursive strategies HEN and 2RA. The accuracy of various strategies decreases when the nonlinearity is increased. For small nonlinearities, however, the accuracy of the BE and CN strategies stops increasing for a decreasing level of nonlinearity. In the case of the FD schemes, the errors introduced by the discretization of the hidden state variables ξ is more important than the errors introduced by the nonlinearly viscoelastic behavior of the

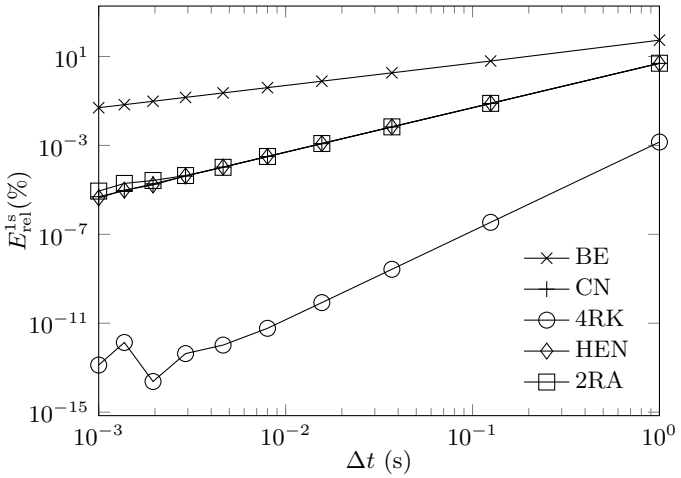

Figure 5.4: Performances of the various algorithms for a constant stress rate tensile loading with respect to the size of the time-step in the case where function a_3 is stress dependent ($\mu_3 = 1000$).

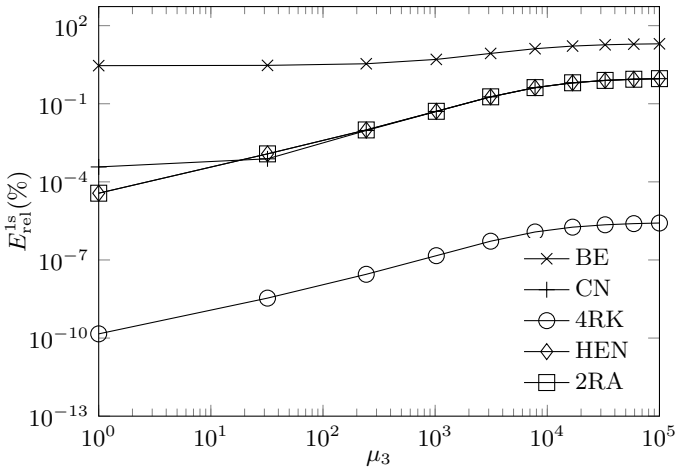

Figure 5.5: Performances of the various algorithms for a constant stress rate tensile loading with respect to the coefficient of nonlinearity μ_3 (functions a_3 is stress dependent) in the case of a fixed size of the time-step ($\Delta t = 0.1s$). The curves of the algorithms HEN, 2RA are superimposed.

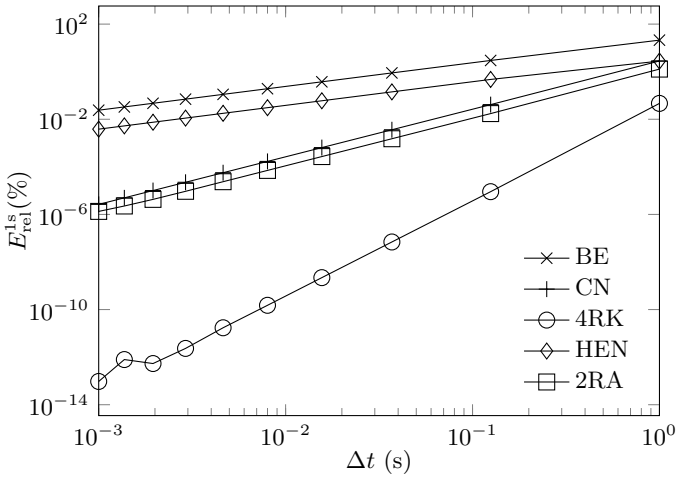

Figure 5.6: Performances of the various algorithms for a constant stress rate tensile loading with respect to the size of the time-step in the case where function a_1 is stress dependent ($\mu_1 = 1000$).

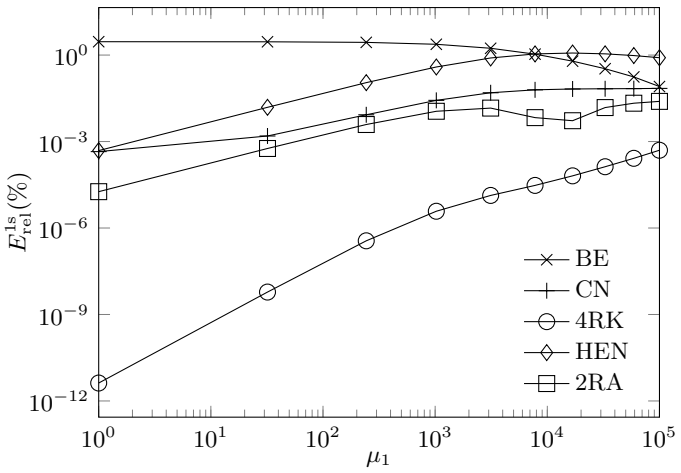

Figure 5.7: Performances of the various algorithms for a constant stress rate tensile loading with respect to the coefficient of nonlinearity μ_1 (functions a_1 is stress dependent) in the case of a fixed size of the time-step ($\Delta t = 0.1s$).

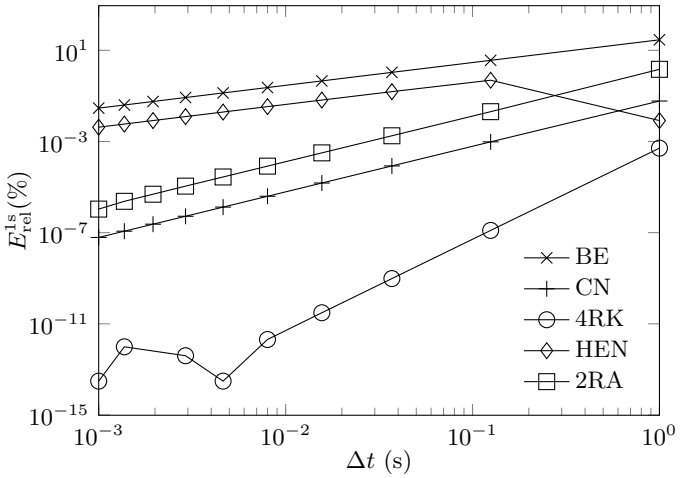

Figure 5.8: Performances of the various algorithms for a constant stress rate tensile loading with respect to the size of the time-step in the case where function a_2 is stress dependent ($\mu_2 = 1000$).

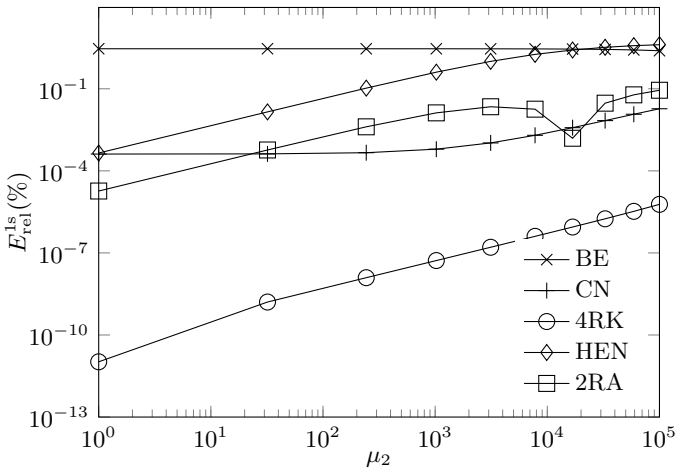

Figure 5.9: Performances of the various algorithms for a constant stress rate tensile loading with respect to the coefficient of nonlinearity μ_2 (functions a_2 is stress dependent) in the case of a fixed size of the time-step ($\Delta t = 0.1s$).

material.

Fig. 5.6 and Fig. 5.8 show that when the nonlinearizing function a_σ is introduced, the recursive strategy HEN exhibits the same linear convergence with that of the Backward-Euler scheme while strategies 2RA and CN both exhibit a quadratic convergence.

To summarize the results obtained above, it should be noted that introducing various loading histories and various kinds of nonlinearities does not have any effect on the convergence rate of the strategies BE, CN, 4RK. The three differential strategies always exhibit a linear, quadratic, and 4^{th} order convergence rate, respectively. However, the accuracy of these strategies is affected.

In the case of the recursive strategies, the convergence rate of the algorithms is affected by the various loading histories and nonlinearities. The solution is theoretically exact when the hypotheses are respected (cancellation errors might appear for small time-steps). However, if a complex loading history is considered then HEN and 2RA both exhibit a quadratic convergence rate. Furthermore, if a nonlinearly viscoelastic material is considered, due to the hypothesis on the reduced-time, the convergence rate of strategy HEN becomes linear and the strategy 2RA exhibits a quadratic convergence.

The results presented above for the nonlinear case are for a constant stress rate tensile loading. However, similar observations can be made for the complex loading history introduced in Equation (5.74) and therefore the results are not presented in this paper. The convergence rate of the various strategies is affected in a similar manner by the size of the time-step, as shown in Fig. 5.4, 5.6 and 5.8.

5.6 Conclusions

The contributions of this study are as follows:

1. A new differential strategy leading to incremental models for the implementation of Schapery-type constitutive theories for fully anisotropic nonlinearly viscoelastic materials into FE software has been proposed. This strategy is more natural than the other strategies introduced before since it uses the equations used for deriving Schapery's constitutive theories.

2. A new recursive strategy to compute the solution of Schapery-type constitutive theories expressed as hereditary integrals has been proposed. In this strategy, the nonlinearizing function a_σ is supposed to be constant piecewise over a time-increment. This hypothesis leads to a better approximation of Schapery-type constitutive theories in the case of a time dependent reduced-time than the recursive strategy used in Henriksen (1984) and Haj-Ali et Muliana (2004).

3. A comparative study of the convergence rate and accuracy of differential and recursive strategies for a few cases of material behaviors and loading histories has shown the advantages and limitations of each strategy.

Even though the differential strategy developed from Schapery's differential equations is a more natural way to obtain incremental models than the recursive strategy or the previously-existing differential strategy, it is not more effective for low order FD schemes. When considering a nonlinearly viscoelastic material, the recursive strategy 2RA and the differential strategy CN have shown similar results, i.e., similar convergence rate, similar accuracy.

Differential strategies have proven to be excellent methods to implement Schapery-type constitutive theories. Furthermore, they have the advantage of allowing for the use of higher order schemes. The 4^{th} Runge-Kutta (4RK) scheme, for example, has a greater convergence rate than any recursive strategies but can be more complex to implement into a FE software. However, in some cases, it might be more computationally efficient to store two times steps and achieve 4^{th} order convergence rate, leading to larger time-steps for the same accuracy, than using lower convergence rate. This is truly an advantage that the differential strategies have over the recursive strategies.

ANNEXE 1: Determination of the internal variables for strain-based theories

In Section 5.4.1, the internal matrices are determined for the stress-based constitutive theory. The same work can be done in the case of strain-based constitutive theories using the same method. For small strains a material can be considered to have a linearly viscoelastic behavior and the internal matrices can be determined while considering the nonlinearizing functions as $p_z = 1$ (for $z = 1, 2, 3, 4$). Following the same steps as in Section 5.4.1 leads to

$$\widetilde{\sigma}_i = \left[L_{ij}^{(1)} - L_{is}^{(2)} \left(pB_{rs}^{(\chi)} + L_{rs}^{(3)} \right)^{-1} L_{jr}^{(2)} \right] \widetilde{\varepsilon}_j \tag{5.81}$$

For a constant strain $\boldsymbol{\varepsilon}^{(0)}$, the linear behavior of a material can be expressed as

$$\sigma_i(t) = \left[C_{ij}^{(0)} + \Delta C_{ij} \right] \varepsilon_j^{(0)} \tag{5.82}$$

where $\mathbf{C}^{(0)}$ is the initial stiffness matrix and $\Delta\mathbf{C}$ is the transient stiffness matrix. The transient stiffness matrix is written as a Prony serie of M terms and so applying the Laplace transform leads to

$$\widetilde{\sigma}_i = \frac{1}{p} \left[C_{ij}^{(0)} + \sum_m^M C_{ij}^{(m)} - \sum_m^M \frac{\omega_m C_{ij}^{(m)}}{\omega_m + p} \right] \widetilde{\varepsilon}_j^{(0)} \tag{5.83}$$

Therefore the internal matrices are

$$L_{ij}^{(1)} = C_{ij}^{(0)} + \sum_{m}^{M} C_{ij}^{(m)} \tag{5.84}$$

and

$$L_{is}^{(2)} \left(pB_{rs}^{(\chi)} + L_{rs}^{(3)} \right)^{-1} L_{jr}^{(2)} = \sum_{m}^{M} \frac{\omega_m C_{ij}^{(m)}}{\omega_m + p} \tag{5.85}$$

which leads to

$$\mathbf{L}^{(2)} = \left(\mathbf{L}^{(2,1)} \middle| \, \mathbf{L}^{(2,2)} \middle| \, ... \, \middle| \mathbf{L}^{(2,m)} \middle| \, ... \, \middle| \mathbf{L}^{(2,M)} \right) \tag{5.86}$$

where $\mathbf{L}^{(2,m)}$ is obtained with a Cholesky decomposition of the matrix $\omega_m \mathbf{C}^{(m)}$, $\mathbf{B}^{(\xi)}$ is the $6M \times 6M$ identity matrix and

$$\mathbf{L}^{(3)} = \begin{pmatrix} [\omega_1]_6 & & & & & \\ & [\omega_2]_6 & & & & \\ & & ... & & & \\ & & & [\omega_m]_6 & & \\ & & & & ... & \\ & & & & & [\omega_M]_6 \end{pmatrix} \tag{5.87}$$

ANNEXE 2: Computation of the Jacobian Matrix

In the fourth step of the FE implementation algorithm in Section 5.4.5, it is necessary to determine the jacobian matrix

$$J_{ij}^{n} = \frac{\partial \Delta \varepsilon_i^n}{\partial \Delta \sigma_j^n} \tag{5.88}$$

For Example, in the case of the lower order incremental model developed in Section 5.4.3, Equations (5.46) can be written

$$\varepsilon_i^{n+1} = -S_{ij}^{(5)} \sigma_j^{n+1} - S_{ir}^{(6)} \left(S_{rs}^{(1)} \right)^{-1} \left[S_{sv}^{(2)} \xi_v^n - S_{sk}^{(3)} \sigma_k^n - S_{sk}^{(4)} \sigma_k^{n+1} \right] \tag{5.89}$$

where

$$S_{rs}^{(1)} = \delta_{rs} + \beta \Delta t^n \frac{a_2^{n+1}}{a_1^{n+1}} A_{rs}^{(3)} \tag{5.90a}$$

$$S_{sv}^{(2)} = \delta_{sv} - (1-\beta) \Delta t^n \frac{a_2^{n}}{a_1^{n}} A_{sv}^{(3)} \tag{5.90b}$$

$$S_{sk}^{(3)} = (1-\beta) \Delta t^n \frac{a_3^{n}}{a_1^{n}} A_{ks}^{(2)} \tag{5.90c}$$

$$S_{sk}^{(4)} = \beta \Delta t^n \frac{a_3^{n+1}}{a_1^{n+1}} A_{ks}^{(2)} \tag{5.90d}$$

$$S_{ij}^{(5)} = a_4^{n+1} A_{ij}^{(1)} \tag{5.90e}$$

$$S_{ir}^{(6)} = \frac{\partial a_3^{n+1}}{\partial \sigma_i^{n+1}} A_{lr}^{(2)} \sigma_l^{n+1} + a_3^{n+1} A_{ir}^{(2)} \tag{5.90f}$$

Combining Equation (5.89) and Equation (5.88) leads to

$$\begin{aligned} J_{ij}^n = & - \frac{\partial S_{ij}^{(5)}}{\partial \Delta \sigma_j^n} \left(\sigma_j^n + \Delta \sigma_j^n \right) - S_{ij}^{(5)} \\ & - \frac{\partial S_{ir}^{(6)}}{\partial \Delta \sigma_j^n} \left(S_{rs}^{(1)} \right)^{-1} \left[S_{sv}^{(2)} \xi_v^n - S_{sk}^{(3)} \sigma_k^n - S_{sk}^{(4)} \left(\sigma_k^n + \Delta \sigma_k^n \right) \right] \\ & - S_{ir}^{(6)} \frac{\partial \left(S_{rs}^{(1)} \right)^{-1}}{\partial \Delta \sigma_j^n} \left[S_{sv}^{(2)} \xi_v^n - S_{sk}^{(3)} \sigma_k^n - S_{sk}^{(4)} \left(\sigma_k^n + \Delta \sigma_k^n \right) \right] \\ & + S_{ir}^{(6)} \left(S_{rs}^{(1)} \right)^{-1} \left[\frac{\partial S_{sk}^{(4)}}{\partial \Delta \sigma_j^n} \left(\sigma_k^n + \Delta \sigma_k^n \right) + S_{sk}^{(4)} \right] \end{aligned} \tag{5.91}$$

where

$$\begin{aligned} \frac{\partial \left(S_{rs}^{(1)} \right)^{-1}}{\partial \Delta \sigma_j^n} = & - \frac{\partial S_{ru}^{(1)}}{\partial \Delta \sigma_j^n} \left(S_{uw}^{(1)} \right)^{-1} \left(S_{ws}^{(1)} \right)^{-1} \\ & - \beta \Delta t^n \frac{1}{a_1^{n+1}} \left(\frac{\partial a_2^{n+1}}{\partial \Delta \sigma_j^n} - \frac{a_2^{n+1}}{a_1^{n+1}} \frac{\partial a_1^{n+1}}{\partial \Delta \sigma_j^n} \right) A_{ru}^{(3)} \left(S_{uw}^{(1)} \right)^{-1} \left(S_{ws}^{(1)} \right)^{-1} \end{aligned} \tag{5.92a}$$

$$\frac{\partial S_{sk}^{(4)}}{\partial \Delta \sigma_j^n} = \beta \Delta t^n \frac{1}{a_1^{n+1}} \left(\frac{\partial a_3^{n+1}}{\partial \Delta \sigma_j^n} - \frac{a_3^{n+1}}{a_1^{n+1}} \frac{\partial a_1^{n+1}}{\partial \Delta \sigma_j^n} \right) A_{sk}^{(2)} \tag{5.92b}$$

$$\frac{\partial S_{ij}^{(5)}}{\partial \Delta \sigma_j^n} = \frac{\partial a_4^{n+1}}{\partial \Delta \sigma_j^n} A_{ij}^{(1)} \tag{5.92c}$$

$$\frac{\partial S_{ir}^{(6)}}{\partial \Delta \sigma_j^n} = \frac{\partial^2 a_3^{n+1}}{\partial \Delta \sigma_j^n \partial \sigma_i^{n+1}} A_{lr}^{(2)} \sigma_l^{n+1} + \frac{\partial a_3^{n+1}}{\partial \sigma_i^{n+1}} A_{lr}^{(2)} \delta_{lj} + \frac{\partial a_3^{n+1}}{\partial \Delta \sigma_j^n} A_{ir}^{(2)} \tag{5.92d}$$

CHAPTER 6

GENERAL DISCUSSION

The aim of this thesis was to study the mechanical behavior of a MVK-10 polyimide matrix submitted to the typical environment of an aircraft engine and to develop numerical tools allowing designers to safely use this material. The results of this study are given in the three papers presented above and discussed in this section

6.1 General behavior of the polymide matrix

6.1.1 Performances and comparison with PMR-15

The MVK-10 matrix was introduced as a potential replacement for the carcinogenic PMR-15 matrix used in high temperature applications for many years. PMR-15 has an operating temperature of 288°C.

According to the study of Ruggles-Wrenn et Broeckert (2009), PMR-15 dogbone samples aged at 288°C in air lost 3.5% of their mass after 1,000 hours. When aged at service temperature, MVK-10 samples were found to have lost about $\sim 1\%$ of their masses after 1,000 hours and $\sim 5\%$ after 10,000 hours. Based on this limited comparison, it would seem that MVK-10 is more stable at its operating temperature than PMR-15.

Table 6.1 recalls the tensile static properties of the PMR-15 matrix at room and service temperatures. Figure 3.8 shows that, at service temperature, MVK-10 matrix Young's modulus, stress at failure and strain at failure respectively decreased by 29%, 50% and 38%, compared to room temperature properties. Therefore, when compared to PMR-15, MVK-10 seems to better preserve its modulus and strength from room to service temperature. The table also shows that these two resins have a lower ultimate strain when the temperature is increased. However, the ultimate strain of MVK-10 is much more affected by temperature than that of PMR-15.

The study dealing with the effects of chemical ageing at the service temperature on MVK10's tensile properties showed that over a 1 month period, the Young's modulus increased by 3.7% and the stress and strain at failure remained constant. However, after 17 month, the Young's modulus, the stress at failure and the strain at failure decreased respectively by 19%, 30% and 10% from the non-aged properties. In comparison, Ruggles-Wrenn et Broeckert (2009) found that after 1,000 hours at service temperature, PMR-15 saw its Young's modulus increased by 13% and its stress at failure decreased by 50%. This shows

Table 6.1: Static properties of the PMR-15 matrix (Chuang, 2001; Ruggles-Wrenn et Broeckert, 2009)

Temperature	Young's modulus	Stress at failure	Strain at failure
Room	3.5GPa	92MPa	2.6%
288°C	1.75GPa	30MPa	2.15%
Overall decreases	−50%	−67%	−17%

that the MVK-10 matrix better retains its mechanical properties during chemical ageing.

However, while the MVK-10 matrix seems to be more stable and to better retain its mechanical properties at service temperature, it still bears some important flaws: *i*) its service temperature is much lower than PMR-15's; *ii*) its stress at failure is much lower at room temperature and service temperature; *iii*) its strain at failure is very low. In fact, it is even lower than typical carbon fibers strain at failure.

Finally, the impact of physical ageing on the viscoelastic properties of the MVK-10 matrix was studied at several temperatures. The experimental results in Figure 6.1 showed that this impact becomes increasingly more important as the physical ageing temperature is increased. However, at service temperature, the impact of physical ageing seemed to be negligible. This was further confirmed with viscoelastic tests performed at various ageing times over a 13 months period. On the other hand, studies on the impact of ageing on the viscoelastic properties of PMR-15 showed that, when aged at service temperature, the stiffness of the material was still increasing after 1,000 hours (Ruggles-Wrenn et Broeckert, 2009). This result for the MVK-10 matrix is surprising. However, one possible explanation would be that the service temperature is far below T_g and thermodynamic equilibrium cannot be achieved, i.e. the volume of the material is too small for the molecular reorganization to happen.

The assumption that, at service temperature, only chemical ageing is happening seems confirmed by the thermogravimetric results in Figure 3.6. At service temperature, mass and volume losses are correlated which could indicate that volume losses are due to evaporation of the chemical species created during chemical ageing. Physical ageing, by definition, only results in volume shrinkage.

6.1.2 Impact of chemical ageing

Initially, the impact of chemical ageing on the material was assumed to be minimal. However, TGA and T_g tests performed on matrix samples showed that the onset of thermal degradation and the material's dry-T_g were very close. This can be explained by the fact that the material's T_g is in the vicinity of the temperatures needed to break the covalent bonds

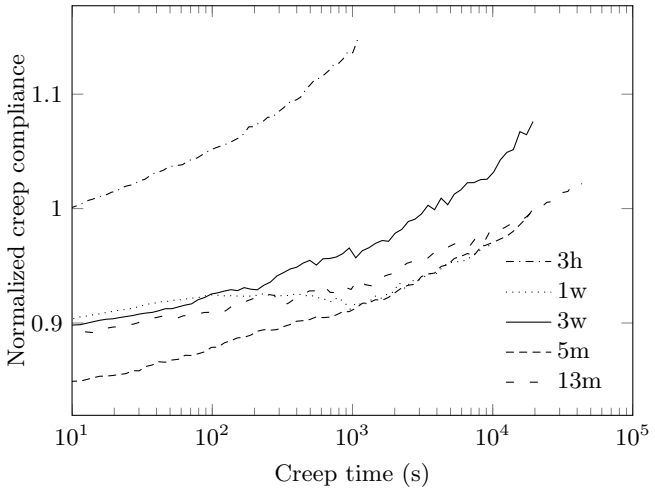

Figure 6.1: Impact of physical ageing on the tensile creep response of the MVK-10 resin at service temperature after 3 hours, 1 week, 3 weeks, 5 months and 13 months.

between the molecules inside the polyimide. The amount of chemical ageing was measured at various temperatures for a short amount of time and its impact on the material's performances was assessed at service temperature for over a year. It should be kept in mind that, during actual flight, service temperature is achieved only at take-off. Therefore, the chemical ageing rate is at its maximum for about 20 minutes per flight, and a year of chemical ageing at service temperature corresponds roughly to 26,000 flights or 20 years of service (4 flights per day).

One unsuspected consequence of chemical ageing was most important when designing tests for evaluating physical ageing. Typically, when using the methodology developed by Struik (1978), the first step consists in rejuvenating the material, i.e. erasing all former physical ageing history, by heating the material a few degrees above its T_g. However, in this case, this proved to be impossible since heating the material a few minutes at those temperatures led to the formation of bubbles on the samples surfaces. The impossibility to rejuvenate the material was very problematic when designing the testing matrix. It was initially decided to use tensile tests following Struik's methodology and to reuse each sample after a rejuvenation period. This would have required much less material that having a pristine sample for each test. Moreover, only two matrix panels were available for the whole project. Therefore, the testing matrix had to revised and tensile tests were replaced by 3-point bending tests. The samples were not rejuvenated before each test which means it was impossible to estimate the amount of physical ageing inside the material prior to testing. However, since the samples were kept at room temperature, which is much lower than service temperature, prior physical ageing was assumed to be minimal and to remain constant during storage. Also, since all

samples tested with three-point bending were obtained from the same sheet of material, they were all submitted to the same thermal history and storage conditions. Therefore, the data obtained should be consistent.

An other indirect consequence of chemical ageing concerned the investigation of the 3D behavior of the material at high temperatures. The 3D behavior could only be evaluated at service temperature on typical tensile test samples with rosettes (since only three-point bending tests were performed at higher temperatures). At this temperature, the viscoelastic Poisson's ratio ν was found to remain constant with time. However, since at higher temperatures, only three-point bending tests could be performed, the impact of temperature and physical ageing on ν could not be assessed. Therefore, ν was assumed to remain constant.

6.1.3 Impact of stress, temperature and physical ageing on the viscoelastic behavior

A major assumption of this thesis was that MVK-10 would exhibit a viscoelastic behavior dependent on stress, temperature and physical ageing, thus requiring the development of a nonlinear constitutive theory. To that end, it was chosen to develop a Schapery-type constitutive theory since this kind of theory fulfilled the requirements of being thermodynamically admissible, physically-based and able to represent the material behavior for all kind of loading histories. Furthermore the impact of stress, temperature and physical ageing could be easily included with explicit nonlinearizing functions. However,the experimental data at high temperature revealed that: *i*) the material always remained inside its linearly viscoelastic range due to its relatively low ultimate stress; *ii*) the infinitesimal strains hypothesis is valid due to the materials low strain at break. Coupled with the assumption of a constant viscoelastic Poisson's ratio, those consequences led to significant simplifications for the viscoelastic model. The fact that the material remained in its linearly viscoelastic range with a constant ν meant that a 3D constitutive theory could be obtained by simply inserting a compliance tensor $\mathbf{S}$ such as proposed in Equation (4.11) inside the 1D viscoelastic model proposed in Equation (4.12). Furthermore, only temperature- and physical ageing-dependent nonlinearizing functions were required.

6.1.4 Implementation in a FE software

Finite-Element software such as `ABAQUS` requires users to write subroutines in order to use internally-developed constitutive theories. In the case of viscoelasticity, those subroutines usually requires the strain tensor and strain increment for each element in order to update the stress tensor. This means that strain-based theories such as Equation (1.25) are better

suited to be implemented into Finite-Element software. However, for practical reasons, tri-dimensional viscoelastic properties are often obtained from creep-recovery tests (Lévesque *et al.*, 2008), leading to stress-based theories such as Equation (1.26).

When dealing with stress- or strain-induced nonlinearly viscoelastic behavior, there is no easy way to go from the strain-based to the stress-based equation and vice-versa. Therefore, when dealing with nonlinearly viscoelastic materials in Finite-Element software, obtaining the stress tensor requires to go through a computationally-expensive optimization process which is explained in Section 5.

However, since the MVK-10's viscoelastic behavior is independent of stress, it is possible to transform the stress-based constitutive theory into a strain-based constitutive theory using a so-called interconversion process. When dealing with viscoelastic functions expressed as Prony series, such as is the case in this thesis, it is possible to obtain an exact interconversion. One such method was developed and published during the course of this project (Luk-Cyr *et al.*, 2013).

CONCLUSIONS AND RECOMMENDATIONS

This thesis investigated the performances of a MVK-10 polyimide matrix submitted to elevated temperatures, high mechanical loadings and an oxidative environment. The purpose was to evaluate the impact of chemical ageing on the material's properties, to develop a viscoelastic model taking into account stress, physical ageing and temperature, and to develop numerical tools for the industrial partners.

The impact of chemical ageing was first studied. Kinetic TGA tests in an oxidizing atmosphere were performed at various heating rates on powder samples. Those tests showed that the onset of thermal degradation was in close proximity with the material's T_g. A three-step degradation model leading to an excellent fit of the data was developed. The thermal stability was studied from isothermal TGA tests conducted on powder samples for 24 hours at various temperatures. For temperatures above wet-$T_g + 37\,^{\circ}\mathrm{C}$, an instantaneous and severe degradation was observed. Below wet-$T_g + 37\,^{\circ}\mathrm{C}$, an oxidation layer formed on the surface. Tensile samples were stored at service temperature (wet-$T_g - 28\,^{\circ}\mathrm{C}$) for 17 months. Those samples were quite stable, exhibiting less than 5% mass loss. However, decreases of 19%, 30% and 10% from the non-aged properties were observed for E, σ_f and ε_f, respectively and simple models were developed.

The impacts of temperature, stress and physical ageing on the polyimide's mechanical properties were thoroughly studied. Isothermal tensile and three-point bending creep tests were performed over a range of temperatures, stresses and ageing times. It was shown that stress had no impact and that the material remained in its linearly viscoelastic range. Furthermore, the Poisson's ratio was found to be independent of time. Those two observations led to the development of a simplified Schapery-type constitutive theory. This theory was successfully validated with complex thermo-mechanical histories.

Finally, the last step consisted in implementing the constitutive theory into a finite-element software. To that end, a new procedure was developed. Instead of the classical methods which deal with Schapery's hereditary integral, the method went back to the evolution equations which are the basis of the integral. The evolution equations were solved with well-known finite-difference schemes such as Backward-Euler, Crank-Nicholson or Runge-Kutta. The numerical model thus obtained could then easily be implemented into finite-element softwares.

In overall, the results of this thesis suggest that the MVK-10 polyimide is a potentially good candidate for applications requiring less than 1,000 hours exposition at service temperature and compares well with other existing matrices. However, the service temperature of

MVK-10 is much lower than that of PMR-15.. However, severe degradation occurred after longer exposition times at that temperature. Severe matrix cracking was observed in the composite after 10,000 hours (without load). Significant degradation in properties seems to be triggered by chemical ageing.

Recommendations for future studies

The previously listed conclusions lead to the following recommandations:

- **Modeling the chemical ageing of polymers:** In elevated temperature applications, chemical ageing is of major concern since it leads to massive decreases in mechanical properties. Therefore, a proper study should be performed both for the in-volume degradation of the polymeric chains and for the growth of the surface oxidation layer and their impact on the polymer's properties. Then, chemical ageing-dependent non-linearizing functions could be developed and inserted into a Schapery-type constitutive theory.
- **Effect of a protecting agent:** Decrease in the samples mechanical behavior seemed to be the results of surface crackings. Therefore, it could be interesting to study the impact of a protecting agent. This would reduce the formation of the surface oxidation layer. In parallel, chemical degradation in an inert atmosphere should be investigated.
- **Investigation of the tri-dimensional properties:** In this work, the scarcity of material limited the investigation of physical ageing to three-point bending tests only and the Poisson's ratio was assumed to remain constant. Therefore, it would be interesting to study the tri-dimensional behavior of the matrix at temperatures closer to the material's T_g.

REFERENCES

ANDREWS, R. D. et TOBOLSKY, A. V. (1951). Elastoviscous properties of polyisobutylene. IV. Relaxation time spectrum and calculation of bulk viscosity. *Journal of Polymer Science*, 7, 221 – 242.

BAŽANT, Z. P. (1972). Matrix differential equation and higher-order numerical methods for problems of non-linear creep, viscoelasticity and elasto-plasticity. *International Journal for Numerical Methods in Engineering*, 4, 11 – 15.

BEIJER, J. G. J. et SPOORMAKER, J. L. (2002). Solution strategies for FEM analysis with nonlinear viscoelastic polymers. *Computers and Structures*, 80, 1213 – 1229.

BEYLER, C. L. et HIRSCHLER, M. M. (2001). *SFPE Handbook of Fire Protection Engineering*, NFPA, Quincy, MA, chapitre Thermal Decomposition of Polymers. Troisième édition.

BIOT, M. A. (1954). Theory of Stress-Strain Relations in Anisotropic Viscoelasticity and Relaxation Phenomena. *Journal of Applied Physics*, 25, 1385 – 1391.

BOULEAU, N. (1992). Interprétation probabiliste de la viscoélasticité linéaire. *Mechanics Research Communications*, 19, 15 – 20.

BOWLES, K. J., ROBERTS, G. D. et KAMROUVIS, J. E. (1995). Long-Term Isothermal Aging Effects on Carbon Fabric-Reinforced PMR-15 Composites: Compression Strength. Rapport technique, NASA Technical Memorandum 107129.

BRADSHAW, R. D. et BRINSON, L. C. (1997a). Physical Aging in Polymers and Polymer Composites: An Analysis and Method for Time-Aging Time Superposition. *Polymer Engineering and Science*, 37, 31 – 44.

BRADSHAW, R. D. et BRINSON, L. C. (1997b). Recovering Nonisothermal Physical Aging Shift Factors Via Continuous Test Data: Theory and Experimental Results. *Journal of Engineering Materials and Technology*, 119, 233 – 241.

BRADSHAW, R. D. et BRINSON, L. C. (1999). A continuous test data method to determine a reference curve and shift rate for isothermal physical aging. *Polymer Engineering and Science*, 39, 211 – 235.

BUDRUGEAC, P. et SEGAL, E. (2001). Some Methodological Problems Concerning Nonisothermal Kinetic Analysis of Heterogeneous Solid–Gas Reactions. *International Journal of Chemical Kinetics*, 33, 564 – 573.

BUDRUGEAC, P., SEGAL, E., PÉREZ-MAQUEDA, L. A. et CRIADO, J. M. (2004). The use of the IKP method for evaluating the kinetic parameters and the conversion function of the thermal dehydrochlorination of PVC from non-isothermal data. *Polymer Degradation and Stability*, 84, 311 – 320.

CARPENTER, W. C. (1972). Viscoelastic stress analysis. *International Journal for Numerical Methods in Engineering*, 4, 357 – 366.

CARUTHERS, J. M., ADOLF, D. B., CHAMBERS, R. S. et SHRIKHANDE, P. (2004). A thermodynamically consistent, nonlinear viscoelastic approach for modeling glassy polymers. *Polymer*, 45, 4577 – 4597.

CHUANG, K. (2001). High T_g Polyimides. Rapport technique, NASA Glenn Research Center.

CHUANG, K. (2005). High T_g Polyimides for resin transfer molding. *International SAMPE Symposium and Exhibition*. vol. 50, 811 – 820.

COATS, A. W. et REDFERN, J. P. (1963). Thermogravimetric Analysis - A Review. *Analyst*, 88, 906 – 924.

COLEMAN, B. D. (1964). Thermodynamics of materials with memory. *Archive for Rational Mechanics and Analysis*, 17, 1 – 46.

CROCHON, T., SCHÖNHERR, T., LI, C. et LÉVESQUE, M. (2010). On finite-element implementation strategies of Schapery-type constitutive theories. *Mechanics of Time-Dependent Materials*, 14, 359 – 387.

CUNAT, C. (2001). The DNLR Approach and Relaxation Phenomena. Part I – Historical Account and DNLR Formalism. *Mechanics of Time-Dependent Materials*, 5, 39 – 65.

DROZDOV, A. D. (1997). A constitutive model in finite viscoelasticity with an entropy-driven material clock. *Mathematical and Computer Modelling*, 25, 45 – 66.

DROZDOV, A. D. (2000). Viscoelastoplasticity of amorphous glassy polymers. *European Polymer Journal*, 36, 2063 – 2074.

FAN, W. et LI, J.-L. (2013). Rapid Evaluation of Thermal Aging of a Carbon Fiber Laminated Epoxy Composite. *Polymer Composites*.

FLYNN, J. et WALL, L. (1966). A quick, direct method for the determination of activation energy from thermogravimetric data. *Journal of Polymer Science Part B: Polymer Letters*, 4, 323 – 328.

GREENBAUM, G. A. et RUBINSTEIN, M. F. (1968). Creep analysis of axisymmetric bodies using finite elements. *Nuclear Engineering and Design*, 7, 379 – 397.

GUO, Y. et BRADSHAW, R. D. (2007). Isothermal physical aging characterization of Polyether-ether-ketone (PEEK) and Polyphenylene sulfide (PPS) films by creep and stress relaxation . *Mechanics of Time-Dependent Materials*, 11, 61 – 89.

GUO, Y. et BRADSHAW, R. D. (2009). Long-term creep of polyphenylene sulfide (PPS) subjected to complex thermal histories: The effects of nonisothermal physical aging. *Polymer*, 50, 4048 – 4055.

GUO, Y., WANG, N., BRADSHAW, R. D. et BRINSON, L. C. (2009). Modeling mechanical aging shift factors in glassy polymers during nonisothermal physical aging. I. Experiments and KAHR-a$_{te}$ model prediction. *Journal of Polymer Science, Part B (Polymer Physics)*, 47, 340 – 352.

GURMAN, J. L., BAIER, L. et LEVIN, B. C. (1987). Polystyrenes: A Review of the Literature on the Products of Thermal Decomposition and Toxicity. *Fire and Materials*, 11, 109 – 130.

HAJ-ALI, R. M. et MULIANA, A. H. (2004). Numerical finite element formulation of the schapery non-linear viscoelastic material model. *International Journal for Numerical Methods in Engineering*, 59, 25 – 45.

HENRIKSEN, M. (1984). Nonlinear viscoelastic stress analysis - A finite element approach. *Computers and Structures*, 18, 133 – 139.

HUTCHINSON, J. M. (1995). Physical aging of polymers. *Progress in Polymer Science (Oxford)*, 4, 703 – 760.

JANG, B. N. et WILKIE, C. A. (2005). The thermal degradation of bisphenol A polycarbonate in air. *Thermochimica Acta*, 426, 73 – 84.

JONES, D. C. (2009). *Nanomechanical Characterization of High Temperature Polymer Matrix Composite Resin: PMR-15 Polyimide*. Thèse de doctorat, University of Kentucky Master's Theses.

KIM, J., LEE, W. I. et TSAI, S. W. (2002). Modeling of mechanical property degradation by short-term aging at high temperatures. *Composites: Part B*, 33, 531 – 543.

KINGSTON, C. T., MARTÍNEZ-RUBÍ, Y., GUAN, J., BARNES, M., SCRIVER, C., STURGEON, R. E. et SIMARD, B. (2010). Coupled thermogravimetry, mass spectrometry, and infrared spectroscopy for quantification of surface functionality on single-walled carbon nanotubes. *Analytical and Bioanalytical Chemistry*, 396, 1037 – 1044.

KIRBY, A. J. (1992). *Polyimides: Materials, Processing and Applications*, vol. 5, Number 11, Report 59. Rapra Technology Limited.

KLÖPFFER, W. (1984). *Introduction to Polymer Spectroscopy*. Springer-Verlag.

KNAUSS, W. G. et EMRI, I. (1981). Non-Linear Viscoelasticity Based on Free Volume Consideration. *Computers and Structures*, 13, 123 – 128.

KNAUSS, W. G. et EMRI, I. (1987). Volume Change and the Nonlinearly Thermo-Viscoelastic Constitution of Polymers. *Polymer Engineering and Science*, 27, 86 – 100.

KOVACS, A. J. (1963). Transition vitreuse dans les polymères amorphes. Etude phénoménologique. *Fortschr. Hochpolym.-Forsch.*, 3, 394 – 507.

KOVACS, A. J., AKLONIS, J. J., HUTCHINSON, J. M. et RAMOS, A. R. (1979). Isobaric volume and enthalpy recovery of glasses. II. A transparent multiparameter theory. *Journal of Polymer Science, Part B (Polymer Physics)*, 17, 1097 – 1277.

LAI, J. et BAKKER, A. (1996). 3-D Schapery representation for non-linear viscoelasticity and finite element implementation. *Computational Mechanics*, 18, 182 – 191.

LANDRY, F. (2010). *Modeling of the Thermomechanical Behavior of an Epoxy Resin Subjected to Elevated Temperatures and Experimental Verification.* Thèse de doctorat, École Polytechnique de Montréal.

LÉVESQUE, M., DERRIEN, K., BAPTISTE, D. et GILCHRIST, M. D. (2008). On the development and parameter identification of schapery-type constitutive theories. *Mechanics of Time-Dependent Materials*, 12, 95 – 127.

LI, F., HUANG, L., SHI, Y., JIN, X., WU, Z., SHEN, Z., CHUANG, K. C., LYON, R. E., HARRIS, F. W. et CHENG, Z. D. (1999). Thermal degradation mechanism and thermal mechanical properties of two high-performance aromatic polyimide fibers. *Journal of Macromolecular Science, Part B: Physics*, 38, 107 – 122.

LI, J., ZHENG, W., LI, L., ZHENG, Y. et LOU, X. (2009). Thermal degradation kinetics of g-HA/PLA composite. *Thermochimica Acta*, 493, 90 – 95.

LIANG, G., ZHANG, Z. et YANG, J. (2007). Study on Properties of Low Dielectric loss Resin Matrix. *Polymer Bulletin*, 58, 1021 – 1029.

LUK-CYR, J., CROCHON, T., LI, C. et LÉVESQUE, M. (2013). Interconversion of linearly viscoelastic material functions expressed as Prony series: a closure. *Mechanics of Time-Dependent Materials*, 17, 53–82.

LUO, W. (2007). Application of time-temperature-stress superposition principle to nonlinear creep of poly(methyl methacrylate). *Key engineering materials*, 340, 1091 – 1096.

LUSTIG, S. R., SHAY JR., R. M., R. M. et CARUTHERS, J. M. (1996). Thermodynamic constitutive equations for materials with memory on a material time scale. *Journal of Rheology*, 40, 69 – 106.

LYON, R. E. (1997). An integral method of nonisothermal kinetic analysis. *Thermochimica Acta*, 297, 117 – 124.

MARAIS, C. et VILLOUTREIX, G. (1998). Analysis and modeling of the creep behavior of the thermostable PMR-15 polyimide. *Journal of Applied Polymer Science*, 69, 1983 – 1991.

MATERAZZI, S. (1997). Thermogravimetry – Infrared Spectroscopy (TG-FTIR) Coupled Analysis. *Applied Spectroscopy Reviews*, 32, 385 – 404.

MENG, X., HUANG, Y., YU, H. et LV, Z. (2007). Thermal degradation kinetics of polyimide containing 2,6-benzobisoxazole units. *Polymer Degradation and Stability*, 92, 962 – 967.

MULIANA, A. H. et SAWANT, S. (2009). Responses of viscoelastic polymer composites with temperature and time dependent constituents. *Acta Mechanica Sinica*, 204, 155 – 173.

NAM, J.-D. et SEFERIS, J. C. (1991). A Composite Methodology for Multistage Degradation of Polymers. *Journal of Polymer Science Part B: Polymer Physics*, 29, 601 – 608.

OHASHI, F., HIROE, T. et FUJIWARA, K. (2002). Strain-rate and temperature effects on the deformation of polypropylene and its simulation under monotonic compression and bending. *Polymer Engineering and Science*, 42, 1046 – 1055.

OLASZ, L. et GUDMUNDSON, P. (2005). Viscoelastic model of cross-linked polyethylene including effects of temperature and crystallinity. *Mechanics of Time-Dependent Materials*, 9, 23 – 44.

OZAWA, T. (1965). A New Method of Mnalyzing Thermogravimetric Data. *Bulletin of the Chemical Society of Japan*, 38, 1881 – 1886.

PEREJÓN, A., SÁNCHEZ-JIMÉNEZ, P. E., CRIADO, J. M. et P (2011). Kinetic Analysis of Complex Solid-State Reactions. A New Deconvolution Procedure. *The Journal of Physical Chemistry B*, 115, 1780 – 1791.

POCHIRAJU, K. V. et TANDON, G. (2006). Modeling Thermo-Oxidative Layer Growth in High-Temperature Resins. *Journal of Engineering Materials and Technology*, 128, 107 – 116.

POON, H. et AHMAD, F. (1998). A material point time integration procedure for anisotropic, thermo rheologically simple, viscoelastic solids. *Computational Mechanics*, 21, 236 – 242.

POON, H. et AHMAD, F. (1999). A finite element constitutive update scheme for anisotropic, viscoelastic solids exhibiting non-linearity of the schapery-type. *International Journal for Numerical Methods in Engineering*, 46, 2027 – 2041.

REGNIER, N. et GUIBE, C. (1997). Methodology for Multistage Degradation of Polyimide Polymer. *Polymer Degradation and Stability*, 55, 165 – 172.

RIMEZ, B., RAHIER, H., VAN ASSCHE, G., ARTOOS, T., BIESEMANS, M. et VAN MELE, B. (2008). The thermal degradation of poly(vinyl acetate) and poly(ethylene-co-vinyl acetate), Part I: Experimental study of the degradation mechanism. *Polymer Degradation and Stability*, 93, 800 – 810.

RUGGLES-WRENN, M. B. et BROECKERT, J. L. (2009). Effects of Prior Aging at 288C in Air and in Argon Environments on Creep Response of PMR-15 Neat Resin. *Journal of Applied Polymer Science*, 111, 228 – 236.

RYCHLÝ, J., MATISOVÁ-RYCHLÁ, L., KATARÍNA CSOMOROVÁ, K., JANIGOVÁ, I., SCHILLING, M. et LEARNER, T. (2011). Non-isothermal thermogravimetry, differential scanning calorimetry and chemiluminescence in degradation of polyethylene, polypropylene, polystyrene and poly(methyl methacrylate). *Polymer Degradation and Stability*, 96, 1573 – 1581.

SÁNCHEZ-JIMÉNEZ, P. E., PÉREZ-MAQUEDA, L. A., PEREJÓN, A. et CRIADO, J. M. (2010). Generalized Kinetic Master Plots for the Thermal Degradation of Polymers Following a Random Scission Mechanism. *Journal of Physical Chemistry*, 114, 7868 – 7876.

SÁNCHEZ-JIMÉNEZ, P. E., PÉREZ-MAQUEDA, L. A., PEREJÓN, A. et CRIADO, J. M. (2011). Constant rate thermal analysis for thermal stability studies of polymers. *Polymer Degradation and Stability*, 96, 974 – 981.

SAWANT, S. et MULIANA, A. H. (2008). A thermo-mechanical viscoelastic analysis of orthotropic materials. *Composite Structures*, 83, 61 – 72.

SCHAPERY, R. A. (1964). Application of Thermodynamics to Thermomechanical, Fracture, and Birefringent Phenomena in Viscoelastic Media. *Journal of Applied Physics*, 35, 1451 – 1465.

SCHAPERY, R. A. (1966a). An engineering theory of nonlinear viscoelasticity with applications. *International Journal of Solids and Structures*, 2, 407 – 425.

SCHAPERY, R. A. (1966b). A theory of nonlinear thermoviscoelasticity based on irreversible thermodynamics. *Proceedings of the* 5^{th} *U.S. National Congress on Applied Mechanics, ASME*, 511, 1 – 20.

SCHAPERY, R. A. (1968). On a Thermodynamics Constitutive Theory and its application to Various Nonlinear Materials. *Proceedings of IUTAM Symposium on Thermoinelasticity*. 259 – 284.

SCHAPERY, R. A. (1969a). *Further development of a thermodynamic constitutive theory : stress formulation*. Purdue University, School of Aeronautics.

SCHAPERY, R. A. (1969b). On the characterization of nonlinear viscoelastic materials. *Polymer Engineering and Science*, 9, 295 – 310.

SCHAPERY, R. A. (1997). Nonlinear Viscoelastic and Viscoplastic Constitutive Equations Based on Thermodynamics. *Mechanics of Time-Dependent Materials*, 1, 209 – 240.

SCHAPERY, R. A. (2000). Nonlinear viscoelastic solids. *International Journal of Solids and Structures*, 37, 359 – 366.

SESTAK, J., SATAVA, V. et WENDLANDT, W. W. (1973). The study of heterogeneous processes by thermal analysis. *Thermochimica Acta*, 7, 333 – 333.

STRUIK, L. C. E. (1978). *Physical Aging in Amorphous Polymer and other Materials*. Elsevier Scientific Publishing Company.

STRUIK, L. C. E. (1988). Dependence of relaxation times of glassy polymers on their specific volume. *Polymer*, 29, 1347 – 1353.

SULLIVAN, J. L., BLAIS, E. J. et HOUSTAN, D. (1993). Physical aging in the creep behavior of thermosetting and thermoplastic composites. *Composites Science and Technology*, 47, 389 – 403.

TALON, O. (2007). Polyimides linéaires. Techniques de l'ingénieur.

TAYLOR, R. L., PISTER, K. L. et GOUDREAU, G. L. (1970). Thermomechanical analysis of viscoelastic solids. *International Journal for Numerical Methods in Engineering*, 2, 45 – 59.

TOUATI, D. et CEDERBAUM, G. (1998). Postbuckling of non-linear viscoelastic imperfect laminated plates part 1 : material considerations. *Composite Structures*, 42, 33 – 41.

TSUJI, L. C., MCMANUS, H. L. et BOWLES (2000). *Time Dependent and Nonlinear Effects in Polymers and Composites, ASTM STP 1357*, American Society for Testing and Materials, West Conshohocken, PA, chapitre Mechanical Properties of Degraded PMR-15. 3 – 17.

TUTTLE, M. E. et BRINSON, H. F. (1986). Prediction of the long-term creep compliance of general composite laminates. *Experimental Mechanics*, 26, 89 – 102.

VRANDEČIĆ, N. S., ERCEG, M., JAKIĆ, M. et KLARIĆ, I. (2010). Kinetic analysis of thermal degradation of poly(ethylene glycol) and poly(ethylene oxide)s of different molecular weight. *Thermochimica Acta*, 498, 71 – 80.

ŠIMON, P. (2004). Isoconvertinal Methods. Fundamentals, meaning and application. *Journal of Thermal Analysis and Calorimetry*, 76, 123 – 132.

VYAZOVKIN, S. (2000). Kinetic concepts of thermally stimulated reactions in solids: A view from a historical perspective. *International Reviews in Physical Chemistry*, 19, 45 – 60.

WHITE, J. R. (2006). Polymer ageing: physics, chemistry or engineering? time to reflect. *C. R. Chimie*, 9, 1396 – 1408.

WILLIAMS, M. L., LANDEL, R. F. et FERRY, J. D. (1955). The temperature dependence of relaxation mechanisms in amorphous polymers and other glass-forming liquids. *Journal of the American Chemical Society*, 77, 3701 – 3707.

XIAO, X. R., HIEL, C. C. et CARDON, A. H. (1994). Characterization and Modeling of Nonlinear Viscoelastic Response of PEEK Resin and PEEK Composites. *Composites Engineering*, 4, 681 – 702.

ZHANG, S. et TSAI, L. W. (1994). Computer simulation of creep damage at crack tip in short fibre composites. *Acta Mechanica Sinica*, 10, 282 – 288.

ZHAO, R. (2008). Application of time-ageing time and time-temperature-stress equivalence to nonlinear creep of polymeric materials. *Materials science forum*, 575, 1151 – 1156.

ZIENKIEWICZ, O. C. et TAYLOR, R. L. (1991). *The finite element method. In : Solid and fluid mechanics, dynamics and non-linearity, vol. 2.* McGraw-Hill, London.

ZIENKIEWICZ, O. C., WATSON, M. et KING, I. P. (1968). A numerical method of visco-elastic stress analysis. *International Journal for Mechanical Science*, 10, 807 – 827.

ZOCHER, M. A. et GROVES, S. E. (1997). A three-dimensional finite element formulation for thermoviscoelastic orthotropic media. *International Journal for Numerical Methods in Engineering*, 40, 2267 – 2288.